Nitric Oxide and Postconditioning: Cardioprotective Methods for Acute Care of Ischemia Reperfusion Injury

Dissertation Advisor

Paul L. Huang, MD/PhD

Author

Terrence Kwok Cay Pong

Nitric Oxide and Postconditioning: Cardioprotective Methods for Acute Care of Ischemia Reperfusion Injury

Abstract

Timely coronary artery reperfusion is essential to prevent myocyte death following myocardial infarction. The act of restoring blood flow however, paradoxically reduces the beneficial effects of reperfusion. This phenomenon, termed myocardial reperfusion injury, refers to the injury of cardiac myocytes that were viable immediately before reperfusion.

Recent studies have shown that the timing and hemodynamic sequence of events which govern reperfusion can help to minimize the severity of reperfusion injury. The term postconditioning describes a modified form of reperfusion that involves a series of flow interruptions which confer significant cardioprotection to the heart. This thesis investigates ischemic postconditioning and endothelial nitric oxide synthase (eNOS) phosphorylation as cardioprotective therapies against reperfusion injury.

In the first half of this thesis, we test the hypothesis that phosphorylation of eNOS serves as a cardioprotection nodal point for ischemic postconditioning. We show that phosphorylation of eNOS increases enzyme activity and that its product, nitric oxide, plays a critical role in cardioprotection. A number of cardiac dysfunctions arise after reperfusion and we address the effects of postconditioning on infarct size and myocardial blood flow.

The second half of this thesis introduces the use of magnetic relaxometry sensors to detect cardiac biomarkers. The ability to non-invasively measure infarct size in small animals would be helpful in studying models of myocardial ischemia-reperfusion injury. We investigate the use of implantable biosensors in vivo and show that the cumulative detection of cardiac biomarkers correlates with infarct severity.

Table of Contents

Abstract iii
Table of Contents v
List of Figures viii
Acknowledgements xi
Dedication xiii

1. Introduction 1
1.1. Problem Statement and Hypothesis 2
1.2. Specific Aims 5
1.3. Myocardial Ischemia-Reperfusion Injury: Past to Present 6
1.4. Thesis Outline 9

2. Ischemic Postconditioning: Protection Against Myocardial Ischemia-Reperfusion Injury 11
2.1. Motivation 12
2.2. Targeting Reperfusion Injury with Ischemic Postconditioning 13
2.3. eNOS: Structure to Function with one Aspartic Substitution 15
2.4. Mediators of Lethal Reperfusion Injury 16
2.4.1. Inflammation 17
2.4.2. Mitochondrial Permeability Transition 18
2.4.3. Generation of Reactive Oxygen Species 19
2.4.4. pH restoration 19
2.4.5. Intracellular Ca^{2+} Overload 20
2.5. The Role of Nitric Oxide Response in Reperfusion Injury 21
2.6. Genetic Mouse Models of Endothelial Nitric Oxide Synthase 24

2.7. Mouse Model of Myocardial Ischemia-Reperfusion Injury and Postconditioning 26
2.8. Results 29
2.8.1. Modulation of Nitric Oxide Levels 29
2.8.2. In Vivo Tolerance to Reperfusion Injury 31
2.8.3. Activation of Cardioprotective Pathways 33
2.9. Discussion 35
2.10. Materials and Methods 37

3. In Vivo Quantification of Myocardial Blood Flow and No-Reflow Phenomena 40
3.1. Motivation 41
3.2. No-reflow Phenomenon 42
3.3. Laser Doppler Flowmetry 44
3.4. Dynamic Imaging of Blood Flow: Myocardial Contrast Echocardiography 47
3.5. Active Contours for Image Segmentation 54
3.6. Results 64
3.7. Discussion 72
3.8. Materials and Methods 75

4. In Vivo Quantification of Infarct Size 77
4.1. Motivation 79
4.2. Magnetic Relaxation Switch Sensors 82
4.3. Extravasation of Cardiac Biomarkers 84
4.4. Biomarker Dosimeter Characterization 88
4.5. In Vivo Validation 93
4.5.1. Cardiotoxicity 97
4.6. Discussion 98
4.7. Material and Methods 101

5. Conclusions and Future Work 104
5.1. Conclusions 105

5.2. Future Directions 107

Bibliography 109

List of Figures

1.1 Potential contribution of ischemia-reperfusion injury to infarct size. 4

1.2 Classic presentation of myocardial ischemia. 6

1.3 Thesis roadmap. 9

2.1 Traditional and postconditioning reperfusion algorithms. 14

2.2 Schematic Representation of eNOS homodimer and Aspartic S1176D substitution. 16

2.3 Overview of survival kinases pathway in ischemic postconditioning. 22

2.4 Generation of phosphomimetic eNOS mice 25

2.5 Location of Surgical Incision and Ligation. 27

2.6 Ligation of the Left Anterior Descending Coronary Artery. 28

2.7 Ex vivo evaluation of infarct size. 29

2.8 Phosphomimetic modulation of eNOS increases available nitric oxide in the myocardium. 30

2.9 eNOS S1176 phosphorylation protects against IR injury in vivo. 32

2.10 Postconditioning activates Akt and eNOS. 34

3.1 Implementation of Laser Doppler Flowmetry on the murine myocardium. 45

3.2 Blood flow profile measured with Laser Doppler Flowmetry. 46

3.3 Myocardial Contrast Echocardiography. 48

3.4 Sonic cracking of a contrast microbubble. 50

3.5 Method of quantifying mean myocardial blood flow 52

3.6 Image processing chain of myocardial contrast echocardiography image slices.57

3.7 External image force. 60

3.8 Snake movement towards endocardial border. 61

3.9 Segmentation of the left ventricle. 62

3.10 Myocardial contrast echocardiography replenishment curve. 63

3.11 Development of myocardial blood flow deficit over time 65

3.12 Phosphomimetic eNOS modulation improves myocardial blood flow. 67

3.13 Regional analysis of improvement in myocardial perfusion. 68

3.14 Effect of postconditioning and S1176D mutation on no-reflow zones. 70

4.1 Timing release of cardiac biomarkers after acute ischemic myocardial infarction. 80

4.2 Magnetic resonance switch (MRSw) activation 83

4.3 Murine cardiac biomarker serum dynamics following acute myocardial infarction. 85

4.4 Cardiac biomarker peritoneal space extravasation dynamics 85

4.5 Cardiac biomarker flank space extravasation dynamics. 87

4.6 Biosensor design 89

4.7 Biosensor calibration in vitro. 90

4.8 Cumulative exposure to analyte in vitro. 92

4.9 MRI interrogation of implanted biosensors 93

4.10 Sensor response differs markedly between MI and sham/control groups 94

4.11 Biosensor correlation with ex vivo infarct size..... 96

4.12 An implanted MRSw sensor device can detect the cardiotoxic effect of the chemotherapeutic drug doxorubicin in vivo..... 98

Acknowledgements

I would like to thank my classmates, colleagues, friends and family for their unyielding support, encouragement and advice. I would not be here without you. Yibo Ling, my fellow classmate in the Division of Health Sciences and Technology, was a fantastic collaborator and a good friend. He was full of innovative ideas and an amazing colleague to work with. He performed the cardiac biosensor experiments in Chapter 4.

The MGH Cardiovascular Research Center and all of its members have provided a nurturing environment over the course of my graduate research. Dmitry Atochin taught me everything I know about mice surgery, he took me under his arm and molded me into a competent animal surgeon. I have also had the pleasure of working with Satoshi Kashiwagi, Qian Li, Shenjun Zhu, Leo Chang, Ahmed Mady and Helen Swanson in my lab.

I had the privilege of working with Marielle Scherrer-Crosbie who helped advance my research in myocardial contrast echocardiography. I also want to thank Ken Bloch for welcoming me into his lab and Farouc Jaffer who introduced me to the concept of ischemic postconditioning.

I would like to especially thank my advisor Paul L. Huang. Paul guided me down my research journey while giving me the freedom to solve problems on my own. I would also like to thank my committee members: Kit Parker and Neel Joshi. Kit welcomed me with open arms when I first set foot on the Harvard campus.

Finally, I cannot thank enough the members of my close and extended family. I thank you for your unwavering love and support. In particular, I want to thank Alice Ching for providing me with year round sustenance by way of air-mail. This thesis is dedicated to my mother Carmen, my sister Tiffany and my father T.C. for their endless enthusiasm, who constantly challenged me, encouraged me to think critically, and taught me to be hard on myself but easy on others. I could not have done this or succeeded without all of your support.

This thesis work was supported by an American Heart Association Pre-doctoral fellowship (#09PRE2250760).

Dedication

For T.C., Carmen and Tiffany.

業精於研
救人爲本

Chapter 1

Introduction

Coronary artery disease is the leading cause of death in the world and is responsible for the death of 3.8 million men and 3.4 million woman each year [1]. Ischemic heart diseases are the most common cause of heart failure accounting for over 50% of heart failure cases alone [2]. Reperfusion is essential in order to prevent tissue necrosis following myocardial infarction (MI) and coronary artery reperfusion following MI has been widely used to restore blood flow and limit infarct progression. The timing and effectiveness of myocardial reperfusion are major requirements for functional recovery and great efforts are made to achieve reperfusion in a timely fashion [3]. The most successful strategies for treating patients following acute MI involve early restoration of myocardial reperfusion with the use of thrombolytic

therapy or percutaneous coronary intervention. However, the act of restoring blood flow paradoxically induces further injury, indicating that tissues and cells tolerate some levels of ischemia only to lose viability after reperfusion [4]. This phenomenon, termed myocardial ischemia-reperfusion injury, can counteract the beneficial effects of myocardial reperfusion (Figure 1.1).

Ischemia-reperfusion (IR) injury is a multifaceted process which involves multiple cell types, for which damage can be transient or lethal in nature [5]. Recent studies have demonstrated that the timing and hemodynamic sequence of events which govern reperfusion can help to minimize the severity of reperfusion injury. The term postconditioning describes a modified form of reperfusion that involves a series of flow interruptions during the first few minutes of reperfusion. Postconditioning has been shown to confer significant cardioprotection by reducing infarct size and cellular apoptosis [6]. However, given the short time since the discovery of ischemic postconditioning, the precise molecular mechanisms responsible for providing cardioprotection are not yet known.

1.1. Problem Statement and Hypothesis

Recent studies have implicated endothelial nitric oxide synthase (eNOS), a nitric oxide synthesizing enzyme, as a potential mediator of ischemic cardioprotection. Nitric oxide plays an important role in normal cardiovascular function and during myocardial ischemia. In this thesis, we test the hypothesis

that eNOS phosphorylation plays an integral role in conferring cardioprotection during postconditioned reperfusion. We investigate whether modulation of eNOS phosphorylation, a physiologic mechanism for regulation of *in vivo* eNOS catalytic activity, can serve as an effective treatment for preventing IR injury. Our overall goal is to utilize novel contrast-enhanced ultrasound imaging tools to investigate to role of eNOS and its involvement in the cardioprotection of IR injury and postconditioning. Our proposed approach makes use of eNOS knockout and knock-in mice models to investigate the physiological events that occur during IR injury *in vivo*. Therefore, in this thesis, we aim to serially investigate the pathogenesis of IR injury and define the relationship between eNOS, eNOS phosphorylation and the early events that occur at the onset of reperfusion.

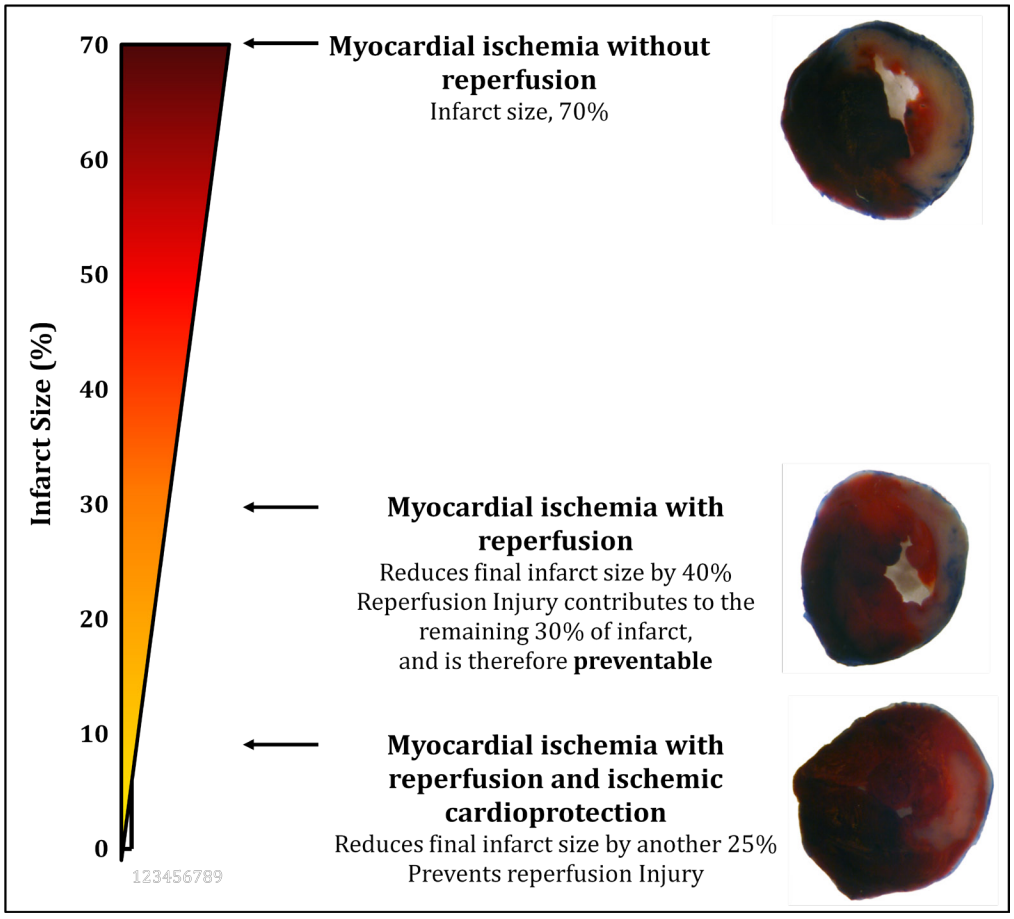

1.1 Potential contribution of ischemia-reperfusion injury to infarct size. Theoretical schematic showing the potential reductions in final infarct size realized through early and successful reperfusion of an ischemic myocardium. Despite reperfusion, the full benefits are not achieved without cardioprotective intervention due to the presence of ischemia-reperfusion injury. Cardioprotective measures performed at the onset of reperfusion can prevent reperfusion injury further reducing infarct size. Infarcted myocardial tissue is represented in white, while the viable, at risk myocardium is stained red, and the healthy myocardium blue.

1.2. Specific Aims

1. To investigate the pathogenesis of lethal reperfusion-injury and the role of eNOS phosphorylation in ischemic postconditioning after myocardial infarction *in vivo.*

2. To investigate the role of eNOS phosphorylation and postconditioning on myocardial blood flow and the no reflow phenomenon in myocardial ischemia-reperfusion injury.

3. To develop an implantable biosensor capable of measuring cardiac biomarkers in vivo and correlate biomarkers with infarct size severity.

1.3. Myocardial Ischemia-Reperfusion Injury: Past to Present

Necropsy (Dr. Hektoen).—The heart was of normal size, but both coronary arteries were markedly sclerotic, with calcareous districts and narrowing of the lumen. A short distance from its origin the left coronary artery was completely obliterated by a red thrombus that had formed at a point of great narrowing. The wall of the left ventricle showed well-marked areas of yellowish and reddish softening, especially extensive in the interventricular septum. At the very apex the muscle was decidedly softer than elsewhere. The beginning of the aorta showed a few yellowish spots, these areas becoming less marked as the descending part was reached. An acute fibrinous pericardial deposit, which showed no bacteria in smears, was found over the left ventricle. (The pericarditis probably explains the slighter pain complained of a few hours before death.) There was marked edema of the lungs. In other respects the anatomic findings were those of health.

1.2 Classic presentation of myocardial ischemia. Excerpt from James B. Herrick's landmark 1912 description of the "Clinical Features of Sudden Obstruction of the Coronary Arteries." Myocardial ischemia is caused by blockage of a coronary artery or of any of its large branches. Blockage of these vessels prevents blood flow to the myocardium causing tissue ischemia and cell death if not treated promptly, reproduced from Herrick [7].

The classic description of patients presenting with acute myocardial infarction and its cause was described by James Herrick in his landmark JAMA article in 1912 [7]. Herrick attributed the cause of myocardial infarction to a coronary thrombotic event (Figure 1.2). Since then, it has been established that the severity and duration of myocardial ischemia are important determinants of final infarct size [8]. Reimer et al documented the wave-front phenomena of ischemic cell

death whereby myocyte necrosis progresses from the endocardium towards the epicardium as the duration of coronary occlusion increases [9].

The diagnosis and treatment of acute MI has evolved to employ the use of methods to either dissolve, compress, remove or bypass the occluding thrombi to achieve early myocardial reperfusion, reduce the size of the infarction and improve clinical outcome [10]. However, the process of reperfusion itself can induce further injury to the ischemic myocardium. This phenomenon, referred to as myocardial reperfusion injury, can reduce the beneficial effect of myocardial reperfusion.

The concept of myocardial ischemia-reperfusion injury was proposed in 1960 by Jennings who reported structural and electrophysiological changes to the heart after coronary reperfusion [11]. In their histological findings Jennings et al reported that reperfusion caused irreversible damage to myocytes, which displayed explosive swelling, contraction bands of the myofibrils and architectural disruption to the sarcolemma suggesting that the act of reperfusion itself may contribute to myocardial apoptosis and necrosis.

Reperfusion of the heart primarily causes four types of cardiac dysfunction, these consist of: 1) myocardial stunning, 2) reperfusion arrhythmias, 3) no-reflow phenomena and 4) lethal reperfusion injury [12]. The first, myocardial stunning refers to relatively mild, sub-lethal injury to myocytes in the presence of near-normal blood flow where contractile abnormality is reversible. The dysfunction is not caused by a primary deficit in myocardial blood flow and the myocardium

usually recovers from this form of injury in days to weeks [13]. The second type of cardiac dysfunction describes arrhythmias that can arise as a consequence of myocardial reperfusion and the resulting electrophysiological imbalance. The cause and treatment of reperfusion-induced arrhythmias has been reviewed in depth by Manning et al [14]. The third type, no-reflow phenomenon, refers to the breakdown or obstruction of the coronary microvasculature in the infarct zone despite an open infarct related artery. Successful restoration of coronary artery patency does not necessarily translate into improved tissue perfusion with no-reflow phenomenon [15]. The last type of cardiac dysfunction, lethal reperfusion injury, relates to the paradoxical reduction in the beneficial effects of myocardial reperfusion following MI. Lethal reperfusion injury results from factors initiated at the onset of reperfusion that lead to the death of cardiac myocytes that were viable immediately before reperfusion [16].

In this thesis, we focus on the effects of postconditioning and eNOS activity on no-reflow phenomenon and lethal reperfusion injury. We address lethal reperfusion injury in Chapter 2 while Chapter 3 focuses on myocardial blood flow and the no-reflow phenomenon.

1.4. Thesis Outline

This thesis focuses on cardioprotective strategies for the treatment and monitoring of acute myocardial infarction and can be divided into two sections. The thesis roadmap is summarized in Figure 1.3.

The first half of this thesis focuses on methods of ischemic cardioprotection. We investigate the cardioprotective role of postconditioning and eNOS phosphorylation in reperfusion injury. In chapter 2 we address lethal reperfusion injury and the ability of postconditioning to reduce infarct size. We also investigate eNOS phosphorylation as a central integrating nexus that influences infarct size and ischemic cardioprotection.

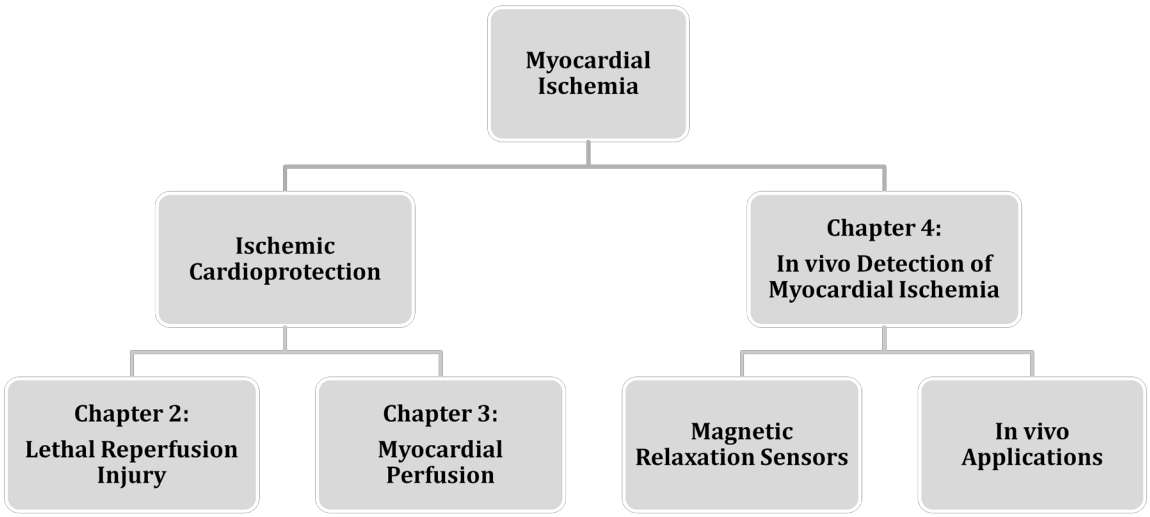

1.3 Thesis roadmap.

Chapter 3 addresses the effects of postconditioning on myocardial blood flow. In this chapter we utilize myocardial contrast echocardiography to obtain a temporal understanding of the myocardial blood flow dynamics that occur after reperfusion. We address the challenge of accurately estimating blood flow when provided with non-EKG gated ultrasound videos and propose the use of an automated active contours image segmentation algorithm to identify and track the myocardium.

The second half of this thesis describes the development and characterization of implantable biosensors for the detection of cardiac biomarkers. Chapter 4 presents a proof-of-concept biosensor based on magnetic relaxation switch technology that allows for estimation of infarct size in vivo.

Chapter 2

Ischemic Postconditioning: Protection Against Myocardial Ischemia-Reperfusion Injury

This chapter describes the use of genetic mouse models to study the role of eNOS activity and nitric oxide production in ischemic postconditioning. We develop a murine model of myocardial ischemia-reperfusion injury and study the effects of ischemic postconditioning on lethal reperfusion injury. Our study employs the use of S1176D phosphomimetic eNOS knock-in mice which simulate the effects of constitutively phosphorylated eNOS to generate increased levels of nitric oxide in myocardial tissue. We determine the effects of phosphomimetic eNOS modulation on known cardioprotective molecular pathways as well as its effect on infarct size following IR injury.

2.1. Motivation

eNOS and its product, nitric oxide, play an important role in cardioprotective signaling, platelet aggregation and leukocyte-endothelial interaction [17, 18]. Among the regulators of NO, phosphorylation of eNOS appears to be an important means of regulating enzyme activity [19, 20]. In this chapter we test the hypothesis that increased eNOS phosphorylation provides a protective benefit against lethal ischemia-reperfusion injury. In particular, the importance of eNOS phosphorylation at the Serine^{1176} residue has been studied *in vitro* using a mutant form of eNOS.

S1176D eNOS contains a single aspartate for serine amino acid substitution that mimics the negatively charged phosphate group of phosphorylated eNOS. The resultant eNOS enzyme has higher catalytic activity and increased production of NO at basal levels. We have generated S1176D mice which express this mutant form of eNOS and use these mice to develop an understanding of the molecular mechanisms that influence infarct size following myocardial IR injury. The combined use of eNOS knock-out and S1176D knock-in mice models help provide an *in vivo* understanding of how eNOS phosphorylation is centrally integrated into the cardioprotective survival pathway.

2.2. Targeting Reperfusion Injury with Ischemic Postconditioning

Postconditioning describes a series of brief mechanical interruptions to blood flow performed at the onset of reperfusion. Postconditioning initiates a cascade of cardioprotective signals that ultimately lead to a reduction in infarct size and myocyte apoptosis. The concept of postconditioning was first reported in 2003 by Zhao et al. who demonstrated in canines that postconditioning conferred similar cardioprotection against MI injury when compared to preconditioned hearts [21]. Since then, these occlusion-reocclusion algorithms have been shown to attenuate damage successfully in rabbits, mice and humans [22, 23]. The algorithms employed in these studies typically last for a few minutes with the optimal duration of occlusion varying between species. Postconditioning algorithms differ from those of preconditioning because they can be applied at the onset of reperfusion in conjunction with other clinical services such as angioplasty. Importantly, they do not require foreknowledge of the ischemic event. A typical flow profile comparing traditional vs. postconditioned reperfusion as applied to mice is shown in (Figure 2.1), 10 second intervals are used between reperfusion cycles for postconditioning in mice.

IR injury is a complex process and the means by which postconditioning exerts its protective effects remain unclear. Multiple physiological pathways have been suggested to be involved, including reduction in the degree of: endothelial cell

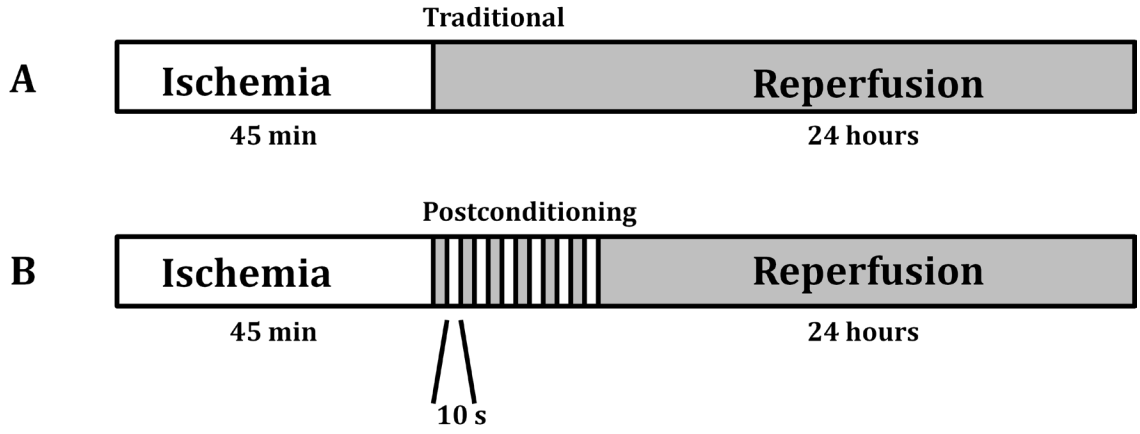

2.1 Traditional and postconditioning reperfusion algorithms. Following 45 minutes of ischemia, mice are subjected to either traditional reperfusion or cardioprotective postconditioning. A) Traditional reperfusion is achieved by immediate reperfusion of the myocardium. B) Postconditioning is accomplished by implementing 6 cycles of 10 sec reperfusion followed by 10 sec occlusion. The extent of reperfusion injury is evaluated 24 hours after reperfusion.

dysfunction, reactive oxygen species generation, leukocyte activation and mitochondrial damage [24-26]. While the net effectiveness of postconditioning has been reported by multiple independent laboratories, the importance and role of myocardial blood flow as well as nitric oxide availability remain unknown. A temporal understanding of the effects of postconditioning on IR injury will help us better understand the chronology of events that are required to protect the heart after MI. In addition, the protective role of eNOS phosphorylation and its central role in postconditioning have yet to be investigated. The purpose of this chapter is to define the role of eNOS phosphorylation at Serine^{1176} in postconditioning and against myocardial IR in vivo.

2.3. eNOS: Structure to Function with one Aspartic Substitution

eNOS catalyzes the reaction of oxygen with L-arginine to generate nitric oxide and L-citrulline [27]. It is part of the first mammalian pathway known to synthesize a gas as a signaling molecule. Structural studies have suggested that active eNOS is associated with dimerization that facilitates electron flow through the active site pocket. This interface includes the binding site for BH_4, heme and L-arginine (Figure 2.2). The presence of BH_4, heme and L-arginine stabilize the active dimeric form of eNOS. eNOS activity can be regulated by Ca^{2+} dependent interaction at the calmodulin (CM) binding domain as well as by phosphorylation. Studies have shown that $Serine^{1176}$ is phosphorylated by protein kinase AKT [19, 20], which results in increased electron flux through the reductase domain and an increase in NO production [28].

In order to mimic the gain of function achieved through phosphorylation of $Serine^{1176}$, we have implemented a single aspartic acid for serine substitution (Figure 2.2). The negative charge associated with the carboxyl group on aspartic acid mimics the charged phosphate group of activated $Serine^{1176}$ (serine phosphorylation occurs at eNOS S^{1176} in mice, S^{1177} in humans and S^{1179} in cow) [28, 29]. This mutation removes the steric hindrance imparted by the non-catalytic insert and permits better electron flux through the reductase domain to facilitate NO generation in the oxygenase domain [30].

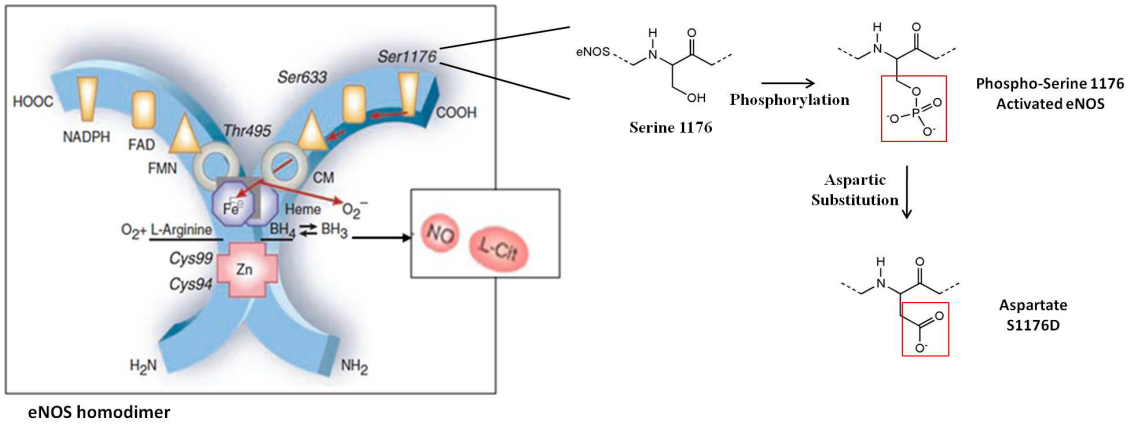

2.2 Schematic Representation of eNOS homodimer and Aspartic S1176D substitution. We have engineered genetic S1176D knock-in mice with a single aspartic acid substitution to mimic phosphorylation of eNOS at S1176, eNOS homodimer image adapted from Goligorsky [31].

2.4. Mediators of Lethal Reperfusion Injury

The lethal aspect of reperfusion-injury refers specifically to the injury caused by the act of reperfusion after an ischemic episode. Studies in MI animal models suggest that reperfusion injury can account for up to 50% of the size of the final infarct [1]. The development of therapeutic treatments for ischemia-reperfusion injury have been targeted at a multitude of biological pathways; these range from minimizing the oxidative stress generated during reperfusion to attenuating a myriad of factors that result from the innate inflammatory response [32].

Experimental models have demonstrated that modified forms of reperfusion, such as postconditioning, can reduce reperfusion injury and confer cardioprotective effects, raising hopes for clinical therapy. Recent demonstrations of the beneficial

effects of ischemic postconditioning during reperfusion have generated immense interest in the reperfusion phase as an opportune window for establishing cardioprotection. However, a more concrete understanding of the factors responsible for regulating lethal reperfusion injury is necessary before we can design successful therapies to attenuate the damage caused by reperfusion. Here we provide an overview of the mediators of lethal reperfusion injury and the potential role of postconditioning in limiting these factors.

2.4.1. Inflammation

The innate inflammatory response following an acute MI is characterized by the release of chemo attractants and the recruitment of neutrophils and macrophages to the injured myocardium. The degree of leukocyte activity is likely affected by the choice of reperfusion (traditional or postconditioned). The inflammatory response rapidly recruits neutrophils to the site of damage within the first 6 hours where they begin to remodel the local microenvironment and facilitate healing over the next 24 hours. Efficient cardiac repair involves the generation of oxygen free radicals, the release of proteases and the additional recruitment of inflammatory cells [33]. In the process however, the release of degradative enzymes and generation of reactive oxygen species can cause vascular plugging and other detrimental effects.

An understanding of how reperfusion affects leukocyte recruitment will provide valuable information for future MI treatment. Studying postconditioning and

its effect on vascular function will enable us to augment this repair process in the future.

2.4.2. Mitochondrial Permeability Transition

The mitochondrial permeability transition pore (mPTP) is a non-specific, high conductance protein channel of the inner mitochondrial membrane that is normally closed under physiologic conditions but opens under cellular stress [34]. During ischemia, the mPTP remains closed, but opens shortly after reperfusion as a result of mitochondrial Ca^{2+} overload, stress from reactive oxygen species, and the rapid restoration of tissue pH. Opening of the mPTP allows for free passage of molecules across the inner mitochondrial membrane which initiates a variety of adverse effects such as osmotic pressure changes, mitochondrial swelling and ultimately cell death. The mitochondrial permeability transition causes the collapse of the mitochondrial membrane potential, uncouples oxidative phosphorylation and accelerates the hydrolysis of ATP [35]. It leads to the release of inner mitochondrial proteins and the irreversible activation of pro-apoptosis pathways. Pharmacological intervention of the mPTP with cyclosporine A or specific inhibitors of the mPTP have been shown to protect against the onset of lethal reperfusion injury [36]. Postconditioning has been shown to inhibit the mPTP in rabbits [37].

2.4.3. Generation of Reactive Oxygen Species

Oxygen free radicals have been studied extensively as mediators of lethal reperfusion injury. There is an increase in the generation of free radicals once oxygen is reintroduced to ischemic myocardium [38, 39]. Most reactive oxygen species (ROS) are generated by neutrophils and the mitochondria and the burst of ROS within the first moments of reperfusion is associated with cardiac dysfunction. In addition, the propagation of ROS induced ROS release may amplify its harmful effects [40]. This has led to the suggestion of the oxygen paradox, where re-oxygenation of the myocardium is necessary but its action generates additional oxidative stress that contributes to myocardial injury exceeding the injury induced by ischemia alone [12]. Furthermore, oxidative stress has been shown to reduce the bioavailability of nitric oxide, reducing the cardioprotective effects of NO [41]. The protective effects of NO include the inactivation of superoxide radicals, inhibition of neutrophil accumulation and improved tissue blood flow.

2.4.4. pH restoration

During myocardial ischemia, the ischemic tissue becomes acidotic and develops a large reduction in pH [42]. Ischemia causes anoxia and the generation of lactic acid through anaerobic glycolysis and ATP depletion. Reperfusion washes out any lactic acid that has built up in the ischemic myocardium causing a rapid return to physiologic pH. The recovery of pH to normal levels is a stress that can precipitate

myocyte death. Although tissue acidosis may seem detrimental in ischemia, numerous studies have highlighted a "pH paradox" where acidosis strongly protects against lethal reperfusion injury. Bond et al showed protection with acidotic pH perfusate when neonatal rat cardiac myocytes were reoxygenated in a pH 6.2 environment versus a pH of 7.4 [43]. The mechanisms responsible for this pH paradox remain poorly understood but acidosis may inhibit harmful proteases and other destructive enzymes that require a neutral or alkaline pH [44, 45]. pH-dependent reperfusion injury may involve the reactivation of pH dependent enzymes that accelerate intracellular damage. In addition, the rapid restoration of physiologic pH may be responsible for the opening of mitochondrial permeability transition pore [35].

2.4.5. Intracellular Ca^{2+} Overload

Reperfusion also causes intracellular and mitochondrial Ca^{2+} overload. The increase of intracellular Ca^{2+} is caused by sarcolemmal-membrane damage and ROS related dysfunction of the sarcoplasmic recticulum. Excess myocardial Ca^{2+} precipitates myocyte death by causing sarcolemmal contraction and opening of the mitochondrial permeability transition pore [12]. Treatment of reperfusion injury with intracoronary calcium channel agonists can decrease infarct size in experimental models [46] but the results of clinical trials have been unsuccessful [47].

2.5. The Role of Nitric Oxide Response in Reperfusion Injury

Although reperfusion is essential in preventing tissue death, the restoration of blood flow to the ischemic myocardium results in further injury to the surrounding area [3]. Following reperfusion, the time course of vascular dysfunction begins early after the onset of reperfusion. The endothelium becomes dysfunctional within minutes, resulting in a marked decrease in NO bioavailability; this is supported by experimental evidence demonstrating impaired endothelium dependent vasodilatory relaxation after ischemia-reperfusion [48]. This represents a pressing concern because post-MI survivors with persistent vascular dysfunction are more likely to develop heart failure.

NO plays numerous roles in the heart and low levels of NO are required to regulate vascular tone, inhibit leukocyte-endothelial adhesiveness and prevent mitochondrial mediated apoptosis [3]. NO bioavailability is necessary for cardioprotection and experimental treatments have identified eNOS activation as an integral component of pro-survival pathways against lethal reperfusion injury. For example, the pharmacological use of HMG-CoA reductase inhibitors has been shown to regulate eNOS mRNA levels [49] and attenuate the severity of myocardial IR injury [50, 51]. Other pharmacological studies have documented the powerful cardioprotective effects of gaseous hydrogen sulfide [52] and volatile anesthetics such as isoflurane at the onset of reperfusion. [53, 54] while the use of insulin

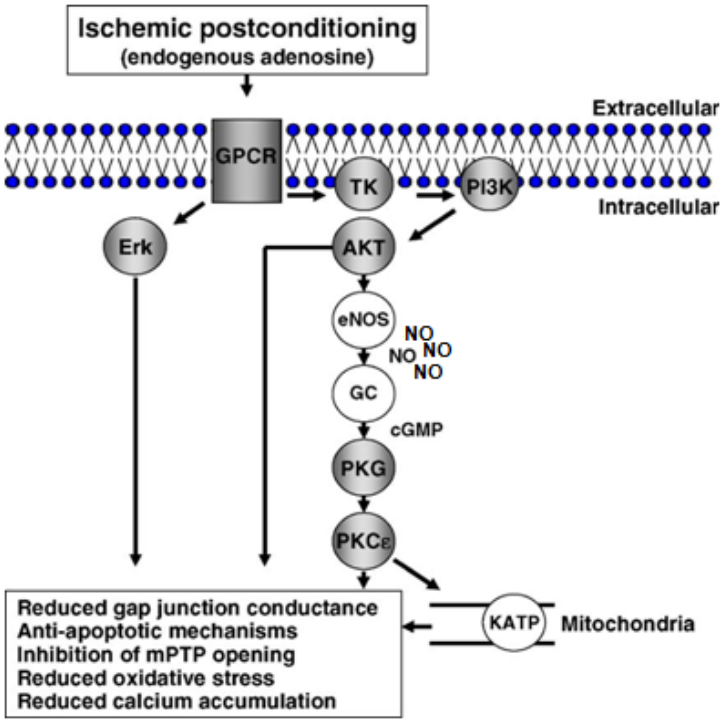

2.3 Overview of survival kinases pathway in ischemic postconditioning. A simplified scheme of important transduction pathways recruited in the setting of cardioprotective ischemic postconditioning. Generation of nitric oxide (NO) through eNOS contributes to the protection of the ischemic heart, adapted from [55].

therapy has been shown to inhibit leukocyte-endothelial adherence via an NO-dependent mechanism [56-58].

The interactions of NO with various pathways are an important defense against IR injury and serve as endogenous protectants for the heart. In the myocardium, the protective effect of NO is supported by the fact that knock-out mice deficient in eNOS develop infarct sizes significantly larger than wild-type mice following reperfusion injury [59]. NO protection is also important in the inhibition of the mitochondrial permeability transition through the reperfusion injury salvage

kinase (RISK) signaling pathway (Figure 2.3). NO interacts with soluble guanylate cyclase and its downstream effectors to inhibit the opening of the mPTP [55].

Since postconditioning reduces infarct size caused by lethal reperfusion injury, we assess the role of postconditioning and its ability to regulate NO bioavailability. This chapter focuses on the importance of eNOS S1176 phosphorylation as a critical step in the regulation of eNOS activity and treatment of IR injury.

2.6. Genetic Mouse Models of Endothelial Nitric Oxide Synthase

In order to study the importance of eNOS phosphorylation on the *in vivo* disease pathogenesis of ischemia reperfusion injury we utilize two murine models of mutant eNOS: an eNOS knock-out model and S1176D phosphomimetic knock-in model of eNOS. The knock out model of eNOS mice was previously generated in our lab by Huang et al [60]. eNOS mediates basal vasodilation and the blood pressure in eNOS knock-out mice is significantly higher that wild-type mice. Studies of cardiac function in eNOS knock-out mice demonstrate that baseline cardiac contractility measures are similar between knock out and wild-type mice [61].

We used the S1176D knock-in model to study the specific effects of eNOS phosphorylation on reperfusion injury. Figure 2.4 depicts the construct used by our lab to generate this phosphomimetic form of eNOS. The eNOS gene of S1176D ki mice contains a single amino acid mutation, where serine^{1176} is replaced by aspartate (S1176D) to achieve a phosphomimetic gain-of-function mutation [19, 20]. Aspartate contains a carboxyl moiety that mimics the negatively charged group when eNOS is normally phosphorylated at serine^{1176}. Previous *in vitro* studies in endothelial cells expressing the S1176D form of eNOS are characterized by increased basal enzyme activity and augmented NO production at resting levels of intracellular calcium [62]. In addition, we have previously shown *in vivo* that this phosphomimetic S1176D form rescues impaired blood flow in Akt1 deficient mice

subjected to wound healing assays [63], and improves vessel reactivity and decreases stroke size when challenged with cerebral ischemia [64]. Both the eNOS knock-out and S1176D knock-in mice were backcrossed to C57BL/6J background to eliminate the confounding variability of genetic background.

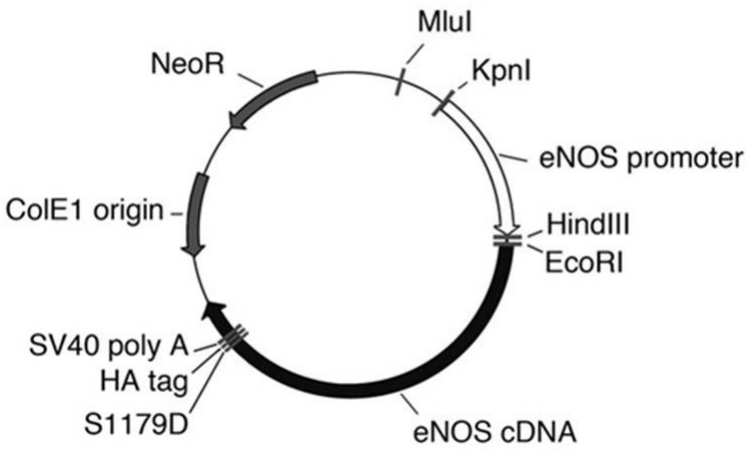

2.4 Generation of phosphomimetic eNOS mice. Schematic of the transgenic construct used to generate eNOS knock-in mice. A 1.6-kb fragment from the eNOS promoter drives the eNOS cDNA carrying a phosphomimetic eNOS mutation, an HA tag and SV40 polyadenylation site, adapted from Atochin et al. [64].

2.7. Mouse Model of Myocardial Ischemia-Reperfusion Injury and Postconditioning

Mouse models of IR injury are advantageous compared to other animal models (such as rat, rabbit and larger animal models) because of their small size, rapid gestation period (21 days) and large litter numbers. Advancements in gene-targeted knock-out and knock-in techniques to modify the mouse genome have made it possible to study the role of eNOS phosphorylation in cardiovascular disease. With our arsenal of genetically altered eNOS mice, we were interested in developing a murine model of ischemic postconditioning to study the mechanisms responsible for myocardial IR injury. A murine model of postconditioning enables us to model myocardial IR injury and study the importance of phosphomimetic eNOS modulation in vivo.

We developed a mouse model based off of the techniques pioneered by Lloyd et al adopting a model of left anterior descending (LAD) artery occlusion and reperfusion [65]. We applied a LAD artery occlusion for 45 minutes followed by reperfusion allowing flow through the previously ischemic myocardium. Postconditioning was achieved by integration of a snare onto the silk ligature around the LAD (Figure 2.5). Myocardial ischemia was documented visually as well as by laser Doppler and contrast ultrasound in specific cases. Figure 2.6A shows the position of the suture and snare on the LAD coronary artery and the subsequent change in color of the anterior wall achieved by tightening of the ligature (Figure

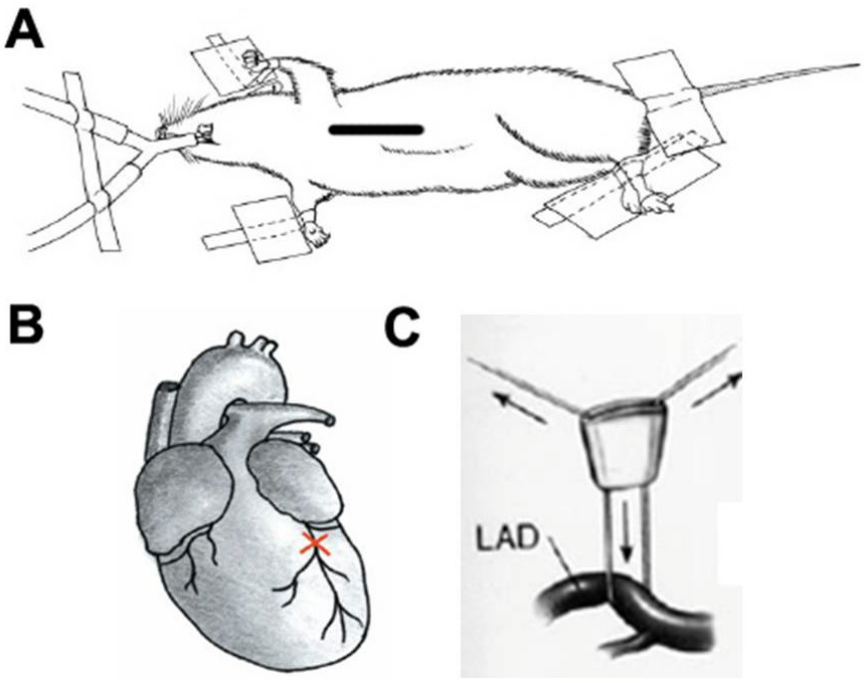

2.5 Location of Surgical Incision and Ligation. A) The mouse is intubated and a surgical thoracotomy is performed left of the sternum. The pericardium is then separated to allow access to the myocardium, image adapted from Tarnavski et al. [66] B) 7-0 silk suture is passed under the left anterior descending (LAD) coronary artery at the level below the left auricle. C) A snare using PE10 tubing is then formed around the suture, application of tension on suture forces the snare onto the LAD creating temporary occlusion of the LAD. Reperfusion of the myocardium is achieved on relaxation of the snare.

2.6B). In our model of IR injury, mice are sacrificed 24 hours after reperfusion to evaluate infarct size.

When performing IR injury studies and comparing infarct size, consistency of the area at risk between groups is important [66]. The gold standard technique for evaluating area at risk and infarct size is accessed via perfusion of Evans blue dye into the carotid artery while the myocardium is re-ligated. Areas of the myocardium

not stained blue are then classified as the 'area-at-risk' (figure 2.7B). The heart is then excised and sectioned transversely into 1mm sections, weighed and stained with triphenyltetrazolium chloride (TTC). After TTC staining, viable myocardium stains red (figure 2.7C) while infarcted myocardium appears white (figure 2.7D). The final size of infarction was determined by a weighted average of the myocardial slices (see methods for detailed description).

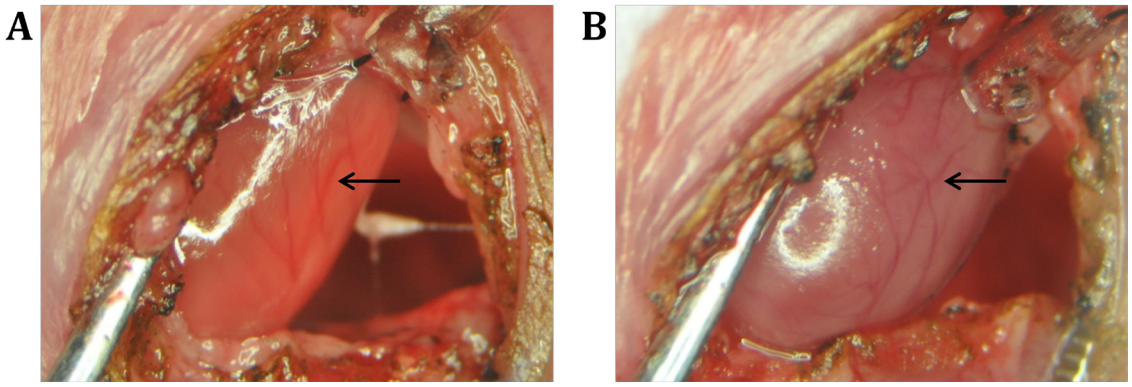

2.6 Ligation of the Left Anterior Descending Coronary Artery. The arrow identifies the LAD coronary artery. A) Normal perfused myocardium, on visual inspection the myocardium appears a robust pink color from a perfused vascular bed. B) Ischemic myocardium achieved by application of snare around LAD coronary artery. An empty coronary artery is identified by the arrow and a significant pallor of the myocardium can be confirmed visually.

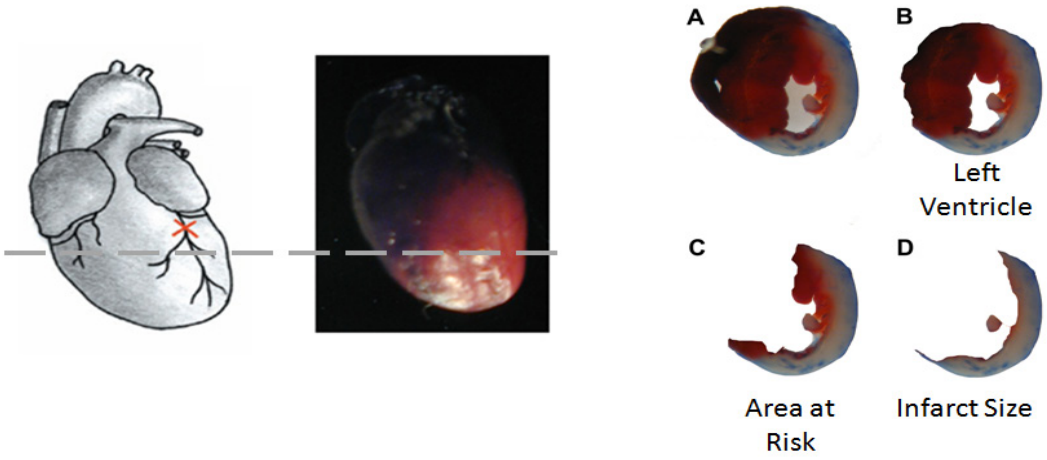

2.7 Ex vivo evaluation of infarct size. 1mm slice of excised myocardium from the level of the dotted line. B) Separation of the left ventricle. C) Area at risk (stained red) D) Infarct Size (stained white).

2.8. Results

2.8.1. Modulation of Nitric Oxide Levels

eNOS phosphorylation modulates myocardial nitric oxide levels.

To investigate the relevance of eNOS phosphorylation as a specific target for protection against myocardial IR injury, we generated genetic knock-in mice expressing a S1176D phosphomimetic mutant form of eNOS. The serine at 1176 of the endogenous eNOS gene was replaced by a single amino acid mutation (S^{1176} for aspartate replacement, S1176D knock-in) that simulated phosphorylation (Figure 2.8A) [62].

To assess whether S1176D knock-in mice can be used as a suitable model for examining eNOS function in the heart, we evaluated the basal level of myocardial NO

production in S1176D knock-in mice versus WT and eNOS ko mice. We used NO specific fluorometry to detect levels of nitrate/nitrite (NOx), the stable breakdown products of NO metabolism [67]. Myocardial tissue isolated from S1176D ki mice

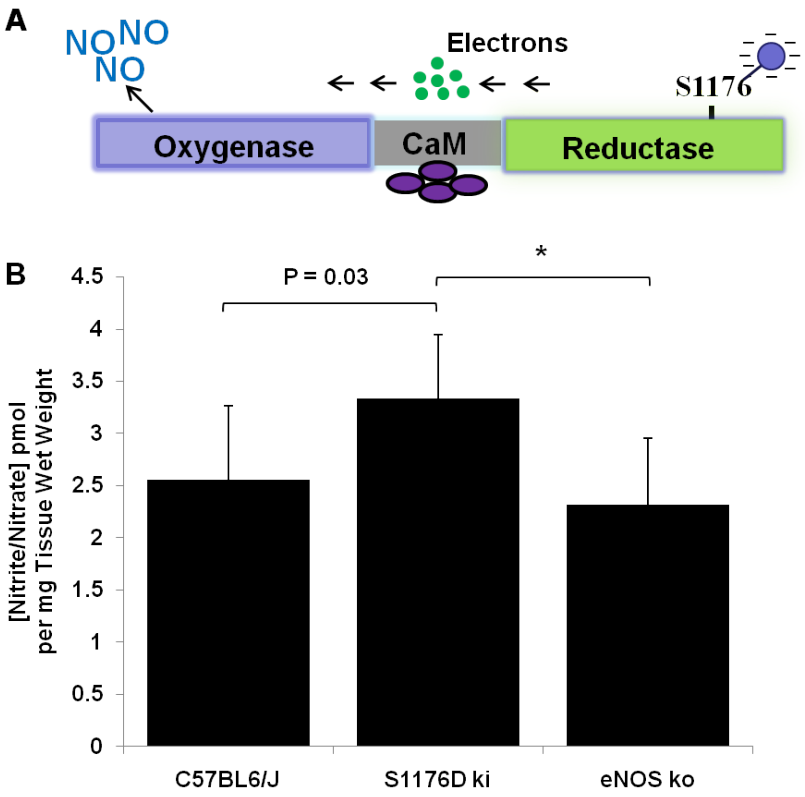

2.8 Phosphomimetic modulation of eNOS increases available nitric oxide in the myocardium. (A) We generated eNOS knock-in mice with a single amino acid mutation replacing Serine1176 with a phosphomimetic aspartate mutation. The aspartate contains a negatively charged carboxyl group that mimics the phosphorylated form of eNOS, increasing electron transfer through the calmodulin (CaM) domain and nitric oxide production. (B) Constitutively active S1176D ki eNOS mice were compared against WT and eNOS ko mice. Myocardial nitrite/nitrate levels were measured via fluorometric assay and normalized by tissue wet weight. n = 7 - 11 mice per group. Data are expressed as the mean ± SD. * $P < 0.05$ compared to WT.

showed greater basal levels of NO when compared to eNOS ko mice and expressed higher levels of NO when compared to WT mice (Figure 2.8B). These results are consistent with previously reported findings from isolated S1176D ki mouse lung endothelial cells, which showed greater basal production of NO compared to wild-type mice**.** Additionally, earlier vascular reactivity studies in S1176D transgenic mice showed increased relaxation in response to stimulation with Acetylcholine compared to WT mice [64]. Here, these data extend our findings by demonstrating that baseline levels of NO in the myocardium can be regulated by constitutive activation of eNOS activity.

2.8.2. In Vivo Tolerance to Reperfusion Injury

Postconditioning and S1176D mice show increased tolerance against IR injury in vivo.

To determine whether myocardial postconditioning is conserved with increased constitutive eNOS phosphorylation, we examined the response to myocardial IR injury in S1176D ki mice. Previous studies in eNOS ko mice have shown that the absence of eNOS exacerbates murine IR infarct size [68] while increased expression of eNOS in transgenic eNOS mice improves tolerance against IR injury [69]. WT, S1176D ki and eNOS ko mice were subjected to ligation of the left anterior descending (LAD) artery for 45 minutes, followed by traditional reperfusion by reopening of the ligation (MIR) or postconditioning (MIPc, 6 cycles of

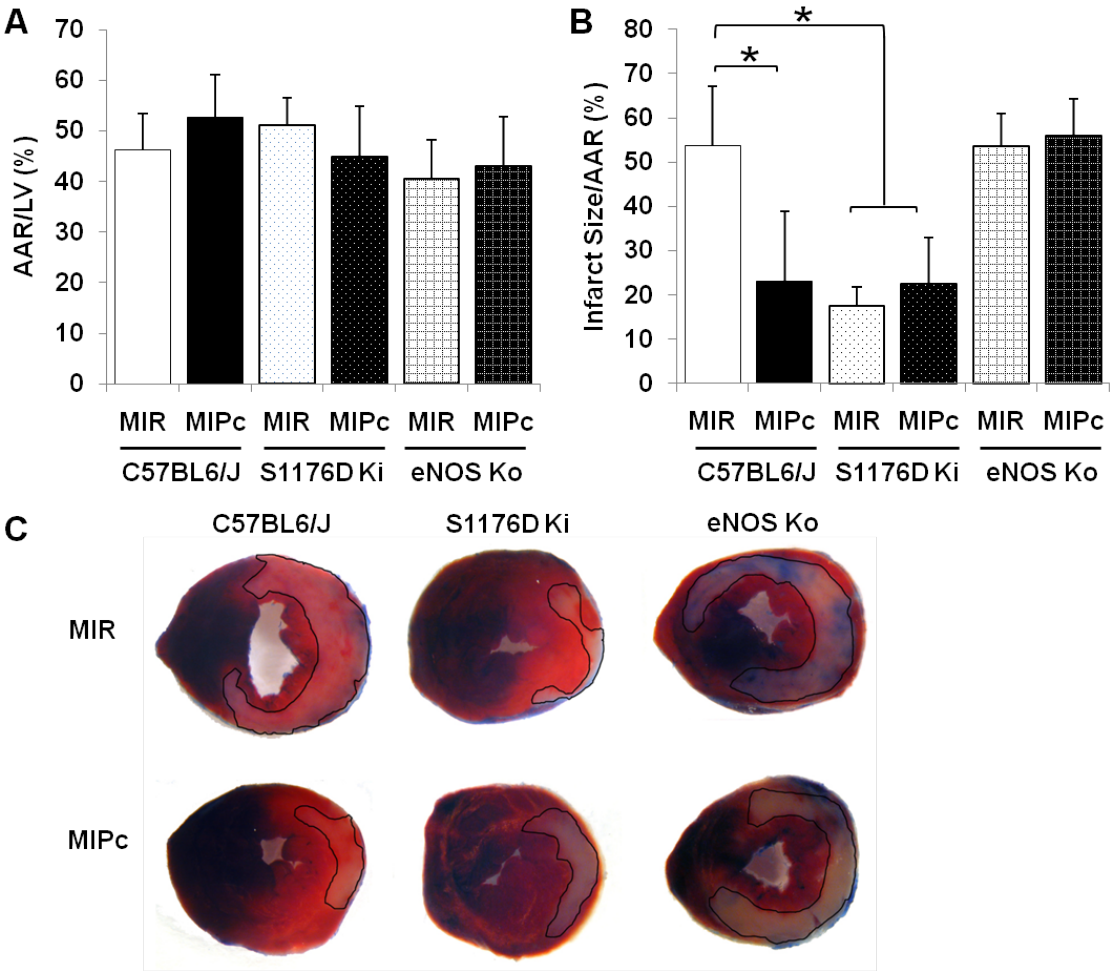

2.9 eNOS S1176 phosphorylation protects against IR injury in vivo. WT, S1176D and eNOS ko mice were subjected to myocardial IR injury (45 minutes ischemia) using a left anterior descending artery ligation model followed by (24 hours) traditional reperfusion (MIR) or postconditioned reperfusion (MIPc: 6 cycles of 10sec reperfusion, 10 sec ischemia). (A) Percentage of left ventricle area at risk, (P = NS). (B) Quantitative analysis of infarct size over area at risk, * $P < 0.05$ compared to WT control. Cardioprotection was activated in S1176D hearts and lost in eNOS ko mice. (C) Representative heart sections perfused with 1% Evans blue and stained with 2% TTC, infarct areas are outlined in black. MIR: Myocardial ischemia with reperfusion, MIPc: Myocardial ischemia with postconditioning, AAR: Area at Risk, LV: Left Ventricle. n = 6 - 9 mice per group. Data are expressed as the mean ± SD.

10 sec reperfusion followed by 10 sec ischemia). The area at risk determined 24 hours after IR was not significantly different across groups (Figure 2.9A). WT mice subjected to postconditioning developed smaller infarct sizes (ratio of infarct size/area at risk) compared to mice subjected to IR. However, when eNOS ko and S1176D ki mice were subjected to myocardial IR injury the effects of postconditioning on infarct size displayed marked differences. Postconditioning was effectively abolished in eNOS ko mice with no reduction in infarct size (Figure 2.9B).

In contrast, S1176D ki mice displayed cardioprotective infarct sparing effects in both the traditional and postconditioned groups with reductions in infarct size comparable to those in postconditioned WT mice. The IR data from S1176D ki mice show that eNOS activity significantly reduces infarct size, regardless of reperfusion technique. These results suggest that S1176D mice subjected to myocardial IR injury are conferred protection against IR injury, even in the absence of protective postconditioning (MIPc) therapy. Representative infarct slices with the infarct zones outlined are shown in Figure 2.9C.

2.8.3. Activation of Cardioprotective Pathways

Cardioprotection by activation of the Akt-eNOS pathway.

To explore the effect of eNOS modulation on the regulation of known cardioprotective signaling pathways, we investigated the expression levels of phospho-AKT and phospho-eNOS in response to IR injury. Western blot analysis

confirmed that phospho-Akt (p-ser473) and phospho-eNOS (p-Ser1176) protein levels increased in postconditioned WT mice (Figure 2.10A and 2.10B). Of interest, phospho-Akt protein levels were also increased in postconditioned eNOS ko mice, though this increase in expression did not result in increased tolerance against infarct size. While postconditioning has been shown to protect the myocardium through PI3K-Akt activation and phosphorylation of eNOS [70, 71] we were interested its effects on Akt in S1176D ki mice. Compared with WT and eNOS ko mice, MIPc did not cause significant changes in phospho-Akt activity in S1176D ki mice.

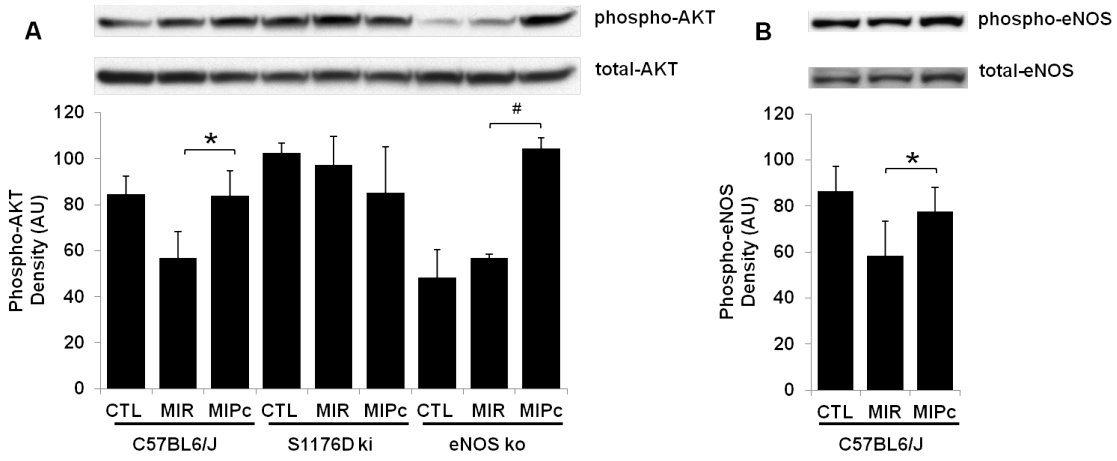

2.10 Postconditioning activates Akt and eNOS. (A and B) Representative Western blots demonstrating phosphorylated and total protein levels of Akt (Ser473) and eNOS (Ser1176) . Densities (in arbitrary units, AU) show that postconditioning phosphorylates Akt in WT and eNOS ko mice. Phosphorylated levels of Akt in S1176D mice are not affected by cardioprotective postconditioning. n = 5 per group. Data are expressed as the mean ± SD. * $P < 0.05$

2.9. Discussion

eNOS activity has been implicated in a wide range of cardioprotective signaling pathways including pre and postconditioning [72-74], halogenated anesthetics [53], hydrogen sulfide [52] and statin [51, 75] therapies. In particular, eNOS S^{1176} can be phosphorylated by various kinases including Akt, AMP and protein kinase A and G, suggesting that S^{1176} phosphorylation may be a common integration point for multiple pro-survival signaling systems. In this chapter, we show that phosphomimetic modulation of eNOS S^{1176} confers protection against IR injury. The introduction of aspartate at the S^{1176} eNOS location mimics a gain-of-function alteration which is associated with greater NO production due to increased electron flux through the eNOS reductase domain [28]. We confirm that basal levels of myocardial NO can be regulated by the degree of eNOS activity. The S1176D ki mouse model provides a valuable tool for exploring the therapeutic benefits of eNOS phosphorylation activity in protecting against IR injury.

Using S1176D ki mice, we demonstrate that activated eNOS imparts profound tolerance against IR injury *in vivo.* It is notable that the reduction in infarct size in S1176D mice is comparable to that observed in postconditioned WT mice. Remarkably, when S1176D mouse hearts were challenged with IR we observed similar levels of protection regardless of the reperfusion method used. NO has been shown to mediate the inhibition of the mitochondrial permeability transition pore which has been strongly implicated in the progression of myocardial apoptosis

resulting from IR injury [37, 76, 77]. The present data provide substantial support for the conclusion that increased eNOS phosphorylation protects the myocardium against IR injury.

Previous studies have reported that postconditioning protects the myocardium through activation of the reperfusion injury salvage kinase (RISK) [78] and survivor activating factor (SAFE) pathways [79]. The RISK and SAFE pathways both phosphorylate eNOS at S^{1176} and are heavily implicated in ischemic postconditioning [80]. Western blot data confirmed that phospho-eNOS and phospho-Akt activity are upregulated with postconditioning. Interestingly, phospho-Akt activity is increased in eNOS ko mice although the infarct sparing effects of postconditioning are lost. This is in contrast to S1176D mice where phospho-Akt activity is left relatively unchanged in the presence of constitutively phosphorylated eNOS. These results support the hypothesis that postconditioned protection against IR is induced directly through the phosphorylation state of eNOS.

2.10. Materials and Methods

Animals
Knock-in mice carrying a S1176D (serine for aspartate) mutation in the endogenous eNOS locus were generated by homologous recombination. The TCT codon for Serine^{1176} in exon 26 of the native eNOS gene was replaced with GAT to produce a S1176D (aspartate) mutation. The targeting construct carrying this mutation in exon 26 was flanked by homologous regions on either side. A neomycin resistance gene flanked by loxP sites adjacent to the mutation allowed for positive selection. A thymidine kinase gene was incorporated at one end of the construct to facilitate negative selection, but was not incorporated into the final genome. The surrounding region of exon 26 was replaced with the mutated exon through homologous recombination. Mice were mated with EIIa-Cre transgenic mice resulting in excision of the neomycin resistance gene. Back-bred S1176D mice were compared with eNOS-deficient mice and C57BL6/J mice as controls.

Nitric Oxide Assay
The extent of baseline nitric oxide production in myocardial tissue was assessed using the commercially available flurometric assay kit in accordance with the protocol supplied by the manufacturer (BioVision). The total concentration of nitrite and nitrate was used as a quantitative measure of NO production. Tissue samples were lysed for 10 minutes on ice with 300µl of tissue-lysis buffer. Tissue homogenates were centrifuged at 10,000g for 5 minutes at 4^{o}C and further filtered through a 10kDa MW cut-off filter (BioVision) the filtrate was collected for the NO assay.

In vivo Myocardial Ischemia Reperfusion Model
Animals were anesthetized under pentobarbital sodium (50 mg/kg ip) and ketamine hydrochloride (50 mg/kg ip) anesthesia was maintained via supplemental doses (15 mg/kg ip) as needed. The depth of the anesthesia was monitored by tail pinch, constant monitoring of respiratory rate and heart rate. Mice were intubated with polyethylene 90 tubing (CWE) and connected to a Harvard respirator (Harvard Apparatus). The respiratory tidal volume was set at 1.0ml/min, and the rate was set at 120 strokes/min and supplemented with 100% oxygen. Mouse left anterior descending coronary artery ligation was performed under through a thoracotomy performed left of the sternum to expose the pericardium. The pericardium was then visualized and opened and the left anterior descending coronary artery identified under stereo microscopy. A 7-0 silk ligature was passed underneath the vessel and through a custom snare to induce ischemia without damaging the artery. Ischemia was achieved by tightening the snare for 45 minutes and occlusion was confirmed by observed blanching of the anterior left ventricular wall. After 45 minutes the

myocardium was reperfused with one of two algorithms 1) traditional myocardial ischemia-reperfusion (MIR) injury where the ligation was simply released or, 2) myocardial ischemia reperfusion with postconditioning (MIPc) where six cycles of 10 sec reperfusion was followed by 10 sec of ischemia. After initiation of reperfusion, the chest cavity was then closed layer by layer. Buprenorphine HCl (0.05–0.1 mg/kg) was administered for post-operative care. The mice were monitored continuously for 6 h, then every 8 h and were treated according to IACUC guidelines if they appeared dyspneic or moribund.

Infarct Size Determination

At conclusion of the 24 hour reperfusion period, the LAD was religated with 7-0 silk suture, and 1ml of 1% Evans blue (Sigma-Aldrich) was perfused retrograde through a left carotid artery catheter the delineate the *in vivo* area at risk (AAR). The heart was excised and fixed in a 2% solution of agarose gel and allowed to solidify. Myocardial tissue was sectioned into 1-mm-thick axial sections using a McIlwain tissue chopper (Brinkmann Instruments). Infarct size was determined by staining with 2,3,5-triphenyltetrazolium chloride (TTC) (Sigma-Aldrich). and stained with 2% TTC for 20 minutes in the dark at 37^{o} C. Each sliced was weighted and visualized under a dissecting microscope equipped with a CCD video camera. The left ventricular area, AAR, and area of infarction for each slice were then determined by computer planimetry software. The final size of infarction was determined by integrating the infarct areas in each myocardial slice over the entire myocardium using a previously described equation [68].

Western Blot Analysis

Myocardial tissues were harvested after 45 min ischemia and 10 min reperfusion. The left ventricular area at risk was isolated through visual identification of blanched myocardium during ischemia. Myocardial tissues were homogenized to obtain protein extracts and 100μg of protein was subjected to electrophoresis in 7% Tris-HCL polyacrylamide gels (Invitrogen). Proteins were transferred to PDVF membranes for western blot analysis and visualized by chemiluminescence (Amersham Biosciences) as previously described [64]. Antibodies to eNOS (Sigma-Aldrich), phospho-eNOS (p-Ser1177 human sequence numbering, BD Bioscience), AKT (Cell Signaling) and phosphor-AKT (p-Ser473, Cell Signaling) were obtained commercially.

Statistics

All results are expressed as mean ± SD, except western blot densities which are expressed as mean ± SEM. Statistical analysis was performed in Matlab (Mathworks) using Kriskal-Wallis analysis of variance and Wilcoxon rank-sum tests with Bonferonni's correction. Differences of $P < 0.05$ were considered significant.

Study Approval

All experiments were conducted in accordance with the guidelines of the Institutional Animal Care and Use Committee (IACUC) of the Massachusetts General Hospital. Mice were euthanized according to the recommendations of the American Veterinary Medical Association Panel on Euthanasia.

Chapter 3

In Vivo Quantification of Myocardial Blood Flow and No-Reflow Phenomena

Endothelial dysfunction and no-reflow phenomenon can present as clinical complications after reperfusion. The degree of no-reflow in a patient has important prognostic value and is an independent predictive factor of patient prognosis and clinical outcome [81, 82]. While experimental studies have established that pathologic myocardial blood flow deficits are propagated at the onset of reperfusion, the role of eNOS phosphorylation in targeting specific mediators of myocardial blood flow and no-reflow phenomena remains unknown.

The ability to measure myocardial blood flow over the dynamic time course of recovery in vivo would be scientifically valuable but existing methods are impractical and limited in application by the small size of murine models. In this

chapter we describe two different imaging modalities, Laser Doppler Flowmetry and Myocardial Contrast Echocardiography (MCE), and evaluate their application in measuring myocardial blood flow and no-reflow phenomena throughout the course of IR injury. We then apply MCE to our genetic mouse models of eNOS to investigate the role of phosphomimetic eNOS modulation on myocardial blood flow.

3.1. Motivation

In the first part of this chapter we evaluate the effectiveness Laser Doppler flowmetry to measure myocardial blood flow. We outline the spatial limitations of laser Doppler and its inability to differentiate between core ischemic and prenumbral areas of the ischemic myocardium. Next, we describe the use of myocardial contrast echocardiography (MCE). MCE provides improved spatial resolution with the same ability to measure blood flow over time but motion of the myocardium during capture is problematic for analysis. In order to accurately identify the myocardium and track its location over time, we propose the use of an active contour image segmentation model guided by external gradient vector flow forces. Our image segmentation algorithm automates the characterization of myocardial blood flow and is capable of generating MCE replenishment curves for the purposes of analyzing myocardial blood flow.

In the second half of this chapter, we use MCE to study the effects of postconditioning on myocardial blood flow. Decreased vascular NO production

results in the clinical manifestation of endothelial dysfunction, vascular wall inflammation and no-reflow phenomenon [83-86]. We extend our MCE studies to S1176D knock-in mice models and demonstrate the effectiveness of phosphomimetic eNOS modulation in improving blood flow following ischemia-reperfusion injury. Using the S1176D knock-in mouse model, we determine the effects of 'activated' eNOS on myocardial blood flow using myocardial contract echocardiography (MCE). Our results demonstrate that enhanced eNOS enzymatic activity protects improves blood flow after myocardial IR. These results reveal the importance of *in vivo* post-translational modification of eNOS in myocardial ischemic protection.

3.2. No-reflow Phenomenon

The no-reflow phenomenon was first described by Kloner et al in 1974 when they reported reductions in blood flow in the infarct zone despite restoration of coronary arterial flow to the ischemic myocardium [87]. At least two mechanisms have been identified to cause no-reflow in the coronary vasculature: micro emboli formation and capillary dysfunction [15]. In the former, micro emboli likely originate from the disruption of lipid rich vulnerable plaques when thrombolytic or percutaneous coronary intervention (PCI) is used to reestablish coronary blood flow. Improved PCI methods that utilize aspiration or thrombectomy have helped to minimize no-reflow lesions caused by micro emboli [88].

The later cause of no-reflow however, can be attributed to the detrimental repercussions of reperfusion itself. Capillary dysfunction due to tissue edema, endothelial disruption and plugging of the capillaries by neutrophil infiltration can be caused factors which are all promoted by coronary reperfusion. The generation of reactive oxygen species, hyper contracture of adjacent myocytes and activation of the mitochondrial permeability transition all contribute in part, to the development of the no-reflow phenomenon [89].

Current treatments for the no-reflow phenomenon include the use of vasodilators. The use of adenosine yields benefits beyond vasodilation by lowering neutrophil count and improving endothelial integrity [90]. While there is diminished basal NO release after reperfusion which promotes neutrophil adherence to the coronary endothelium [91], the use of nitric oxide donors has been shown to reduce myocardial necrosis and neutrophil accumulation [92, 93]. In this chapter we investigate the role of eNOS phosphorylation on no-reflow phenomenon with the use of S1176D knock-in mice to test whether the increased bioavailability of NO improves no-reflow after reperfusion.

3.3. Laser Doppler Flowmetry

In order the study the role of reperfusion on vascular function we developed a method to measure tissue perfusion in the murine heart using Laser Doppler Flowmetry. The application of Laser Doppler imaging to measure tissue perfusion has been previously demonstrated in skin, renal, skeletal muscle and cerebrovascular studies [94-96] but its application in the murine myocardium, which is subjected to significant motion, has not been investigated.

Laser Doppler flowmetry provides information about blood flow by registering the Doppler shift in frequency of reflected monochromatic laser light [97]. In the past, LDF has been applied to static tissues not subjected to the same motion artifacts as the heart. In our hands, we provide evidence that laser Doppler flowmetry can be used for continuous real-time measurement of local myocardial perfusion in the beating murine heart [98]. To assess myocardial micro perfusion a laser Doppler fiber optic probe was attached to the myocardial surface on the left ventricular myocardium lying in proximity to the LAD and away from obvious large vessels using tissue glue. Attachment to the surface of the myocardium resulted in a free floating fiber optic probe which moved in unison with the beating heart (Figure 3.1). Due to the flexibility of the optical fiber, we were able to acquire tissue perfusion measurements virtually free of motion artifacts [99].

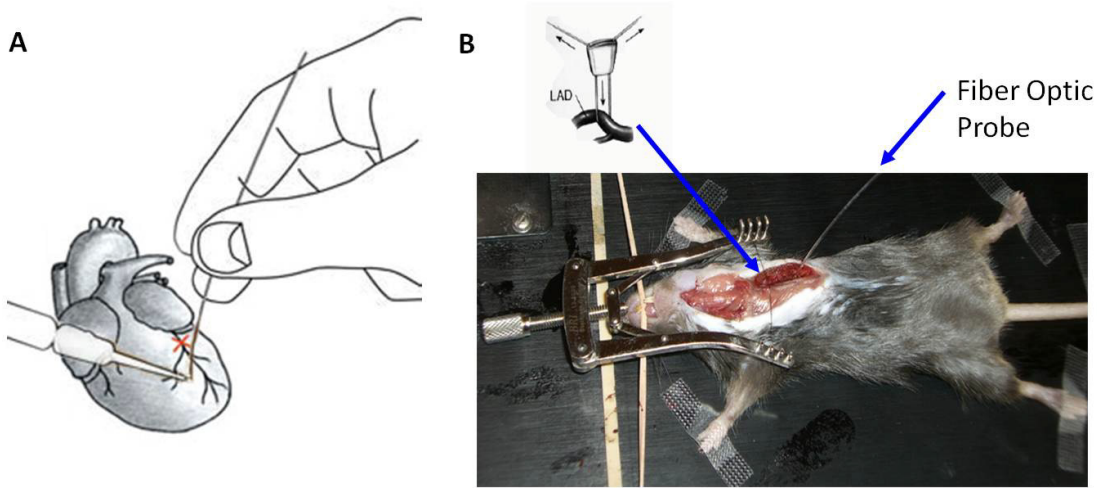

3.1 Implementation of Laser Doppler Flowmetry on the murine myocardium. A) Schematic of fiber optic probe attachment. The laser Doppler probe is secured with tissue glue to the anterior epicardial surface. The location of the probe is place distal from the point of ligation to confirm changes in blood flow post ligation. B) Implementation of the ligation snare and fiber optic probe.

In order to quantify vascular function and tissue perfusion following ischemia, we applied LDF to the epicardial surface of the left ventricle, distal from the location of LAD occlusion. Figure 3.2 depicts LDF measurements of myocardial blood flow after an ischemic event in mice undergoing distal LAD occlusion followed by abrupt reperfusion or postconditioned reperfusion. This data demonstrates the ability to quantitatively measure the degree of tissue perfusion *in vivo*. The top panel depicts a drop in tissue perfusion at the onset of ischemia followed by abrupt reperfusion of the myocardium after 45 minutes of occlusion. LDF also captures the hemodynamic profile of postconditioned reperfusion which is depicted in the bottom panel, showing the 'staccato' occlusion/reperfusion cycles indicative of postconditioning.

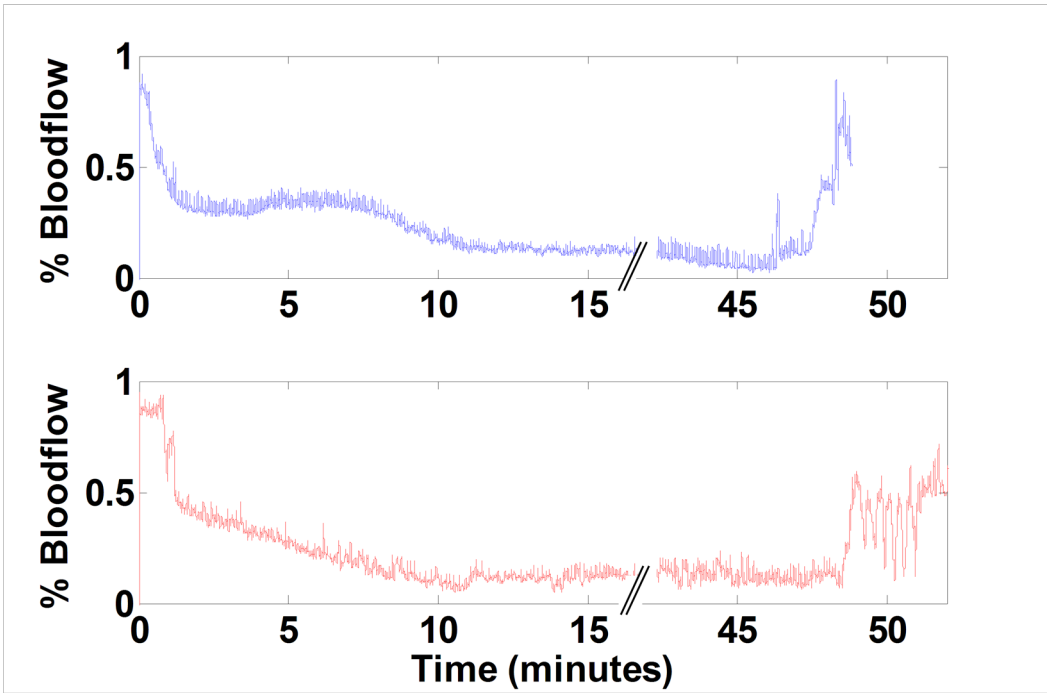

3.2 Blood flow profile measured with Laser Doppler Flowmetry. Myocardial blood flow measurements for traditional reperfusion (top) and postconditioned reperfusion with 6 cycles of 10sec each (bottom). The anterior myocardium was subjected to 45 minutes ischemia followed by reperfusion.

However, we found that fidelity of the LDF signal depends critically on the placement of the fiber optic probe. Placement of the probe in the core ischemic region versus the non-ischemic prenumbra is often difficult and thus, we conclude that LDF has limited application when comes to quantifying the degree of myocardial blood flow deficit in IR injury. With this understanding we explored the use of MCE and its ability to provide added spatial information.

3.4. Dynamic Imaging of Blood Flow: Myocardial Contrast Echocardiography

Myocardial Contrast Echocardiography (MCE) is an ultrasound imaging tool used for the assessment of myocardial blood flow. Blood itself is not a good reflector of ultrasound but the microcirculation of the myocardium can be measured through infusion of echo-opaque microbubbles into the blood stream. These microbubbles average 1 – 3 μm in diameter and are small enough to pass through pulmonary capillaries and the myocardial microvascular bed. Upon sonication the microbubbles oscillate with predictive characteristics generating a measurable acoustic response [100, 101]. The infusion of microbubbles is useful in applications where added contrast and visualization of the myocardial vascular bed is desired. The venous administration of microbubbles has been shown to result in successful myocardial opacification [102-104] and is helpful in identifying regional perfusion deficits [105].

Circulating microbubbles in the blood provides increased backscatter signaling and additional enhancement of the myocardial border. Figure 3.3 illustrates the improved contrast provided during parasternal long-axis imaging of the heart comparing MCE versus normal echocardiographic imaging in mice (a thoracotomy has been performed to minimize shadowing effects from chest wall.) Use of contrast microbubbles ensures that the endocardial border between the ventricular lumen and myocardium is easy to identify. It is important to note

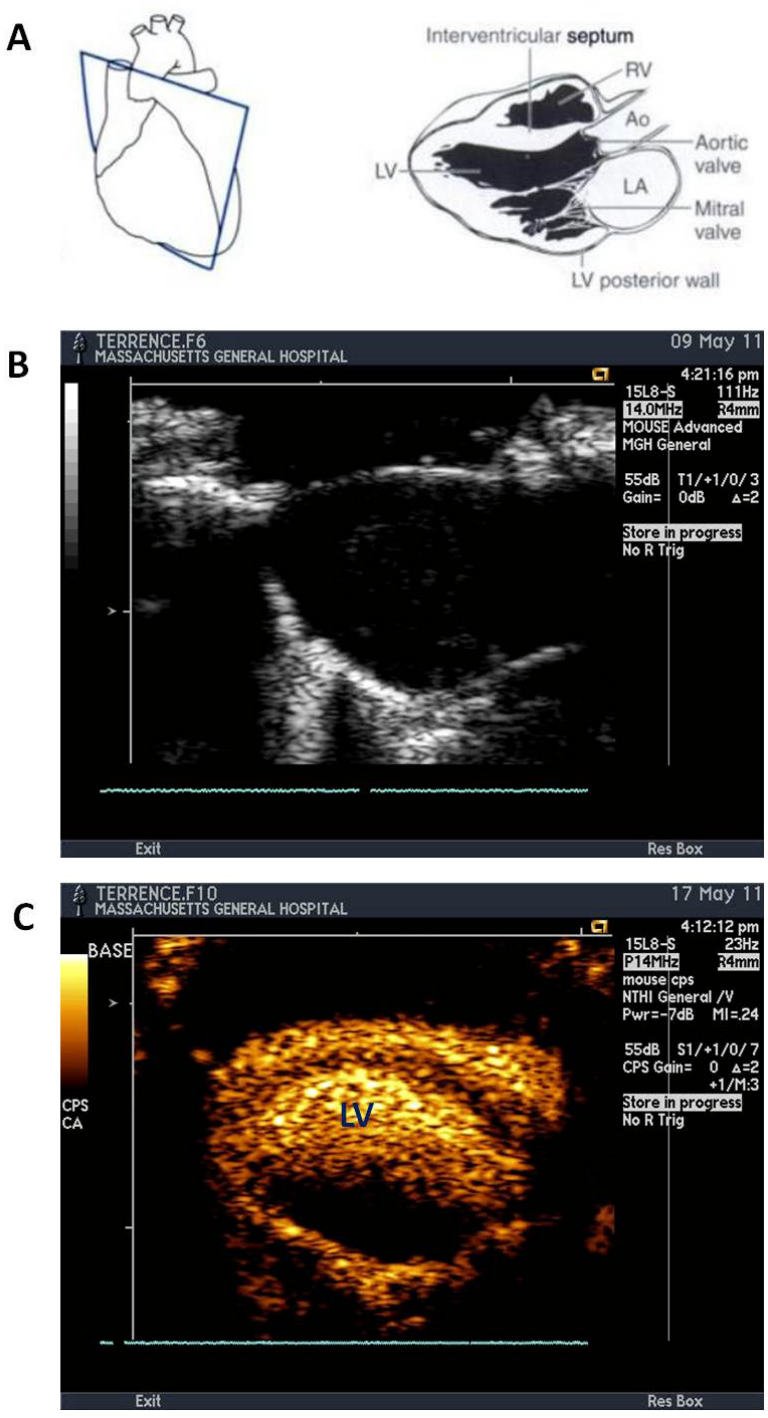

3.3 Myocardial Contrast Echocardiography. A) Schematic of parasternal long axis (PSLA) view of the myocardium, adapted from Lilly, 4th Edition, 2007 [106]. B) Normal PSLA echocardiographic view. C) Enhanced PSLA view with myocardial contrast echocardiography, the left ventricular lumen is labeled LV.

however that contrast agents can cause imaging artifacts that manifest as shadowing of the posterior septum, this makes it difficult to accurately perform MCE analysis in the posterior region. In our study, analysis of myocardial blood flow is thus restricted to the anterior septal region.

Because harmonic vibration signals emanate mostly from the microbubbles rather than tissue, selective reception of these signals provides an increased signal-to-noise ratio, and opacification of myocardial tissue [100]. 'Second generation' high molecular weight gas filled microbubbles were used instead of air-filled microbubbles because the highly diffusible oxygen and nitrogen from air can leak out and dissolve into the blood. Our second generation microbubbles are made of Perflutren lipid microspheres (Definity, Lantheus imaging, Billerica, MA) composed of octafluropropane gas encapsulated in an outer lipid shell. Definity microbubbles are characterized by low solubility and high stability in the blood. Octafluoropropane (empirical formula of C_3F_8) has a molecular weight of 188. Heavy gases are less soluble in blood and thus less likely to leak out of the microbubble to impair echogenicity. The high molecular weight of Definity microspheres means that the microbubbles generate high echogenicity without large fluctuations in size. It is important for bubble size to remain constant because the backscatter of a bubble is related to the sixth power of its radius [107].

While contrast enhanced ultrasound provides a useful tool for visualization of the endocardial border its ability to quantify myocardial blood flow is particularly

valuable in our studies of IR injury. MCE measurement of myocardial blood flow is centered on the ability of ultrasound to induce microbubble destruction and subsequent characterization of the rate of microbubble return. When microbubbles are subjected to high intensity ultrasound, destruction of microbubbles occurs causing the gas to escape, eliminating their echo-opaque properties. Microbubble destruction is dependent on the power output, ultrasound frequency and the duration of imaging. As the acoustic power of the ultrasound beam is increased, the microspheres move from a linear resonance response to a nonlinear harmonic oscillation response. At a critical threshold of power, fracture and destruction of the microbubbles occurs releasing the inert high molecular weight gas into the blood for clearance [101]. More destruction occurs at lower transducer frequency, higher power output and increased imaging duration. Sonic cracking of microbubbles caused by high intensity ultrasound is shown in figure 3.4 below, when gas is released from the confines of the microbubble echo opacity is lost.

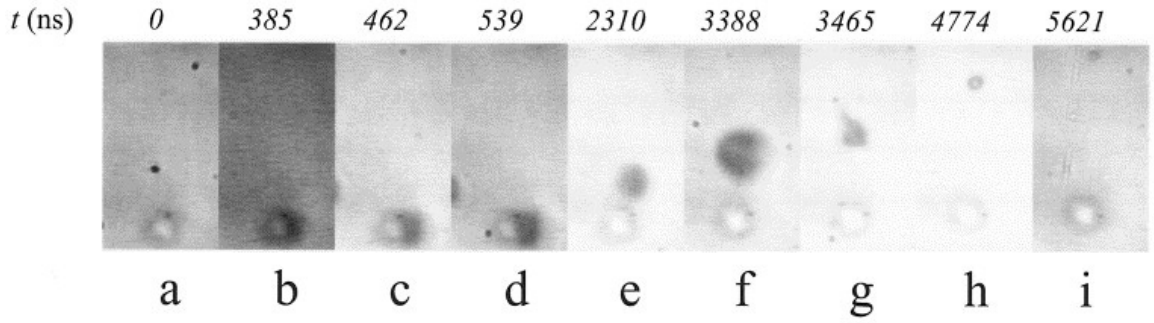

3.4 Sonic cracking of a contrast microbubble. (a-d) Sonic cracking of a 4μm contrast bubble. (e-i) The gas is released from the perforated microbubble, reproduced from Postema et al. [100].

Previous studies by Wei et al. have demonstrated that measurement of the rate of microbubble reappearance after microbubble destruction provides a measure of myocardial blood flow [108]. Measurement of microbubble flow rate to estimate blood flow velocity is supported by findings from Jayaweera et al who reported a correlation between microbubble flow velocity and the mean transit rate of radio labeled red blood cells in dogs [109]. Another study conducted by Keller et al, working with hamsters, found that sonicated albumin microbubbles within the microcirculation accurately mimics red blood cell flow in the myocardium [110]. This concept is illustrated in figure 3.5 where a high energy ultrasound pulse has been applied to eliminate all microbubbles within the field of view. Once the microbubbles have been successfully destroyed the rate of microbubble replenishment within the ultrasound provides a measure of the microbubble velocity.

In order to quantify myocardial blood flow two parameters are measured. First, upon destruction, measurement of the microbubble reappearance rate provides an estimation of the mean myocardial microbubble velocity. Second, the microbubble concentration (and subsequent ultrasound intensity) measured in the myocardium at steady state reflects the sum of the microbubbles in the myocardial cross-sectional area [108]. Together, myocardial blood flow can be calculated with knowledge of the mean myocardial microbubble velocity (ie. the rise parameter), β,

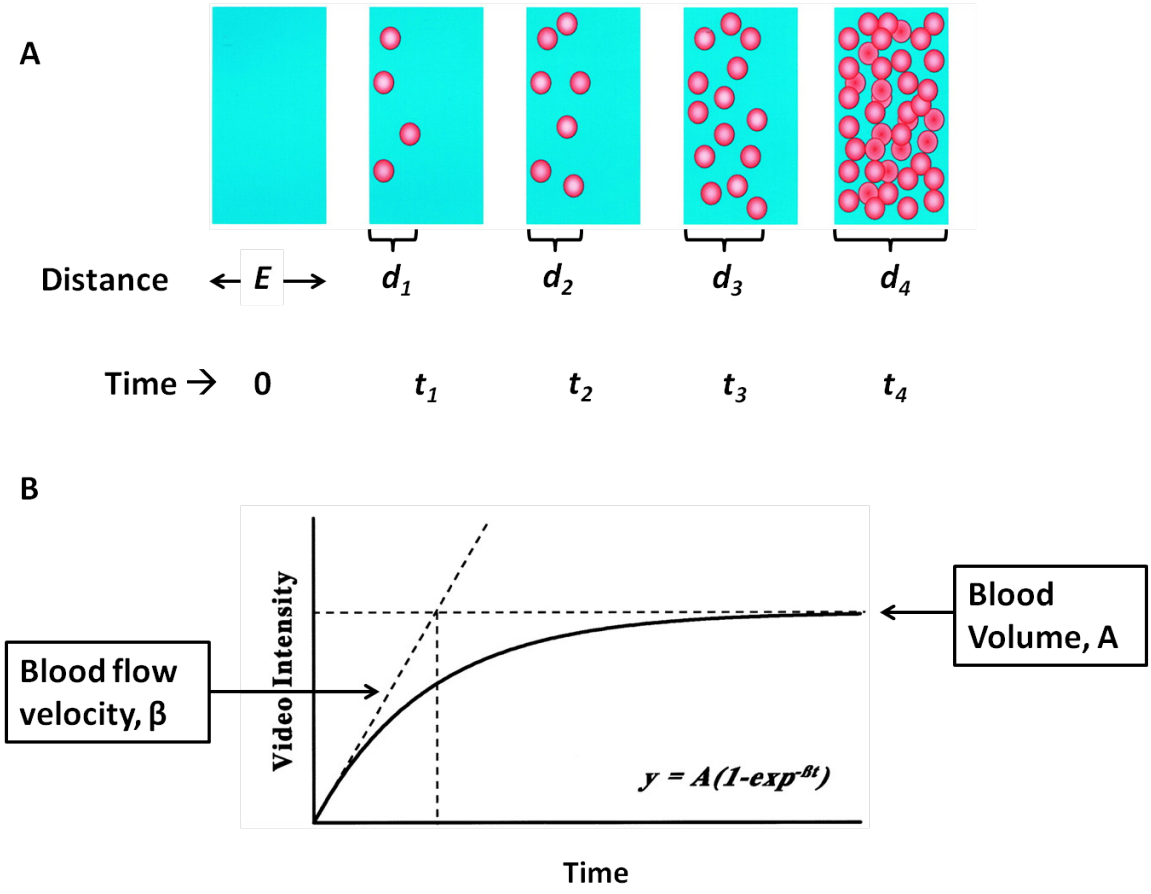

3.5 Method of quantifying mean myocardial blood flow. A) All microbubbles can be destroyed by a pulse of ultrasound at time t_0. The thickness, E of the ultrasound beam causes destruction of all bubbles within that region. Then replenishment of microbubbles within that window can be measured (d_1 through d_4 with respect to time t_1 to t_4). B) The corresponding replenishment curve can be fitted to the inset equation and characterized by two parameters, blood flow velocity (β) and the plateau blood volume, A. Adapted from Wei et al. [108].

and the myocardial microvascular cross-sectional area at steady state (ie. the plateau intensity), A. Using these principles in experiments with dogs with two-dimensional echocardiography, Kaul et al concluded that measurement of the velocity of microbubbles through the myocardium accurately reflects myocardial

blood flow [111]. Thus, MCE provides the unique ability to assess regional deficits in myocardial perfusion in vivo.

Our study focuses on applying MCE to measure myocardial blood flow in a murine model of myocardial ischemia-reperfusion injury. Previous work on MCE in mice has been conducted by Scherrer-Crosbie et al [112] and Raher et al [113]. Implementation of MCE in smaller mice models has a significant number of challenges including the need for smaller ultrasound transducers and the need to obtain and analyze replenishment curves from mice with fast heart rates in the range of 400-600 beats per minute. The fast heart rate limits the application of gated signal acquisition to EKG recordings because the acquisition frame rate of the ultrasound system (at 30 Hz) would omit important microbubble information during the replenishment phase. Video acquisition without EKG gating introduces significant myocardial motion into the MCE video frame. Consequently, analysis of murine MCE videos would be greatly aided by a robust image segmentation algorithm capable of identifying the endocardial and epicardial borders and able to generate accurate replenishment curves despite significant motion of the myocardium.

To aid in the quantification of myocardial blood flow from murine MCE videos we developed an image segmentation algorithm that utilizes active contours to detect and separate the myocardium from a contrast-enhanced ultrasound image.

3.5. Active Contours for Image Segmentation

Problem Objective

Identification of the left-ventricular border from contrast-enhanced echocardiograms is essential for accurate quantification of myocardial blood flow. However, contrast replenishment curves must be obtained from MCE videos that contain motion artifacts caused by the periodic motion of respiratory and myocardial movement as well as external user produced motion through manipulation of the ultrasound transducer. In this setting, manual identification of the ventricular border can be slow and tedious and often susceptible to intra-observer variability. Typical analysis requires manual identification and consistent segmentation across hundreds of video frames (300 frames in each MCE video). Therefore, in order to generate a reproducible replenishment curve, automated segmentation of the endocardial border is desirable to ensure consistency and limit the practical workflow. In this section, we present a tissue tracking algorithm that utilizes active contours to identify the left ventricle in videos obtained from MCE.

Our attempt to automate detection of the left ventricle focuses on replicating human user based identification of edges. We are tasked with developing an image segmentation algorithm for a time series of two-dimensional echocardiographic images. Analysis of MCE videos for the purposes of generating microbubble replenishment curves requires that we first identify the myocardial borders and then track the course of its movement over time. Our tissue tracking algorithm takes

advantage of the enhanced ventricular borders provided by constant infusion of Definity contrast agent. The epicardium and endocardium form the upper and lower boundaries of the left ventricle in the parasternal long axis view. The endocardial border is the curved boundary which separates the ventricular lumen from the inner myocardial surface while the epicardial border separates the outer surface of the myocardium from the pericardium and thoracic cavity. Together, the endocardial and epicardial borders define the ventricular tissue of interest.

The endocardial border represents a promising geometric feature for image segmentation given the high degree of contrast between the two adjacent mediums [114, 115]. The high concentration of contrast agent in the ventricular lumen forms a distinct gradient boundary that we can utilize in the development of our active contours algorithm. Epicardial border detection is considerably more difficult because there is less differentiation in contrast between the epicardial surface and thoracic cavity. Detection of the epicardial border can be assisted by first identifying the endocardial border and then defining a typical distance between the endocardial and epicardial border.

In summary, the resulting algorithm must be capable of wall motion tracking, account for the cardiac cycle (in the absence of EKG gating), background respirator movement and finally generate microbubble replenishment curves from the segmented myocardium. We employ a semi-automatic active contour model for detection of the endocardial border. Active contours represent a special case of

general techniques that match a deformable spline to an image by means of energy minimization. The spline is influenced by constraining conditions and image forces that pull it towards object contours in an iterative fashion. To initiate border detection, an initial guess of the myocardial apex is placed on the image interactively by the user. The surface is then optimized or deformed to a new position in an iterative fashion guided by images features (ie. Edges) associated with the true endocardial border.

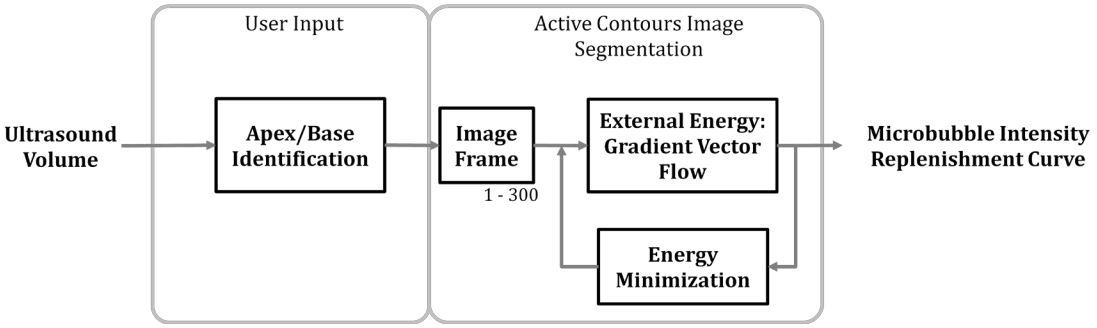

3.6 Image processing chain of myocardial contrast echocardiography image slices. Processing of contrast ultrasound video consists of user defined identification of the myocardial apex and base followed by automatic active contours segmentation of the left ventricular volume.

Active Contour Implementation

Figure 3.6 depicts the data processing chain used for detection of the left ventricle. It consists of two distinct operations: user identification of the myocardial apex and base followed by automated active contours image segmentation. Automated detection of the apex and base is hindered by acoustic interference from speckle noise and artifacts inherent in our ultrasound image, this makes consistent identification of the apex and base difficult and less reliable compared to human identification [115]. Thus, user input is required in the first operation because manual identification ensures proper location of the apex and base which is important for the generation of the initial spline. The apex of the left ventricle is the most anterior and inferior structure of the ventricular chamber while identification of the base is aided by alignment with the aortic root (in frame).

Once the apex and base have been identified, the image frame is cropped and converted to grayscale. A snake is then initialized between the apex and base to begin segmentation of the endocardial border. A snake is an energy minimizing spline guided by external constrain forces and influenced by salient features governed by the image, they are particularly apt at finding image contours such as edges, lines and terminals [116]. The snake is a curve that moves within the spatial domain of our image frame represented by,

$$\boldsymbol{x}(s) = [x(s), y(s)] \tag{3.1}$$

optimized by minimizing the energy functional,

$$E = \int_S \frac{1}{2}[\alpha|\boldsymbol{x}(s)|^2 + \beta|\boldsymbol{x}''(s)|^2] + E_{External}(\boldsymbol{x}(s))dS. \tag{3.2}$$

The energy functional is governed by internal and external energy parameters. The internal energy is composed of a first order term that acts as a membrane and second order term that acts as a thin plate, where α and β are weighting parameters that control the snake's tension and rigidity [117]. The external energy function is derived from the MCE image, $E_{External}$. Many different methods have been used to define the external force of the image, with each method taking a different approach to guide the path of the snake as it moves through an echocardiographic image.

Hommoude [115] and Noble et al [118] review many of the active contour methods applied to the field of echocardiographic image segmentation. For instance Cohen et al modify the snake by adding balloon like behavior to give more stable

results when snakes are initialized away from contours [119]. Chalana et al employ a multiple active contour model for cardiac boundary detection, pooling information from multiple frames because individual echocardiographic images can contain missing boundaries [114]. Mikic et al employ optical flow estimates [120] and Hamarneh et al applied Principal Component Analysis to a frequency-based representation of the left ventricle [121].

We employ an external force model established by Xu et al who compute the external force as a diffusion of the gradient vectors from a gray scale image, termed gradient vector flow [122]. The particular advantage of gradient vector flow derived external forces is that it is insensitive to initialization of the snake, the snake can initially be inside, outside or across an object's boundary and has a large capture range meaning that the snake can be initialized far away from the endocardial boundary. In our application, the external energy functional can be expressed as a weighted combination of several factors to attract the snake to different features in our image. The total image energy can be expressed as a weighted combination of variables,

$$E_{Image} = w_{line}E_{line} + w_{edge}E_{edge} + w_{terminal}E_{terminal} \qquad (3.3)$$

By placing emphasis on w_{edge} we preferentially force attraction of the snake to the endocardial border in our image. The edge functional ensures that the snake is attracted to contours with large image gradients

$$E_{edge} = -|\nabla I(x,y)|^2 \qquad (3.4)$$

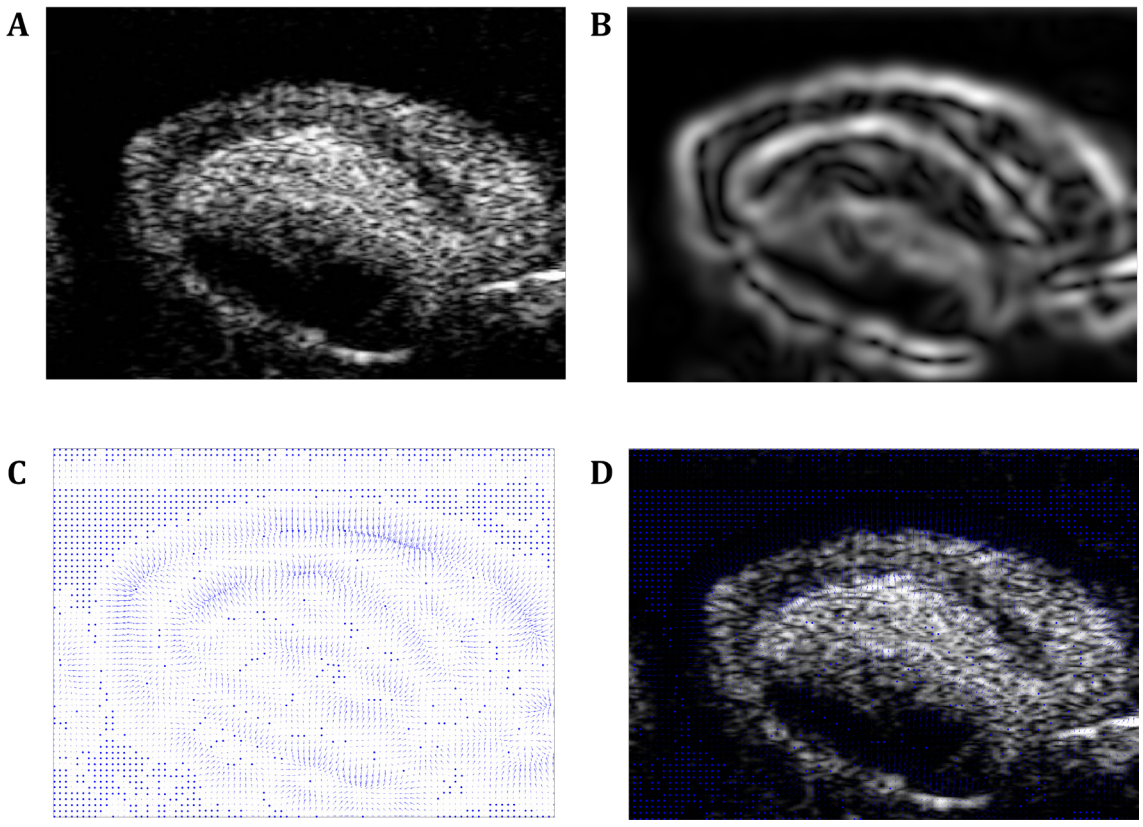

3.7 External image force. A) Greyscale image myocardial contrast echocardiography (MCE) frame. B) Edge functional computed from MCE image. C) Gradient vector flow image. D) External gradient vector flow forces superimposed on grayscale image. The gradient vectors guide the spline towards the endocardial border.

When applied to an MCE image, the endocardial and epicardial borders are made apparent in Figure 3.7B. Calculation of the external force using gradient vector flow from the initial image results in generation of an external force field. The gradient vectors that direct the snake to the endocardial boundary are visible in Figure 3.7C. Figure 3.7D shows the external force field super imposed on an MCE image. Iterative

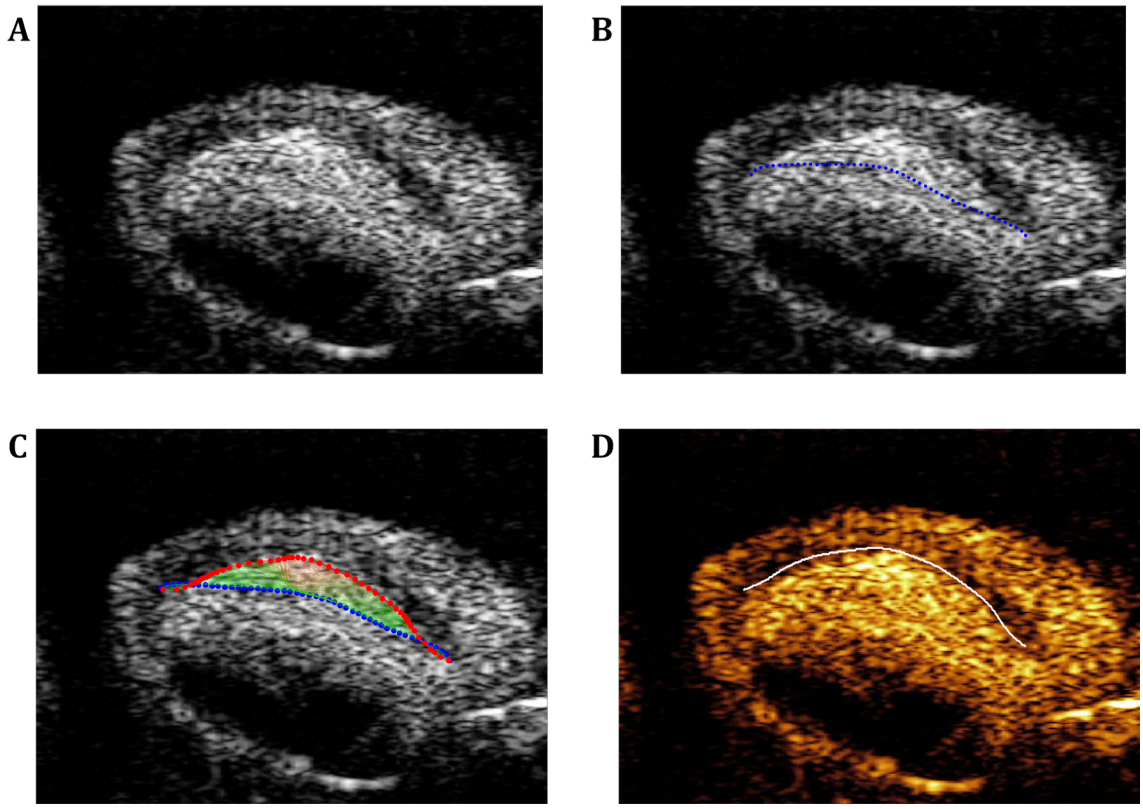

3.8 Snake movement towards endocardial border. A) Greyscale image myocardial contrast echocardiography (MCE) frame. B) User identification of the apex and base enables initialization of a spline between two points. C) Guided by the external image forces, the spline iteratively converges on the endocardial border. D) Final segmentation of the endocardial border.

movement of the snake through the external force field drives the active contour to clamp on the endocardial boundary. The movement of the snake through the MCE image is shown in Figure 3.8. Finally, the left ventricle is segmented into three distinct regions composed of the apical anteroseptum, mid anteroseptum and basal anteroseptum (Figure 3.9). Of note, ligation of the LAD occurs at the intersection of the mid and basal anteroseptum while the apical anteroseptum is distal from the

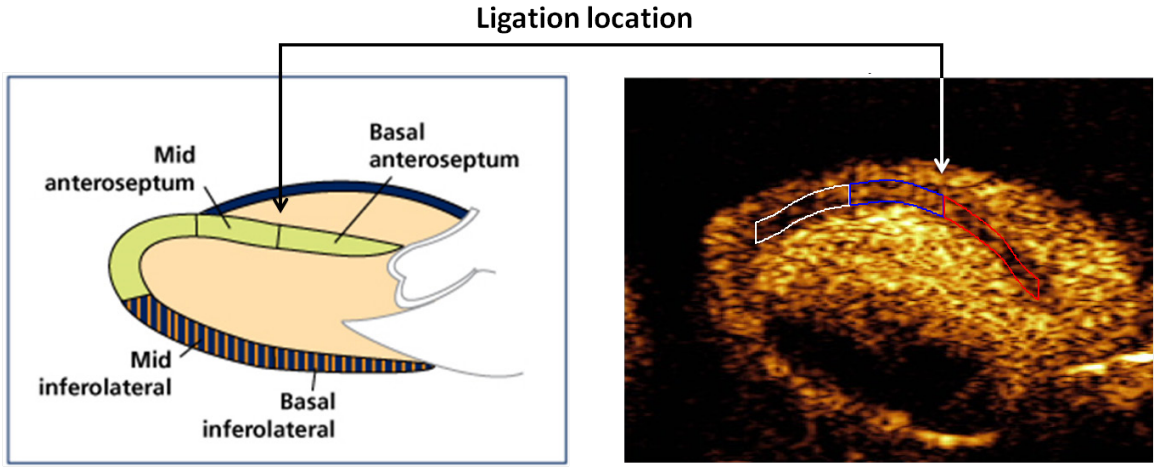

3.9 Segmentation of the left ventricle. Following identification of the endocardial and epicardial borders, the left ventricle is segmented into three regions, the: apical anteroseptum (white), mid anteroseptum (blue) and basal anteroseptum (red). The snare forms a ligation around the left anterior descending coronary artery at the location of the arrow.

ligation site and most prone to blood flow deficits during LAD ligation. Tracking of all three regions over time enables us to generate replenishment curves of the microbubbles refilling the myocardium. Evaluation of distinct regions allows us to examine whether areas furthest away from the point of ligation develop the most significant blood flow deficits.

Estimation of myocardial blood flow from each region of interest was obtained by fitting the replenishment curve to an exponential function

$$y = A(1 - e^{-\beta t}) \qquad (3.5)$$

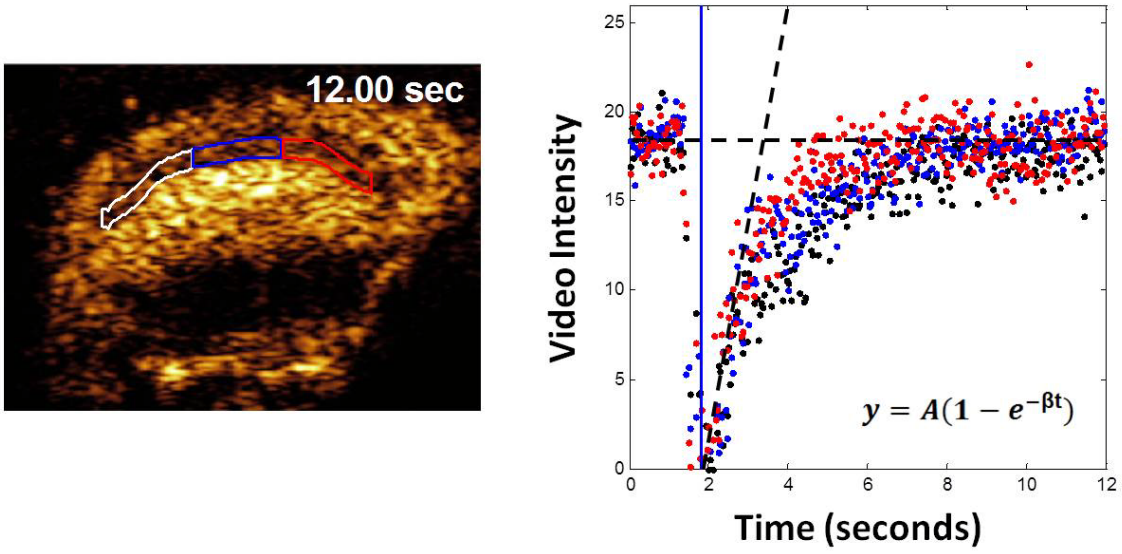

3.10 Myocardial contrast echocardiography replenishment curve. Replenishment curves (at baseline before ischemia) of the apical anteroseptum (white), mid anteroseptum (blue) and basal anteroseptum (red).

where y is the signal intensity, β is the slope of the curve and A is the plateau intensity [108, 113]. An example of replenishment curves derived from all three anteroseptal regions is shown in Figure 3.10. In this figure, MCE was applied at baseline before ligation of the LAD and all three regions have similar replenishment curves. The characteristics of these replenishment curves will be affected differently following ischemia-reperfusion injury.

3.6. Results

In this section, we use the active contours image segmentation algorithm to follow the dynamic time course of myocardial blood flow in mice subjected to IR injury. We test the hypothesis that both postconditioning and phosphomimetic eNOS modulation improves blood flow in the myocardium after reperfusion.

Improved myocardial blood flow in S1176D mice after myocardial IR injury.

eNOS is an important biological regulator of many cardiac functions including myocardial perfusion, leukocyte-endothelial cell interaction, platelet adhesion/aggregation and no-reflow phenomena. Given the central role that NO serves in regulating blood flow, we hypothesized that phosphomimetic modulation of eNOS improves myocardial perfusion after IR injury. We performed myocardial contrast echocardiography (MCE) [113, 123] on mice subjected to 45 min LAD ligation and reperfusion to assess whether improvements in myocardial blood flow could contribute to changes in infarct size.

We obtained high quality two-dimensional parasternal long-axis videos of the myocardium to assess changes in blood flow following IR injury (Figure 3.11A). MCE was performed serially over the time-course of reperfusion to provide a temporal understanding of myocardial blood flow (MBF) deficit. Ligation of the LAD produced a predominantly antero-apical myocardial area at risk (Figure 3.11B).

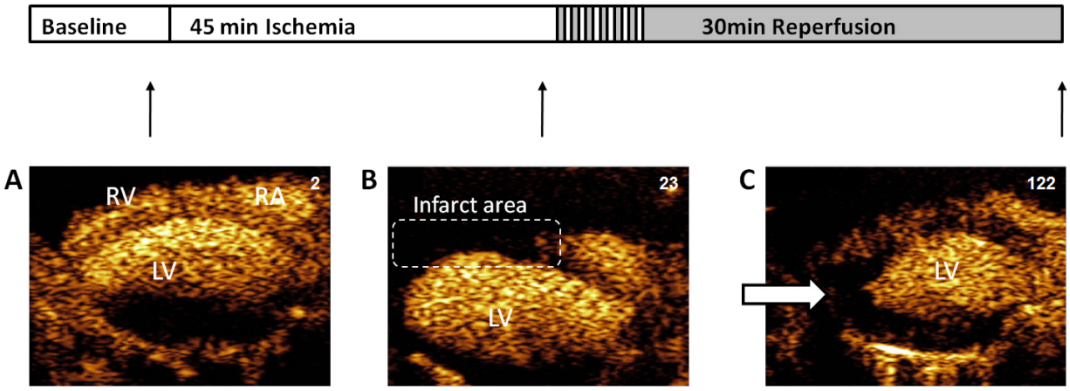

3.11 Development of myocardial blood flow deficit over time. A) Representative myocardial contrast echocardiography images taken at baseline, **B**) the potential infarct area has no myocardial blood flow during ischemia and **C**) 30 minutes after reperfusion, arrow: myocardial blood flow deficit in apical anteroseptum 30 minutes post-reperfusion. RV: Right ventricle, RA: Right atrium, LV: Left ventricle.

Upon reperfusion, myocardial perfusion was markedly impaired with perfusion defects noted in the anteroseptal wall and apex (Figure 3.11C). To quantify these observations, the anteroseptum was divided into three regions during analysis to capture the distinct blood flow deficits in each anatomic region. The three myocardial regions are outlined in Figure 3.12A: region 1) the basal anteroseptum (outlined in red), 2) the mid anteroseptum proximal to the ligation site (blue) and 3) the apical septum distal to the ligation site (black). The location of LAD ligation occurred at the intersection between the mid and basal anteroseptum with the majority of blood flow deficits found in the apical septum (region 3). No significant differences in myocardial blood flow were measured in the basal and mid anteroseptum regions.

MCE replenishment curves were computed from raw MCE videos of infused contrast agent and used to estimate the myocardial blood flow. Significant differences in myocardial blood flow between WT, S1176D ki and eNOS ko mice were found in the apex of the myocardium after 30 minutes of reperfusion. Postconditioning significantly improved blood flow in WT mice while no improvements in blood flow were detected in eNOS ko mice (Figure 3.12B). Interestingly, S1176D ki mice displayed marked improvements in myocardial blood flow after IR injury with blood flow restored close to baseline values. The protective effects of postconditioning against IR injury were associated with increased levels of myocardial perfusion in the apical septum.

To extend our understanding of myocardial blood flow deficit and recovery over time we measured the temporal dynamics of MBF changes using MCE. Figures 3.12C-E show the relative blood flow in the apical septum for WT, S1176D ki and eNOS ko compared to perfusion values at baseline before the onset of ischemia. WT mice subjected to MIR reperfusion exhibited worsening MBF over time, whereas postconditioned WT mice displayed progressive improvement in MBF over time with significantly improved perfusion after 30 minutes. In contrast, postconditioning failed to improve myocardial blood flow in eNOS ko mice. Examination of MBF in S1176D ki mice showed a rapid return to pre-ischemic levels of perfusion. Prompt recovery of blood flow was observed at the onset of reperfusion where MBF levels showed robust recovery to baseline levels. The

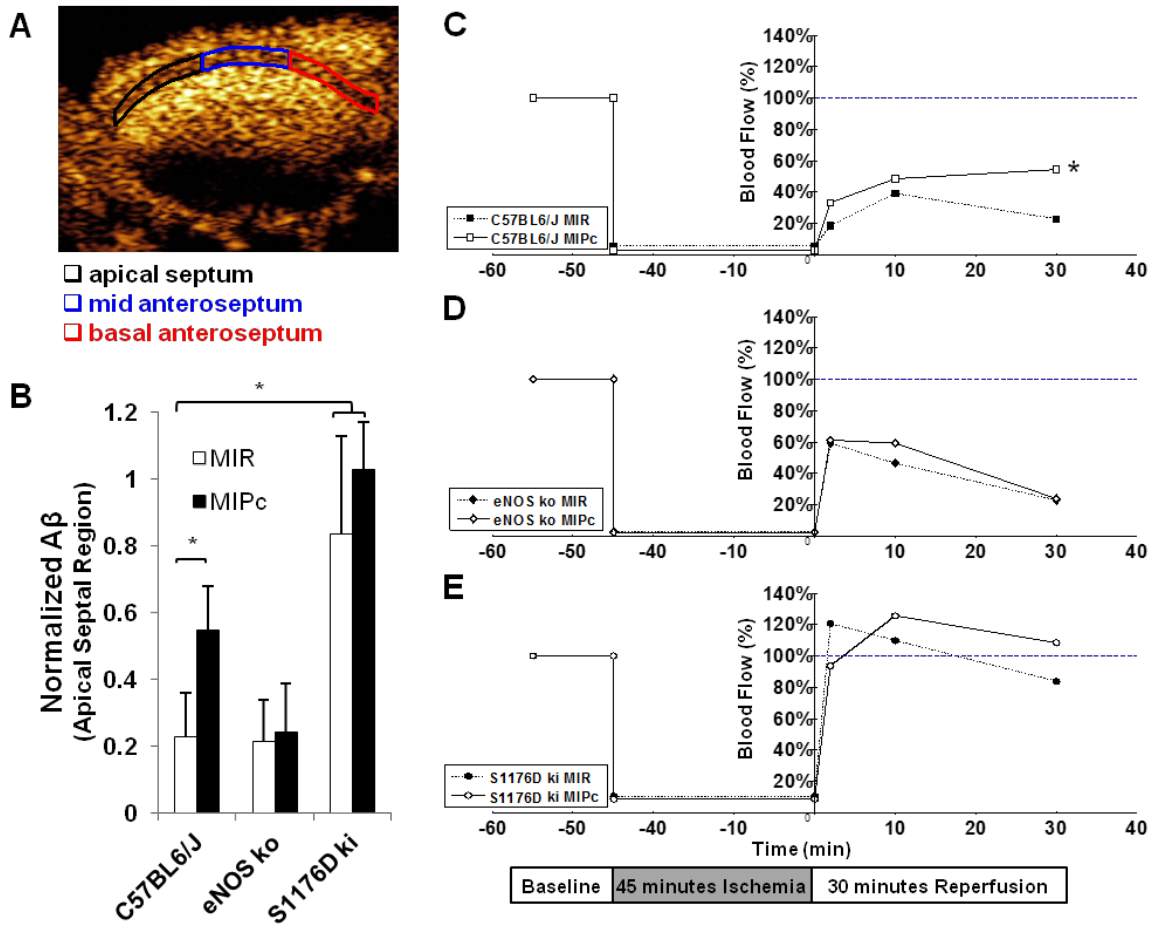

3.12 Phosphomimetic eNOS modulation improves myocardial blood flow.
A) The left ventricular anteroseptum was divided into three regions of interest defined by the apical septum, mid anteroseptum and basal anteroseptum. **B**) Myocardial blood flow deficit, Aβ, in the apical septum 30 minutes after reperfusion. Postconditioning improves myocardial blood flow in WT mice while both S1176D mice groups exhibit improved myocardial perfusion. **C**) Normalized temporal myocardial perfusion profiles in the apical region for C57BL/6J **D**) eNOS knockout and **E**) S1176D knockin mice. Levels of myocardial blood flow were measured at baseline, ischemia, and (2, 10 and 30 minutes) after reperfusion. MIR: Myocardial ischemia with reperfusion, MIPc: Myocardial ischemia with postconditioning. n = 5 - 6 per group. Data are expressed as the mean ± SD. * $P < 0.05$

temporal results of from MCE analysis support the notion that increased eNOS activity enhances myocardial perfusion after IR injury. Mean arterial pressure (MAP) and heart rate (HR) was monitored throughout the course of IR and no significant difference was found between groups, baseline levels of MAP were 70 ± 5 mmHg with an average of 468 ± 30 bpm while MAP after 30 minutes of reperfusion were 42 ± 8 mmHg with an average HR of 453 ± 23 bpm

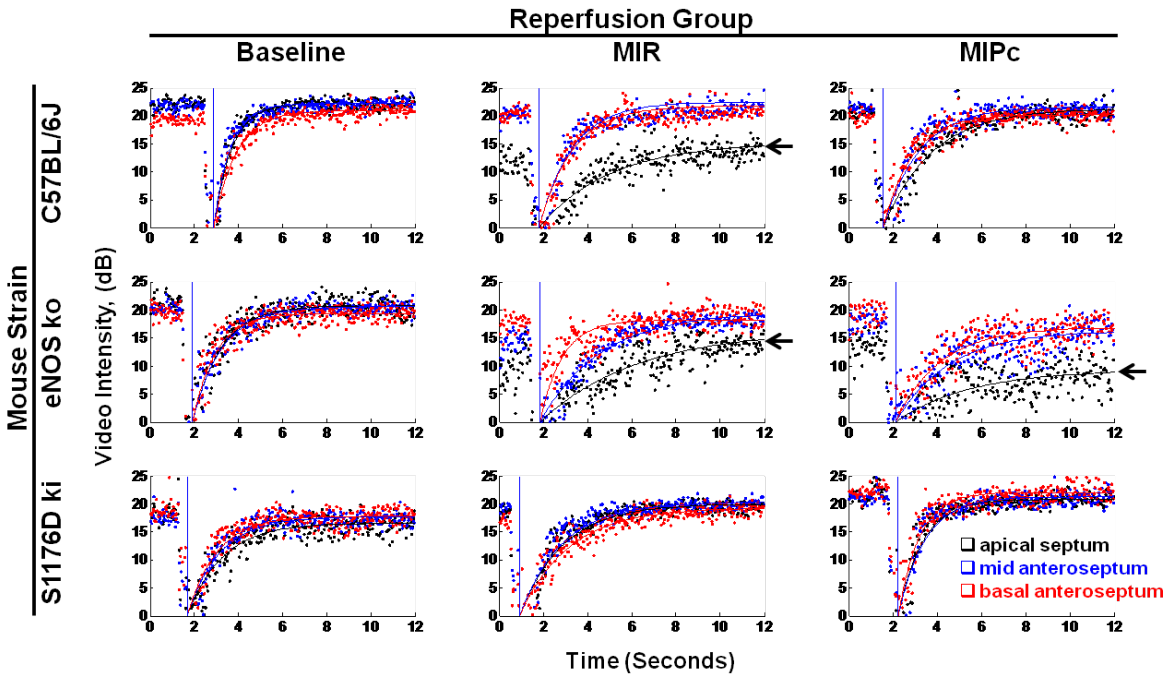

3.13 Regional analysis of improvement in myocardial perfusion. Representative region specific replenishment curves 30 minutes post reperfusion. Segmentation of the left ventricular wall was divided into three regions: apical (black), mid antero (blue), and basal anteroseptal regions (red). Postconditioned WT mice and both S1176D IR mice groups exhibit improved apical perfusion vs. impaired perfusion (arrows).

To investigate regional improvement in myocardial perfusion after IR injury we studied myocardial blood flow characteristics by region. Figure 3.13 shows representative reperfusion curves obtained 30 minutes after reperfusion from the apical, mid and basal anteroseptum of the myocardium. Baseline reperfusion curves were similar across all three regions and across all three mice groups. These findings show that the baseline levels of myocardial perfusion are conserved when eNOS activity is modulated. However, following IR the reperfusion curves differed significantly between mice groups. WT mice treated with traditional reperfusion (MIR) developed significantly larger apical septal deficits compared with WT mice treated with postconditioned reperfusion. Postconditioned WT mice (MIPc) displayed improved replenishment curves.

Both MIR and MIPc treated eNOS ko mice groups showed large apical deficits in post reperfusion blood flow confirming that postconditioning failed to improve MBF in eNOS ko mice. In contrast, S1176D mice showed robust tolerance against myocardial perfusion deficit after IR. Replenishment curves from both S1176D reperfusion groups responded well to IR injury with minimal deficits in MBF. These data show that eNOS activity is crucial to augmenting blood flow in myocardial IR injury. Thus, myocardial perfusion may be involved directly or indirectly in increasing myocardial tolerance against IR.

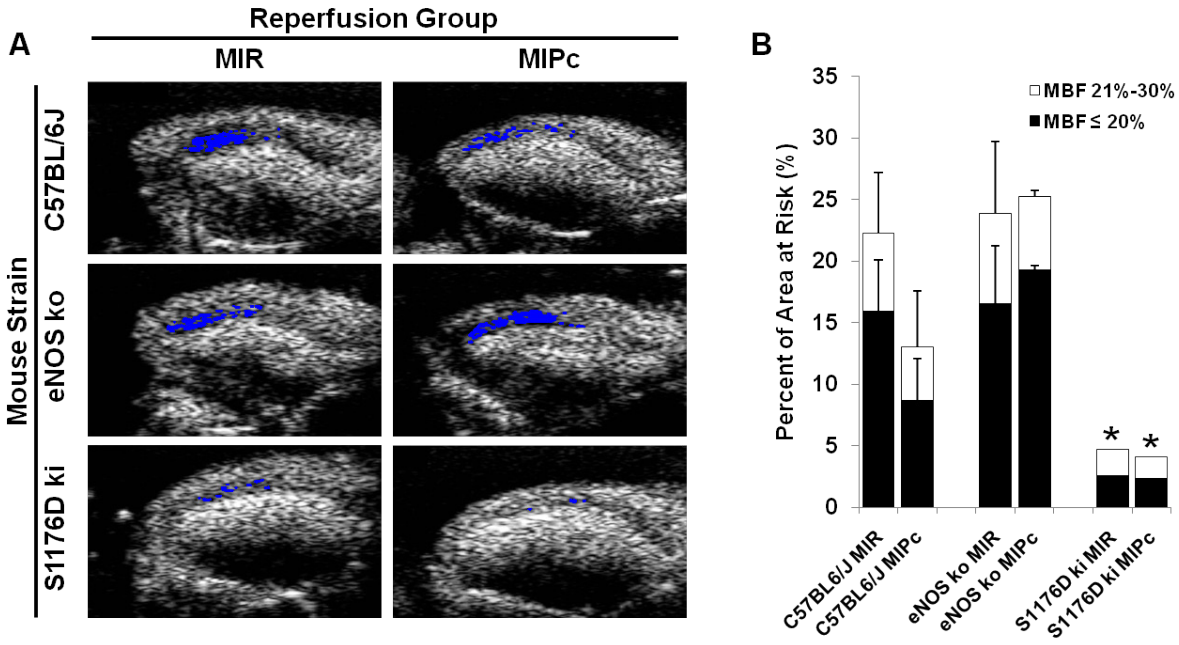

3.14 Effect of postconditioning and S1176D mutation on no-reflow zones. (**A**) Representative images 30 minutes after reperfusion. Superimposed areas (blue) indicate regions with ≤20% residual blood flow. (**B**) Composite graph showing areas of the myocardium with ≤20% (black) and ≤30% (white) residual blood flow compared to preischemic baseline. MBF: myocardial blood flow. n = 5 - 6 per group. Data are expressed as the mean ± SD. * $P < 0.05$

Assessment of myocardial no-reflow phenomena.

To further support the conclusion reached through regional analysis of replenishment curves, we assessed the spatial extent of 'no-reflow' zones using MCE after 30 minutes of reperfusion. This technique provides a quantitative assessment of the functional damage to the micro-vascular bed; obstructed or dysfunctional capillaries prevent contrast microbubbles from entering these areas, resulting in perfusion defects characterized as no-reflow zones [83]. WT MIR and eNOS ko mice developed larger myocardial areas with severe blood flow reduction (≤20% blood

flow calculated using a thresholding-paradigm) compared with WT treated with MIPc (Figure 3.14). Constitutively active eNOS activity in S1176D mice significantly improved residual blood flow. Collectively, these findings indicate that eNOS activity is crucial in protecting against myocardial IR injury.

3.7. Discussion

In this chapter we investigated whether modulation of eNOS activity affects myocardial blood flow and micro-vascular function. eNOS influences leukocyte-endothelial interactions [58], platelet aggregation and adhesion [124]. It is possible that eNOS phosphorylation and the resulting increase in NO production influences the degree of blood flow after IR. Furthermore, in a previous study, we reported that S1176D mice exhibit increased sensitivity to acetylcholine in response to vessel relaxation studies [64]. We used the S1176D mice model to explore the potential of modulating eNOS serine^{1176} phosphorylation activity as a therapy against myocardial IR injury. The ability to measure MBF levels with MCE at baseline and reperfusion allows for the detection of differences in blood flow in response to ischemic challenge.

In our model of IR, ligation of the LAD produces an area at risk predominantly focused towards the apex of the heart. We found that postconditioning improves myocardial blood flow in the apical septum of WT mice while these benefits are lost in eNOS ko mice. Furthermore, modulation of the eNOS serine^{1176} phosphorylation site markedly improves blood flow in the same region. No additional benefit of postconditioning in the S1176 ki mice was observed suggesting that phosphorylation of eNOS reproduces the beneficial effects of postconditioning. These results are important because they demonstrate the *in vivo* effects of eNOS activity on microvascular function. In this regard, improved MBF and

increased NO production through eNOS activation may contribute to the profound tolerance against IR injury found in protected hearts.

We investigated whether postconditioning is an effective treatment for no-reflow phenomena. Previous studies utilizing thioflavine S (a fluorescent marker of capillary perfusion) reported that postconditioning fails to improve no reflow after IR [125]. In the present study, we utilize MCE and report failure to improve no reflow in postconditioned WT mice. However, while postconditioning may not reduce the anatomic area of no reflow, additional insight can be gained about the degree of endothelial dysfunction from analysis of MCE replenishment curves. On one hand, postconditioning may not improve the absolute area of no reflow. On the other hand, we find that the postconditioning improves regional MBF, suggesting that postconditioning influences the degree of endothelial dysfunction. There were no hemodyamic differences between groups. Thus, although no reflow zone may not be significantly reduced, improved perfusion within the area at risk may be involved in increasing myocardial tolerance against IR.

In summary, our results establish that phosphorylation of eNOS at serine^{1176} is an important determinant of myocardial IR injury in mice. While NO availability may potentiate the activation of various pro-survival pathways our findings reveal that eNOS activity also regulates the degree of myocardial blood flow in IR injury. These insights into the effects of eNOS activity on myocardial perfusion in IR injury

suggest that eNOS S^{1176} activation could play an important therapeutic role in myocardial survival.

3.8. Materials and Methods

Myocardial Contrast Echocardiography Studies
MCE studies were performed as previously described [113]. Mice were anesthetized with intraperitoneal injections of pentobarbital sodium (50 mg/kg) and ketamine hydrochloride (50 mg/kg). Heart rate and blood pressure were monitored through a carotid catheter and recorded with a blood pressure analysis module in PowerLab (ADInstruments). A venous line was placed in the left jugular vein for constant infusion of microbubbles. 10% Perflutren lipid microspheres (Definity, Lantheus imaging, Billerica, MA) were diluted 1/10 in sterile saline and infused intravenously at 20μL/min. A thoracotomy was performed to provide unobstructed visualization of the myocardium. A 7-0 silk suture was passed underneath the LAD and through a custom snare. MCE was performed with a linear transducer (14MHz; Acuson Sequoia C512 system, Siemens) using a mechanical index of 0.24. Perfusion images were obtained in real time following destruction of microbubbles using a sequence of 10 high-energy frames (mechanical index 1.9). Signal intensity was obtained for 10 seconds after the high-energy sequence at a frame rate of 30 Hz. Parasternal long-axis views were required at the level of the aortic arch. For temporal monitoring of myocardial blood flow MCE was used to measure blood flow at baseline before ischemia, during ischemia, and at 5, 10, 30 minutes after initiation of reperfusion.

Myocardial Perfusion Analysis
MCE was performed on the anteroseptal wall in the parasternal long-axis view using methods previously described [113]. Detection and segmentation of the left ventricular anteroseptum was accomplished using a shape based snake model of edge detection in Matlab (Mathworks) [116, 126]. The anteroseptum was divided into three regions of interest defined by the apical septum, mid anteroseptum and basal anteroseptum. Average signal intensity within each region of interest was measured in each frame and a curve of signal intensity over time was fitted to an exponential function: $y = A(1 - e^{-\beta t})$, where y is the signal intensity, β is the initial slope of the curve and A is the signal plateau intensity. Two to three curves were averaged per time-point for each animal. Myocardial blood flow (MBF) was estimated by the product of Aβ. Values are expressed as percentage of baseline Aβ.

No-reflow Analysis
Myocardial contrast echocardiography measurements were taken at baseline as a measure of myocardial blood flow before ischemia and compared against MCE measurements taken at the end of the study, 30 minutes after reperfusion. Three consecutive MCE images were averaged for each animal under each condition, the average signal intensity of the left ventricular anteroseptum at baseline was

calculated. Images were converted to relative myocardial blood flow images by using a thresholding paradigm to identify areas of severe (0%-20% residual blood flow, representing the core ischemic region) and moderate (21%-30% residual blood flow, representing penumbra) blood flow relative to baseline [127].

Chapter 4

In Vivo Quantification of Infarct Size

Molecular biomarkers can be used as objective indicators of pathologic processes. Although their levels often change over time, their measurement is often constrained to a single time point. Cumulative biomarker exposure would provide a fundamentally different kind of measurement to what is available in the clinic. In addition, *in vivo* monitoring of MI biomarker levels over time may have useful applications in basic research. In small animals models of myocardial IR injury where serial blood draws are not feasible, the ability to measure myocyte cell death overtime in a single animal would provide valuable information. The current gold standard for evaluating infarct size in small animals prohibits this type of analysis

because existing methods rely upon gross-anatomical staining and end stage sacrifice of the animal. In our hands, the ability to obtain cumulative biomarker measurements would enable us to evaluate the efficacy of cardioprotective therapies in genetic mice models of myocardial IR injury.

Magnetic resonance relaxometry can be used to noninvasively monitor changes in the relaxation properties of antibody-coated magnetic particles when they aggregate upon exposure to a biomarker of interest. We report in this chapter on implantable devices containing such sensors that continuously profile changes in three clinically relevant cardiac biomarkers at physiological levels for up to 72 h. Sensor response differed between experimental and control groups in a mouse model of myocardial infarction and correlated with infarct size. Our prototype for a biomarker monitoring device also detected doxorubicin-induced cardiotoxicity and can be adapted to detect other molecular biomarkers with a sensitivity as low as the pg/ml range.

4.1. Motivation

The physiological levels of molecular biomarkers can be regarded as time-varying continuous signals. However, clinicians seldom take advantage of this temporal information in making diagnostic and prognostic decisions. Biomarker measurements are often made at single time points, which do not adequately capture the dynamics of the underlying signal if they miss transient changes occurring between measurements. For instance, levels of serum cardiac troponin I (cTnI), creatinine kinase (the CK-MB isoform) and myoglobin elevate and return to baseline in a stereotyped manner after acute myocardial infarction (MI). The earliest rising biomarkers are myoglobin and the CK-MB isoform which rise to a peak of 2 to 5 times the upper limit of normal range following acute MI (Figure 4.1) [128]. Cardiac troponin is currently the preferred clinical biomarker for diagnosing myocardial infarction and troponins can rise 20 to 50 times about the normal limit in the setting of large infarctions [129]. The length of time in which the biomarkers remain elevated about the upper limit of normal also varies, with myoglobin and CK-MB exhibiting more transient characteristics and troponin exhibiting extended levels of elevation in serum. Thus, a given measured value could correspond to either the early or late phase of biomarker release.

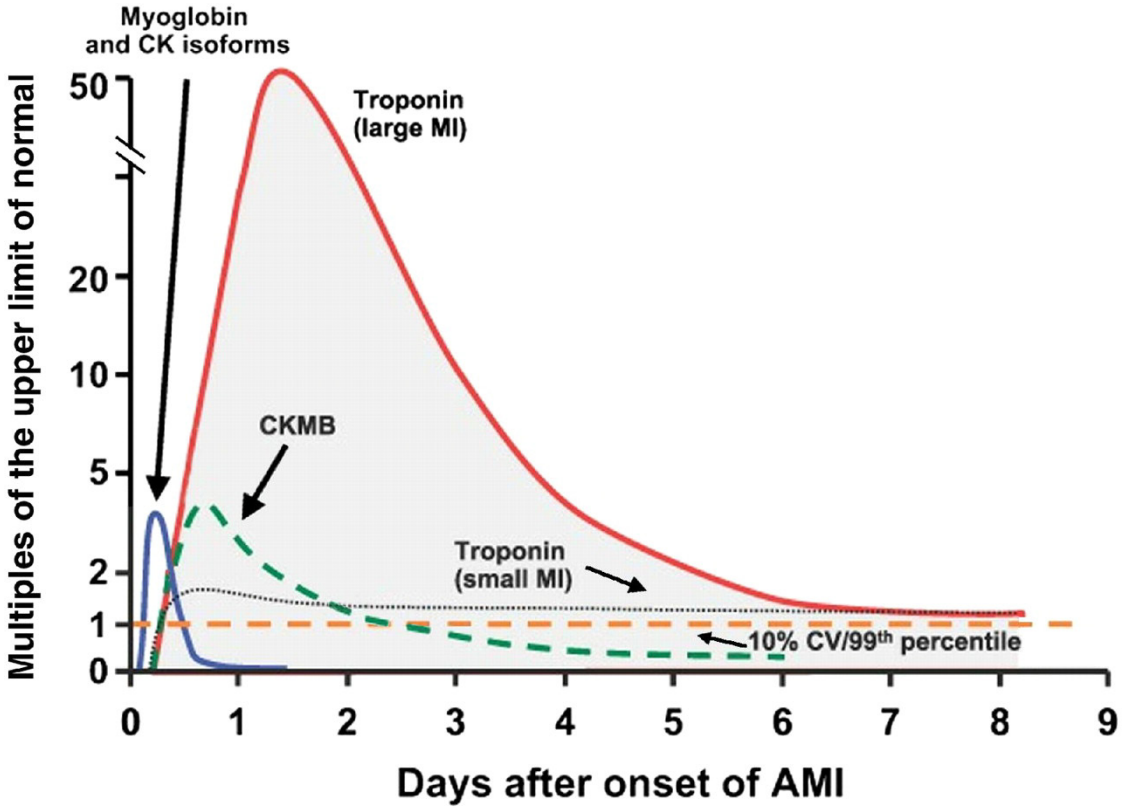

4.1 Timing release of cardiac biomarkers after acute ischemic myocardial infarction. The cardiac biomarkers myoglobin, CK-MB and troponin exhibit increased serum concentration after acute myocardial infarction. While myoglobin and CK-MB levels are the earliest to rise they typically return to normal range within 2 to 3 days, troponins can rise and stay elevated for 7 days or more. The horizontal dashed line shows the upper limit of normal range (defined as the 99th percentile from a normal reference population), adapted from [128].

Here we describe implantable magnetic relaxation sensors that are capable of integrating biomarker levels over time. The signal from such a device corresponds to the entirety of biomarker release long after a pathologic event has occurred, and even after the concentrations have returned to baseline.

Most MIs are characterized by symptoms of severe discomfort. However, a significant minority, defined as unrecognized MIs, are accompanied by minimal or no symptoms. The 30-year follow-up of the Framingham Heart Study reported that 28% and 35% of MIs are unrecognized in men and women, respectively [130]. However, current standards for detecting unrecognized MIs rely primarily on electrocardiographic surveillance. Results vary markedly between such studies because of differing electrocardiographic criteria [131, 132]. Patients at high risk for unrecognized MIs are followed periodically by their cardiologists but MIs timed between these visits can go unnoticed. A sensor that reports on integrated MI biomarker levels throughout these intervals could therefore be used to identify these previously undetectable infarcts.

4.2. Magnetic Relaxation Switch Sensors

A new class of nanoparticle-based magnetic resonance contrast agents makes this type of application feasible. Superparamagnetic iron oxide nanoparticles aggregate about analyte molecules and alter the transverse relaxivity (*T*2) of surrounding water protons [133-137]. Dubbed magnetic relaxation switches (MRSw), the particles can be functionalized to detect a variety of small molecules including proteins, nucleic acids, oligonucleotides, peptides, receptors, ligands and antibodies [137-143]. Our strategy incorporates primary to secondary antibody binding for specific detection of cardiac biomarkers. The antibody functionalized superparamagnetic nanoparticles aggregate in the presence of specific cardiac biomarkers changing the *T2* time of the aqueous solution when interrogated with magnetic resonance analysis (Figure 4.2).

Incorporation of these agents into implantable sensors permits noninvasive biomarker measurements using magnetic resonance relaxometry. We constructed small discrete sensors incorporating MRSw technology to measure cardiac biomarkers and characterized their performance *in vivo* in a murine model of MI characterized by the release of three clinically validated biomarkers at physiological concentrations. MI detection is particularly well matched for MRSw technology as MI size, a clinically relevant feature, is expected to correspond to cumulative biomarker release. A previous effort to explore the *in vivo* efficacy of similar sensors was fundamentally limited by the lack of correspondence between naturally

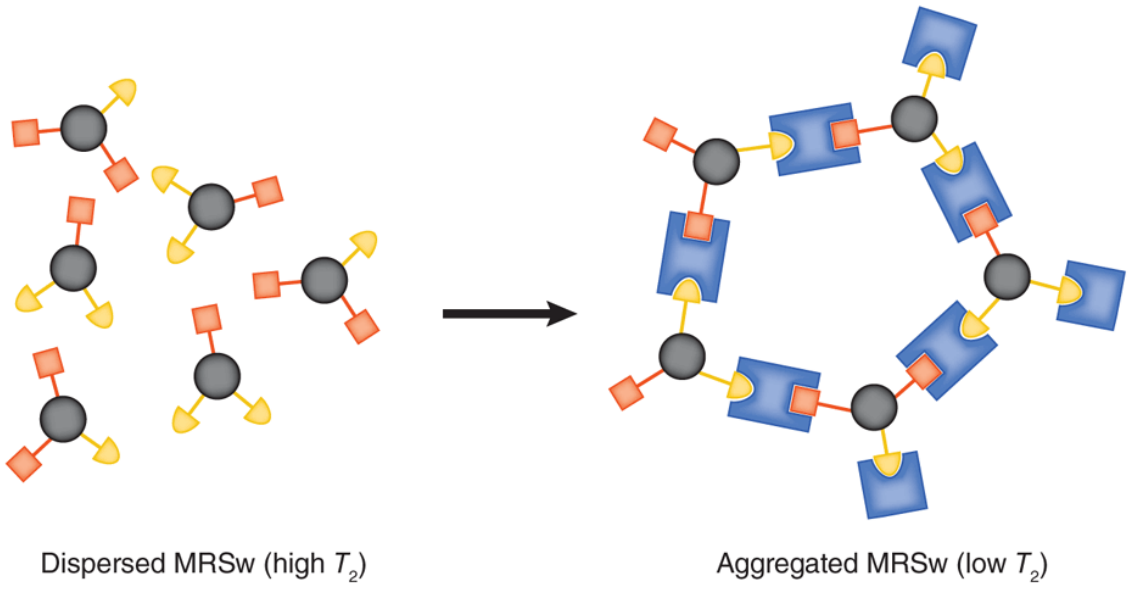

4.2 Magnetic resonance switch (MRSw) activation. Superparamagnetic iron oxide nanoparticles (black) are functionalized with polyclonal antibodies (red and yellow). Magnetic relaxation switching occurs in the presence of biomarkers (blue) which decreases the transverse relaxivity (*T2*) of surrounding protons. The subsequent signal can be detected using magnetic resonance relaxometry, adapted from [129].

occurring cancer and the xenograft tumor model used; the xenograft tumors released biomarkers at concentrations significantly above, and in a temporal fashion that did not resemble, that of physiological tumors [144].

Myoglobin, cTnI and CK-MB are functional proteins released by the ischemic myocardium after an acute infarct. Their serum dynamics are well known in humans: whereas levels of myoglobin rise and fall rapidly over 24 h after MI, levels of cTnI and CK-MB can remain above baseline for up to a week [145]. We adapted a left anterior descending (LAD) artery ligation procedure, as described [146], to experimentally induce acute myocardial infarction in C57BL6 mice.

4.3. Extravasation of Cardiac Biomarkers

The sensors were designed to sample biomarkers in a potential space created within the animal. If *in situ* sensing is to be achieved, the intended cardiac targets traditionally measured in serum (Figure 4.3) must be detectable in the location of sensor implantation. Serum levels of cardiac biomarkers after acute MI are well characterized in the existing literature [147], but their extravasation to the potential spaces had not previously warranted study. We evaluated the effectiveness of two potential spaces by determining the extravasation dynamics of cardiac biomarkers into the peritoneal space and a subcutaneous space created in the flank. The time course of cardiac biomarkers after MI in the serum and peritoneum were evaluated (Figure 4.4). We document a peritoneal 'lag' in myoglobin concentration and the absence of TnI. These results indicate that the peritoneal space is a poor environment for sensor implantation.

Next, we experimentally determined the extravasation dynamics (Figure 4.5) in the subcutaneous flank region under three conditions: MI, sham and control. Whereas MI groups received sensor implantation, thoracotomy and LAD ligation, sham groups received sensor implantation and thoracotomy but no LAD ligation. Control groups received sensor implantation only.

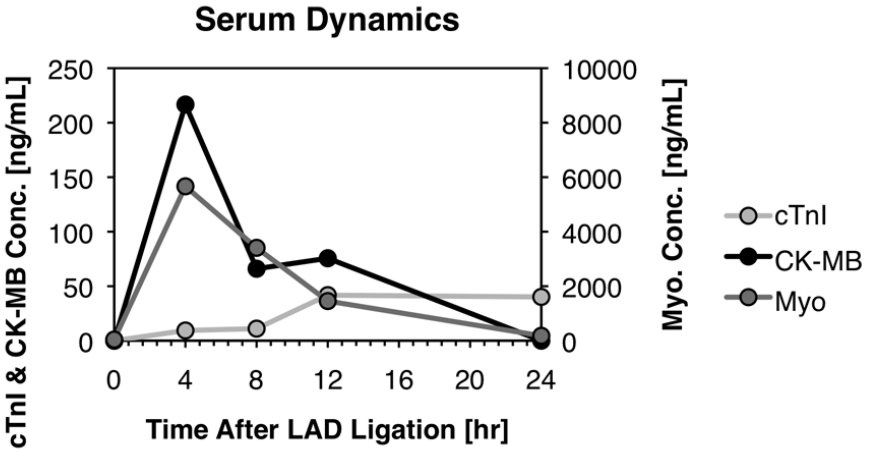

4.3 Murine cardiac biomarker serum dynamics following acute myocardial infarction. cTnI, myoglobin and CK-MB serum profiles after LAD ligation are within the range of literature results and confirm the validity of the MI model used. Approximately 0.5 ml of blood was drawn from each subject, the serum extracted by centrifugation and biomarker levels measured by ELISA at the indicated times after LAD ligation. Results are averages (n = 4).

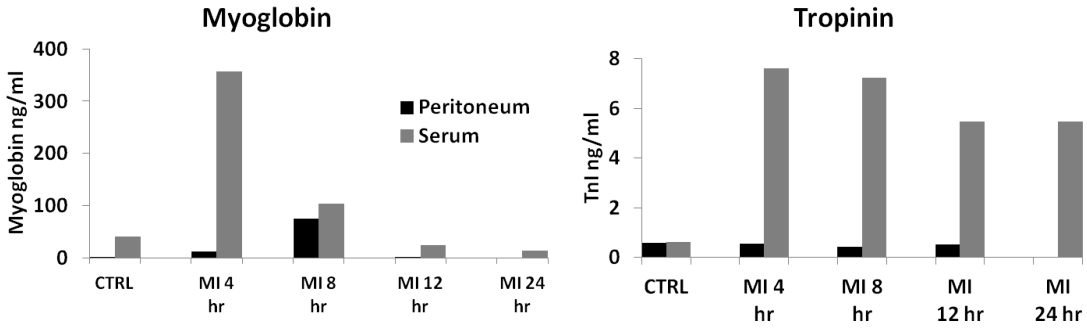

4.4 Cardiac biomarker peritoneal space extravasation dynamics. ELISA measurement of cardiac biomarkers in the peritoneal space demonstrates a significant myoglobin 'lag' and the absence of troponin. The peritoneal space represents a poor implantation site for cardiac biosensors.

These results confirm that the subcutaneous flank space is a viable site for cardiac biomarker detection, as biomarker elevations in the MI group differed significantly ($P < 0.05$) from the sham and control groups. It should therefore be possible to distinguish between the experimental conditions based on measurements acquired from implanted sensors. There are, however, some initial elevations in myoglobin and CK-MB for the control and sham groups that we would expect the sensors to detect. Open chest surgery and subcutaneous device implantation cause substantial noncardiac injury. The early behaviors of these biomarkers are consistent with their differing specificities for cardiac injury; cTnI is highly specific to cardiac damage, but CK-MB is less specific and myoglobin is a marker of general muscle damage. That myoglobin and CK-MB are elevated in the control groups (Figure 4.5b,c, green) suggests local implantation-induced trauma will be visible to the implanted sensors. No significant difference can be found between the sham and control groups for any biomarker, suggesting that thoracotomy-induced trauma should not affect the *in situ* sensor response.

The movement of protein biomarkers from the circulation to the subcutaneous space should depend on the chemical properties of the specific biomarker as well as the vascularization and morphology of the implant site. The reliability of subcutaneously implanted sensors may be limited by these factors. Nonetheless, there is little delay seen here between the peaks in the accumulation of serum (Figure 4.3) and extravasate (figure 4.5) biomarkers.

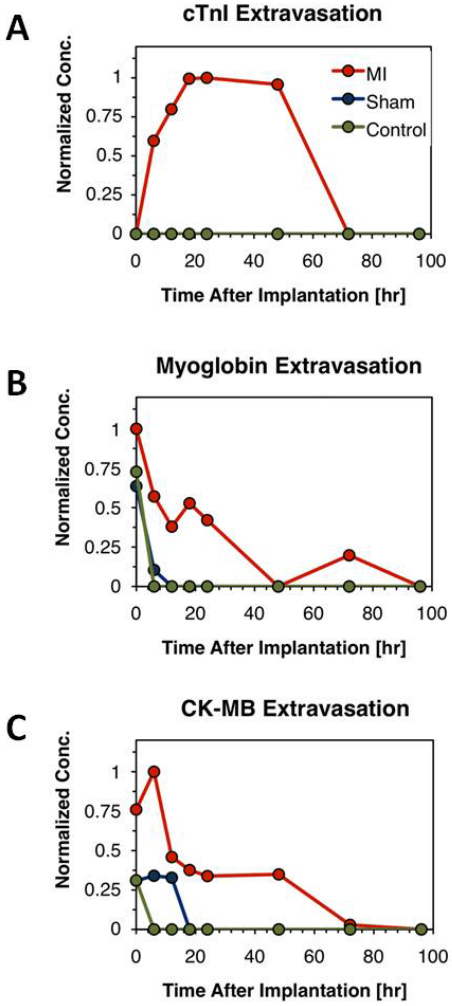

4.5 Cardiac biomarker flank space extravasation dynamics. Three experimental conditions were imposed: control (sensor implantation only), sham (sensor implantation and thoracotomy only) and MI (sensor implantation, thoracotomy and LAD ligation). Each biomarker extravasates, with MI groups exhibiting significantly elevated concentrations, as compared to the corresponding control and sham groups. Presumably, implantation-induced injury caused the low initial cTnI in the setting of high initial myoglobin and CK-MB. The similarity between sham and control groups indicates that any thoracotomy-induced biomarker release is not significantly 'visible' in the sensor implant site. Extravasate samples were obtained by flushing the flank with 1 ml PBS at the indicated times after LAD ligation and measured using ELISA. Values are normalized within each panel to the maximum measured concentration. Results are averages ± s.e.m. (n = 4, normalized); $P < 0.05$ is indicated by black asterisks between MI/sham, red asterisks between MI/control and green asterisks between sham/control.

Rapid subcutaneous availability of these biomarkers, coupled with a sufficiently rapid sensor response, should enable potential applications of MI detection using this technology. The samples were obtained by flushing the subcutaneous space with 1 ml PBS and were assayed by enzyme-linked immuno-sorbent assay (ELISA). We considered these measurements a first-order approximation of biomarker extravasation and used them as a checkpoint for proceeding with sensor implantation.

4.4. Biomarker Dosimeter Characterization

To engineer discrete sensors containing appropriately functionalized MRSw nanoparticles, we enclosed particles in the reservoirs by size-exclusion membranes (Figure 4.6). The dynamic range of each sensor was tuned by adjusting the device transport characteristics and the nanoparticle chemistry. Careful selection of the membrane composition, pore size and surface area permitted control of analyte transport into the device. cTnI sensors were tuned for sensitivity in the 10–100 ng/ml range, whereas sensors to detect myoglobin and CK-MB were tuned to detect in the 100 ng/ml to 1 μg/ml range to reflect the expected subcutaneous levels (Figure 4.7).

Antibody-antigen binding can provide an extremely strong noncovalent interaction. We tested the proposition that antibody-based MRSw sensors would be

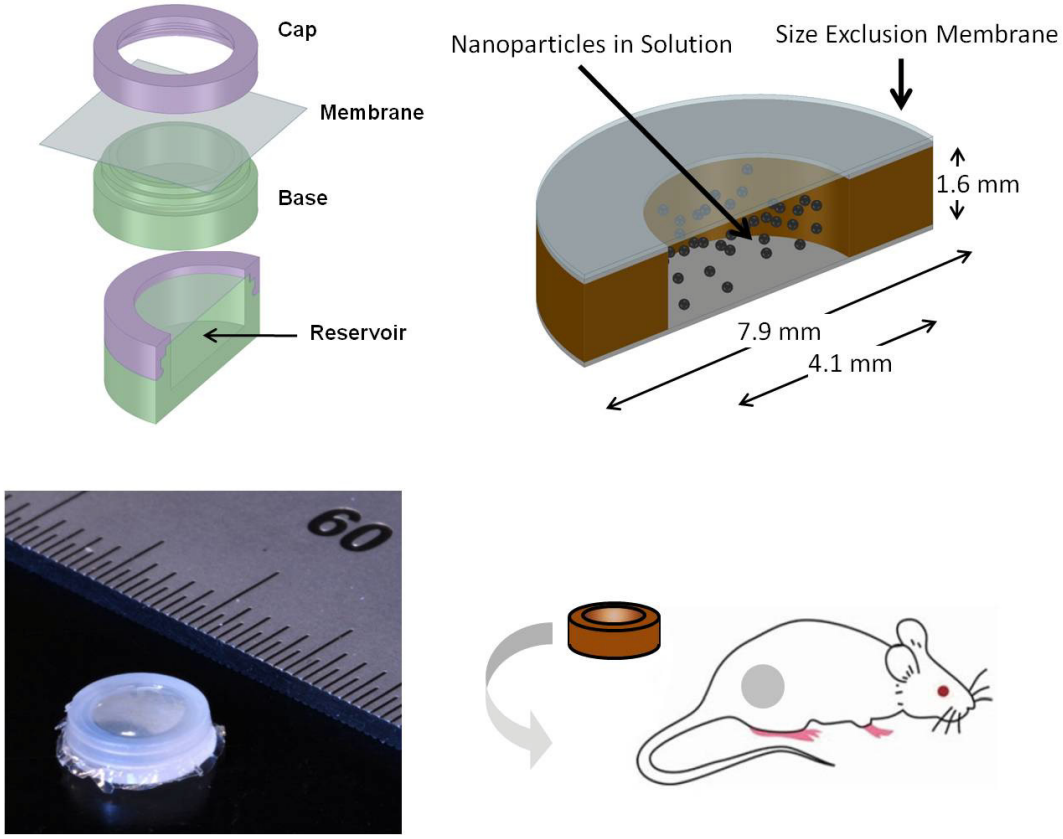

4.6 Biosensor design. The sensor consists of a reservoir containing MRSw particles enclosed by a size-exclusion membrane. T_2 changes are produced when analytes diffuse across the membrane and initiate particle aggregation. The sensor is designed for implantation into the subcutaneous flank, images courtesy of Ling [148].

irreversible and that the degree of $T2$ change would correspond to the cumulative analyte exposure. The sensors were exposed to four different constant myoglobin concentrations (Figure 4.8A) to investigate the integrative capacity of antibody-based MRSw. The overall response rate is proportional to the concentration outside the device, demonstrating that the sensor behavior is dominated by diffusion

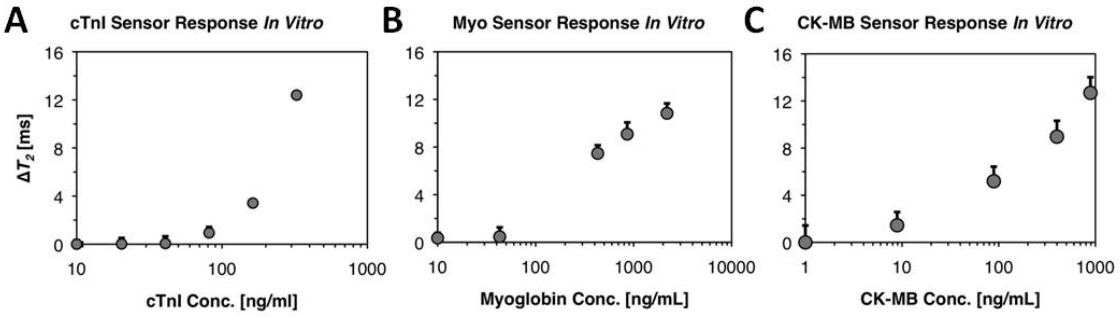

4.7 Biosensor calibration in vitro. Sensor response as a function of analyte concentration was calibrated to match expected *in vivo* concentrations. The measurements were acquired after an incubation time of 72 h for cTnI and 24 h for myoglobin and CK-MB sensors to match the expected duration of elevation for the respective biomarkers. Results are averages ± 95% confidence intervals (n = 4).

transport into the device reservoir. We define exposure as $E(t_m) = \int_{t=0}^{t_m} C(t)dt$,

where $C(t)$ is the analyte concentration as a function of time and tm is the time of measurement. Plotting the measured $T2$ against exposure yields a single curve that is independent of the analyte concentration and verifies that the sensors operate as dosimeters in a diffusion-limited regime (figure 4.8B, solid and dotted lines). The diffusion occurs across the full area of the device reservoir and the devices saturate at ~1.5 μg·h/ml. The saturating exposure level can be tuned to the anticipated *in vivo* biomarker levels by adjusting the area available for diffusion. Reducing the diffusion area by half would, therefore, increase the saturating exposure by a factor of two.

We next studied sensor response to three time varying concentration profiles as shown in Figure 4.8B (inset) (n = 2) because physiologic biomarker levels often

follow nonconstant dynamic patterns. These profiles simulate transient biomarker release when the instantaneous biomarker concentration at the time of measurement is zero. The sensor signal persists after the analyte is no longer present, and the measurements (Figure 4.8B, red/blue/green data points) coincide with the measured $T2$ versus exposure profile (Figure 4.8B, solid and dotted lines). The results from prolonged exposure to constant and transient concentration profiles indicate that the biosensors ultimately function in a manner analogous to radiation dosimeters; they report consistent $T2$ changes independent of the biomarker exposure profile.

The measurement of cumulative analyte release could be useful in detecting biomarker concentrations that are below the level of detection of blood-draw assays. This property also limits antibody-functionalized MRSw to fixed lifetimes reached when the binding sites are saturated. Cumulative sensors can thus only be used for finite durations, necessitating careful engineering of the particles and devices to match the chosen application's required sensitivity and lifetime.

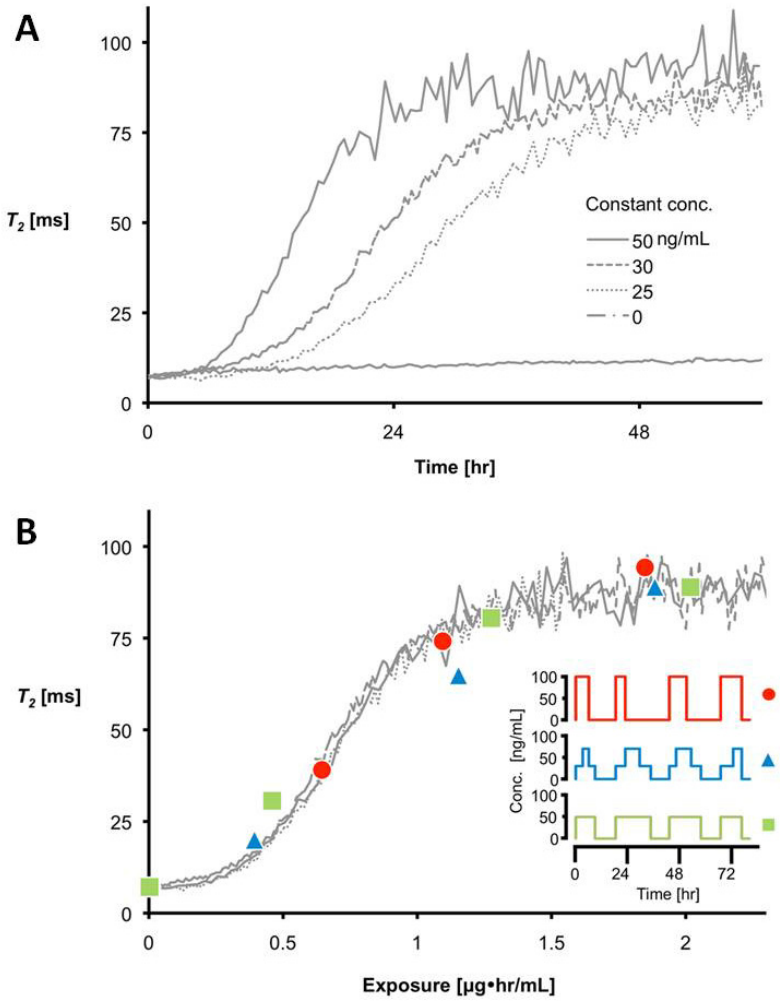

4.8 Cumulative exposure to analyte in vitro. A) Characterization of sensor saturation with exposure to constant concentration profiles. Devices were maintained in a constant concentration of myoglobin solution and the relaxation time T_2 was measured every 20 min. The time to saturation depends on the concentration. All of the devices, with the exception of the control, show a similar response and saturate at the same T_2 value. The total exposure of the device to myoglobin (measured in units of [µg·h/ml]) is defined as the area under the concentration versus time curve up until the measurement time. B) Exposure to constant and temporal concentration profiles demonstrate that MRSw sensors function as dosimeters. Plot of T_2 versus the constant exposure profiles obtained from **e** are shown as curves. The symbols represent the average T_2 of devices exposed to various temporal concentration profiles shown inset. The curves and symbols lie on top of each other, demonstrating that the response depends exclusively on exposure. Most points have deviations smaller than the symbol size. Measurements were made after several hours of incubation at zero concentration.

4.5. In Vivo Validation

We proceeded to implant subcutaneous sensors specific for each biomarker in the flanks of animals from the MI, sham and control groups. It is possible that the sensors might be acutely exposed to intravascular fluid as a result of surgery-induced capillary disruption. Sensors in all three (MI, sham, control) groups were therefore implanted before any further surgery so that their acute post-implant exposures did not vary between groups. Any differences between the three groups can therefore be attributed to true biomarker extravasation. *In situ* MRI measurements demonstrated that the sensors can be interrogated at the implant site (Figure 4.9).

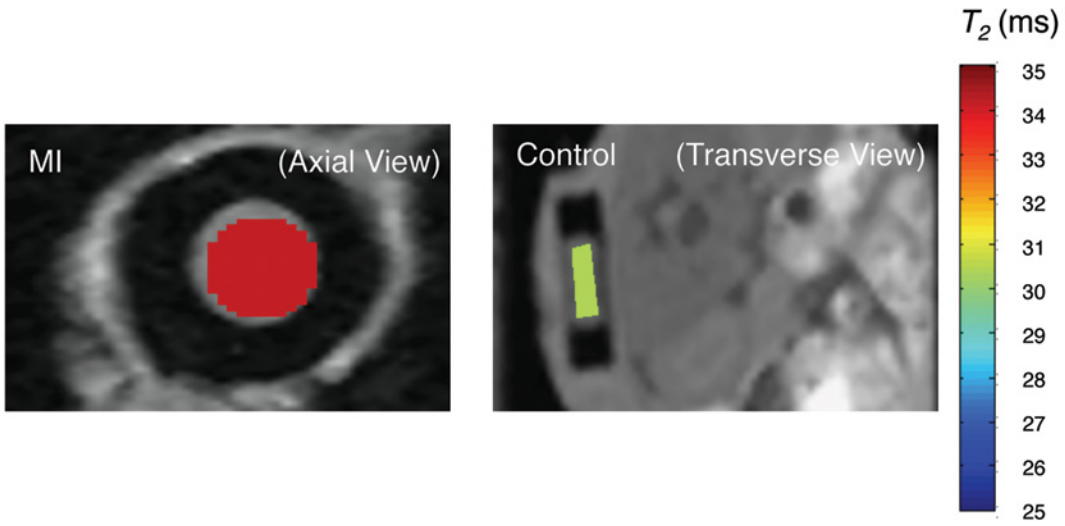

4.9 MRI interrogation of implanted biosensors. A T_2 map (color bar on the right) superimposed on T_2 -weighted images of myoglobin sensors demonstrates the feasibility of MRI-based *in situ* measurements after 24 h implantation with (MI) or without (control) concomitant LAD ligation at the time of sensor implantation. The images show that the sensors can be measured in either the axial or the transverse plane.

Most measurements were obtained from explanted sensors using a single-sided relaxometer. Despite the limited sensitivity of the single-sided system, $T2$ increases of the MI over the sham and control groups for all three biomarkers are evident (Figure 4.10). Wilcoxon rank-sum two-sided tests give significant P values ($P < 0.05$) for cross comparisons between the MI and control groups, and between the MI and sham in levels of myoglobin and CK-MB above baseline in the sham and control groups reflect noncardiac injury caused by the initial surgical procedure. Implanted MRSw sensors functionalized against IgG alone showed negligible increases in $T2$.

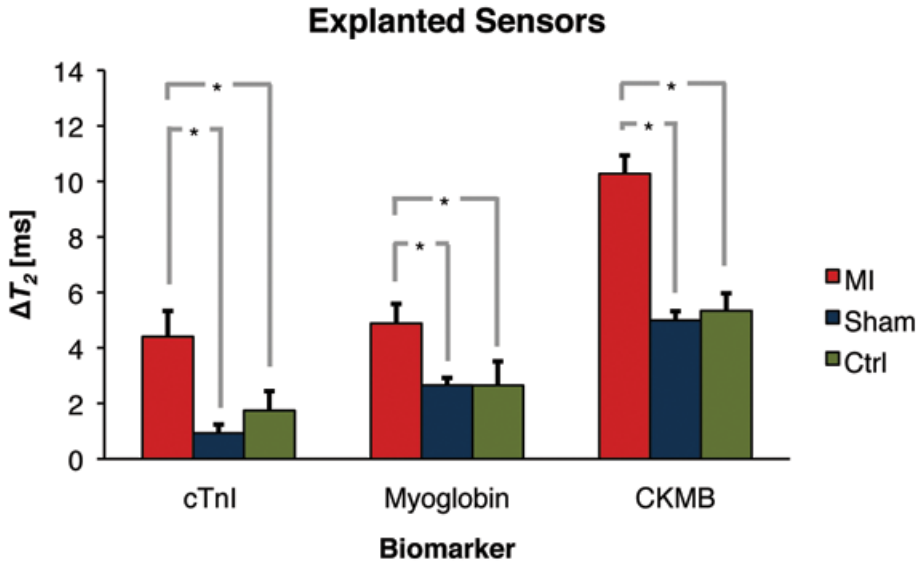

4.10 Sensor response differs markedly between MI and sham/control groups. The T_2 of explanted sensors, as measured by single-sided proton relaxometry (after 72 h implantation for cTnI and 24 h for myoglobin and CK-MB), from the MI group are significantly higher (* indicates $P < 0.05$ using the Wilcoxon rank-sum two-sided test) than from the control/sham groups for all three biomarkers. Increases in the T_2 of myoglobin and CK-MB sensors for both control and sham groups were expected and consistent with the extravasation results. Results are averages ± 95% confidence intervals ($n = 36$; 6 sensors/subject and 6 subjects/group).

The infarct zone can be visualized through 2,3,5-triphenyltetrazolium chloride staining and objectively quantified as the fraction of left ventricular volume [149]. The cumulative release of cardiac biomarkers should be directly proportional to the magnitude of infarction, as the biomarkers are functional proteins directly released from the ischemic tissue. A comparison of sensor readings with infarct size (Figure 4.11) shows a consistent trend for all three biomarkers, despite the relatively large errors. The capability to quantitatively measure infarct size has important implications for risk stratification of MI patients [150, 151]. This factor, usually measured indirectly in the clinic through functional tests or imaging, can be directly quantified by the implantable sensors described here.

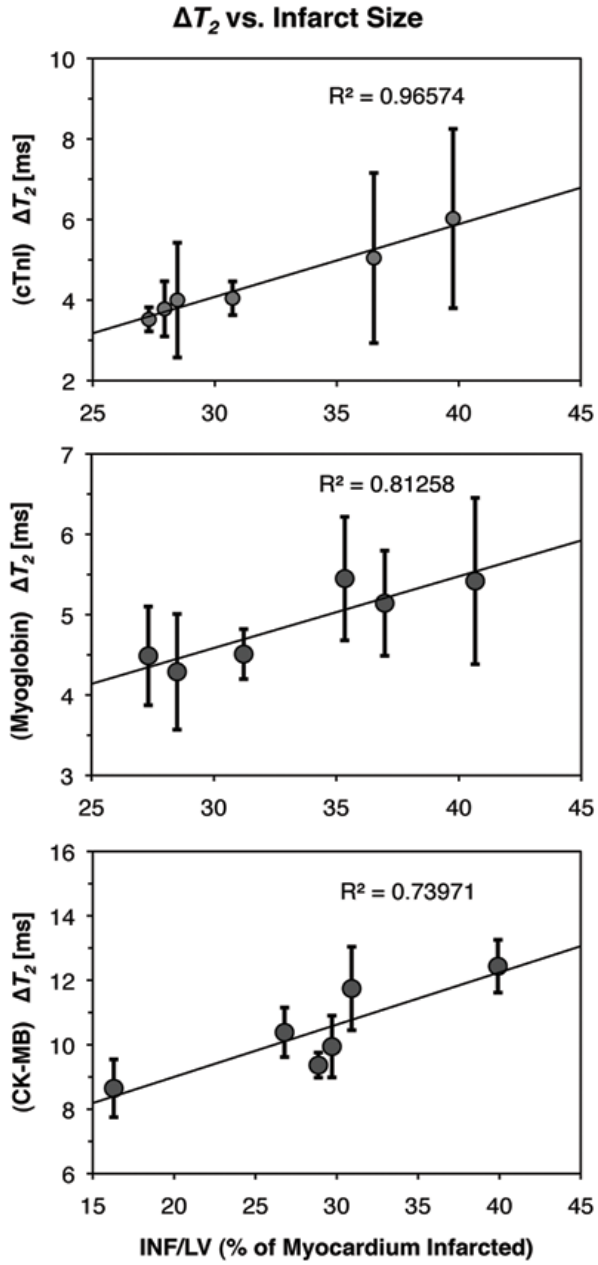

4.11 Biosensor correlation with ex vivo infarct size. T_2 change of the same explanted sensors from figure 4.10, if disaggregated into the individual subjects and replotted as a function of infarct size, correlates positively with infarct size for all three cardiac biomarkers. The cumulative release of biomarkers from the infarcted myocardium generates the final T_2 sensor value. This characteristic may contribute to the correspondence between sensor reading and infarct size. Results are averages ± 95% confidence intervals (n = 6 sensors/subject).

4.5.1. Cardiotoxicity

We further studied application of the sensors to discern drug cardiotoxicity. Doxorubicin is a potent anthracycline antibiotic that has found wide clinical use as a cancer chemotherapeutic [152, 153]. Its cardiotoxic effects are well known; after administration, patients exhibit dose-dependent loss of cardiac myocytes accompanied by serum cardiac biomarker elevation [154]. We confirmed that serum myoglobin increases after doxorubicin administration in a murine model (figure 4.12A), although at an order of magnitude lower concentration than after acute MI (102 ng/ml versus 103 ng/ml). Myoglobin sensors were thus left *in vivo* for 72 h after implantation (as opposed to 24 h for acute MI). The results show a clear distinction in sensor $T2$ between the experimental and control groups, thus validating sensor efficacy in assaying drug cardiotoxicity (Figure 4.12B). These sensors may potentially be used in the future to establish the cardiac side effects of novel pharmaceuticals.

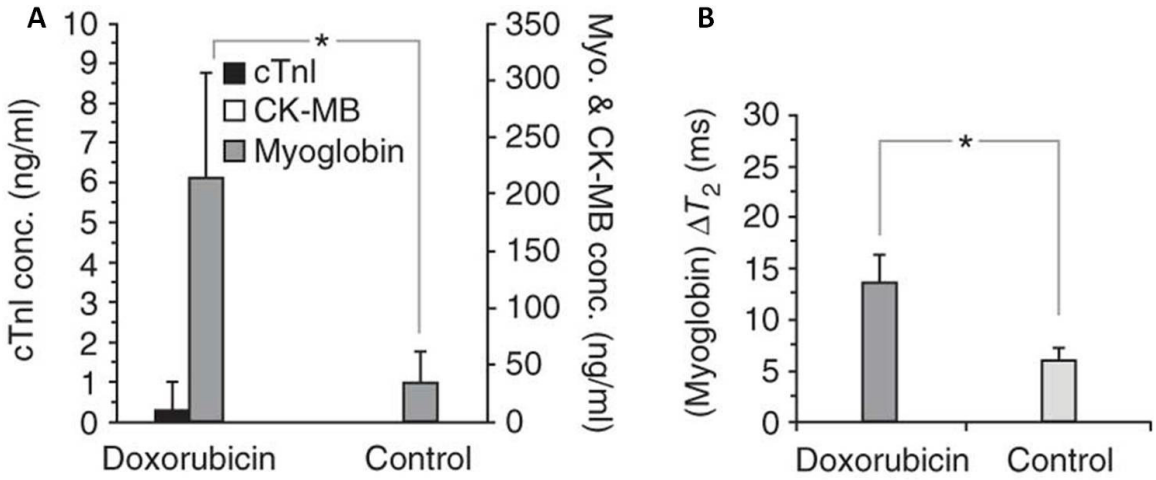

4.12 An implanted MRSw sensor device can detect the cardiotoxic effect of the chemotherapeutic drug doxorubicin in vivo. A) Doxorubicin induces a significant (* indicates $P < 0.05$) increase in serum myoglobin (ELISA measurements). Results are averages ± 95% confidence intervals ($n = 4$). Wilcoxon rank-sum two-sided tests were used to test for statistical significance. B) Myoglobin sensors explanted (after 72 h) from a doxorubicin-administered group show significant increases in T_2 over those from a control group. Results are averages ± 95% confidence intervals ($n = 16$; 4 sensors/subject and 4 subjects/group).

4.6. Discussion

New high-sensitivity troponin assays will lead to an increasing population of patients identified with elevated troponins of nonischemic etiology. Additional assays will need to be developed to help physicians distinguish between acute coronary syndromes and other causes. *In vivo* diagnostic MRSw measurements may prove to be especially useful in discriminating between troponin elevations caused by transient tachyarrhythmias and sustained ischemic episodes. These integrative

sensors are engineered to have lower sensitivity so that they do not saturate upon total exposure to analyte released during and after an MI. The troponin sensor discussed here, for example, has sensitivity in the ng/ml range but could be engineered for even higher sensitivity to the pg/ml range of the newest troponin assays. Thus, integrative sensors may provide prognostic value as sentinels in high-risk patients and for the detection of unrecognized MIs. The ability to track cumulative biomarkers *in vivo* can be advantageous for its ability to capture transient events, which are frequently missed with serial testing. Furthermore, this type of sensor can be useful in research as a tool for monitoring biomarkers in small animals in which serial blood draws may not be feasible. MRSw can be functionalized to detect a variety of small molecules and further study will establish the general efficacy of these sensors. The sensors require single time point measurements that fit comfortably into the traditional clinical paradigm because they are practical to obtain, yet provide information on biomarker levels from the time of sensor implantation to when accumulation is measured. We have shown the utility of cumulative biomarker measurements for applications relevant to heart disease. Such data will in all likelihood prove to possess clinical value for other applications as well. The MRSw molecular sensors described here represent a possible path in that direction. We showed that they perform adequately in the detection of pathologically elevated levels of three soluble disease biomarkers that extravasate from the circulation to the implant site. They are stable over several

months and can be applied as disease sentinels in MI patients at high risk for short-term recurrence.

4.7. Material and Methods

Preparation of magnetic nanosensors. NanoMag-CLD SPIO nanoparticles (50 nm) with amine terminated dextran shells (Micromod) were coupled with monoclonal antibody against goat IgG (Meridian Life Sciences, Saco, ME) using a previously described method 25. These particles were then derivatized against specific targets by incubation with goat-produced polyclonal antibodies against cTnI (BiosPacific, Emeryville, CA), myoglobin (BiosPacific, Emeryville, CA) and CK-MB (BiosPacific, Emeryville, CA). Unless otherwise specified, particles were suspended in PBS with 1% bovine serum albumin (Sigma-Aldrich, St. Louis, MO) and 0.1% penicillin-streptomycin (Invitrogen, Carlsbad, CA) to minimize bacterial contamination and non-specific adsorption.

Device fabrication and implantation. Derivatized particles were encapsulated within small diffusion devices 15. Polycarbonate diffusion membranes (SPI Supplies, West Chester, PA) were affixed by double-sided adhesive to one side of high density polyethylene cylinders (thickness = 1.6 mm, inner diameter = 4.1 mm, outer diameter = 7.9 mm). The opposing end was closed off by single-sided adhesive (3M) after the reservoir was filled with 25 μL particle solution. Devices (n = 6 per animal) were implanted subcutaneously in the flank. The animals were sacrificed and the devices explanted for single-sided relaxometry at specified time points. Devices were sealed with single-sided adhesive and replaced in the implant site for imaging.

Myocardial infarction surgery. All experiments were conducted in accordance with the guidelines of the Institutional Animal Care and Use Committee (IACUC) of the Massachusetts General Hospital. Mouse LAD ligation has been previously described 17. The procedure was performed under 2% isoflurane anesthesia with supplemental oxygen. The depth of the anesthesia was monitored by tail pinch, constant monitoring of respiratory rate and heart rate. An intercostal approach between the 3rd and 4th intercostal spaces was taken to expose the pericardium. The pericardium was then visualized and opened and the LAD identified under stereo microscopy. A silk ligature was passed underneath and tied around the vessel to induce occlusion. Occlusion was confirmed by observed blanching of the anterior left ventricular wall. The chest cavity was then carefully closed layer by layer. Sham-operated mice underwent the same procedure without tying the LAD ligation suture. Buprenorphine HCl (0.05-0.1 mg/kg) was administered for post-operative care. The mice were monitored continuously for six hours, then every 8 hours and were treated according to IACUC guidelines if they appeared dyspneic or moribund.

Independent measurements of biomarker levels. Commercially available enzyme-linked immunsorbent assays were used to independently quantify Myoglobin (Life Diagnostics, West Chester, PA), CK-MB (Oxis International, Foster City, CA), and Troponin I (Life Diagnostics, West Chester, PA) levels following control, sham and MI Procedures. Each kit was strictly used in accordance with included instructions. Extravasate samples were obtained by flushing the flank with 1 mL PBS at the indicated times after LAD ligation. Doxorubicin cardiotoxicity biomarker levels were characterized and studied by administration of 20 mg/kg doxorubicin HCl i.p.

Infarct Size Determination. Area at risk and area of infarction were determined by perfusing Evans blue dye into the carotid artery prior to sacrificing the animal. Hearts were then removed and sectioned perpendicular to the long axis into 1 mm slices using a McIlwain tissue chopper (Sterling, Wood Dale, IL) and stained with 1% 2,3,5-triphenyltetrazolium chloride (TTC) for 5 min at 37˚C. Each slice was analyzed for left ventricular area, area at risk and infarct size.

Measurement of proton relaxation times. Proton relaxation measurements were determined on a custom-built system using a single-sided NMR relaxometer (0.43 T and 25˚C; Profile NMR MOUSE, ACT Center for Technology, Aachen, Germany). The sensor's field gradient enables measurements to be made on a single device positioned above the sensor. Transverse relaxation times for the single-sided MR were measured using a Carr Purcell Meiboom Gill (CPMG) sequence with the following parameters: echo time (TE) = 0.035 ms, 5714 echoes, 16 scans, and recovery time (TR) = 3 s. The echo peak intensities were fit to the equation using a custom script running on MATLAB (The Mathworks).

Measurement of device dynamics and dosage response. Devices were prepared as described above and were individually mounted inside a well on a custom-built holder. Each well was then filled with 400 μL of analyte, and the analyte was changed every 4 to 8 hours. The holder was mounted on an automated motion stage and measurements were acquired automatically. The total exposure is given by the integrating the analyte concentration as a function of time and reported in units of μg•hr/mL. Four devices were incubated in a constant concentration (0 ng/mL to 50 ng/mL) and measured at 20 minute intervals to ascertain the diffusion limited response and the onset of saturation. Six devices were exposed for 4-12 hours to myoglobin concentrations of between 30 ng/mL and 100 ng/mL as shown in Figure 2f (inset). The analyte was then replaced with PBS, and the devices were incubated overnight. The sensor T2 value stabilizes after approximately 12 hours so relaxation times are reported after the overnight incubation. The return to a zero concentration of myoglobin also mimics a transient in vivo event.

Magnetic resonance imaging. MRI measurements were made using a 9.4T animal imager (Bruker Biospin). Imaging protocols included a Tri-plane for localizing the implanted devices. Multi-slice multiecho (MSME) T2-weighted imaging was performed using the following parameters: flip angle = 90°; Matrix size (64 x 64); TR = 2330 ms; TE = 16 equally spaced echoes at 4.07 ms intervals ranging from 4.07 ms to 85.12 ms; field of view (FOV) = 2 cm x 2 cm, slice thickness = 1 mm. Region of interest analysis was performed and T2 fit was performed using a mono-exponential fitting algorithm for the multi-TE data. ROI incorporating the center slice of the devices were analyzed.

Statistics. Statistical comparisons were made by means of the Wilcoxon rank-sum two-sided test. This non-parametric method was considered appropriate here as no assumptions are made on the distribution of the data. P-values of less than 0.05 were taken to be significant.

Chapter 5

Conclusions and Future Work

The work conducted in this thesis identifies eNOS phosphorylation and nitric oxide bioavailability as important factors in the regulation of ischemic postconditioning. The use of genetic mouse models enabled characterization of the role of eNOS phosphorylation on myocardial ischemia reperfusion injury in vivo. Studies were performed to elucidate the effects of postconditioning on lethal reperfusion injury and myocardial blood flow. These studies reveal that postconditioning and eNOS phosphorylation are important protective regulators of lethal reperfusion injury (Chapter 2), myocardial blood flow and the no-reflow phenomenon (Chapter 3). The challenge of identifying the left ventricle from

myocardial contrast echocardiographic images was addressed, and a solution applying active contours for image segmentation was presented.

We encountered limitations in the methods used to evaluate infarct size in animal models over the course of this thesis. The need to sacrifice animals to obtain ex vivo infarct size data challenges our ability to monitor the temporal development of reperfusion injury. In Chapter 4 we present a proof of concept study using implantable magnetic relaxation switch sensors to measure cardiac biomarkers and estimate infarct size. This technology has potential applications in small animal research where cumulative measurements of biomarkers are difficult to obtain.

This chapter discusses the general conclusions that may be drawn from this thesis and outlines possible directions for future work.

5.1. Conclusions

Postconditioning represents an attractive therapeutic option for the treatment of patients with acute myocardial infarction. Preliminary clinical trials examining postconditioning as therapies to treat myocardial infarction have shown promising results in its the ability to limit myocardial infarction size [87]. However, additional basic research is required to further our understanding of cardioprotection and the mechanisms through which postconditioning exerts its protective effects.

In this thesis we have identified eNOS phosphorylation at the serine^{1176} residue as an important regulator of lethal reperfusion injury and myocardial blood flow. Nitric oxide bioavailability is an important determinant of cardioprotective success and phosphomimetic modulation of eNOS augments the production of NO. Experiments in S1176D knock-in mice show that these benefits translate to reductions in infarct size of over 50%. Moreover, myocardial contrast echocardiography studies enable us to evaluate the pathogenesis of myocardial blood flow in a time sensitive manner. We report that blood flow deficits associated with reperfusion injury can worsen over time and that postconditioned therapies provide beneficial vascular effects. These experiments establish the in vivo relevance of posttranslational modification of eNOS in cardioprotection.

Our work in image segmentation of MCE videos also demonstrates the feasibility of automated tracking in contrast-enhanced ultrasound videos of the heart. The rapid heart rate of murine models precludes the use of EKG signals and we use an active contours approach to identify the myocardium. This approach enabled the development of a relatively intuitive and high performance algorithm for the analysis of replenishment curves from MCE videos.

While there are several gold standard methods to evaluate infarct size and myocardial blood flow in animal models of myocardial reperfusion injury, the established techniques provide information at single time points, and do not adequately capture the temporal dynamics of the underlying variable. The Chapter 4

we present cumulative biomarker measurements as an attractive option to measure the pathogenesis of infarction. Because they MRSw biosensors integrate biomarker levels over time, their use in measuring cardiac biomarkers can provide important information on the development of reperfusion injury, long after the initial therapy has occurred. This opens up the possibility of conducting longitudinal studies in small animal models and offers an attractive modality to evaluate the effectiveness of cardioprotective therapies.

5.2. Future Directions

Postconditioning represents an attractive option for the treatment of acute myocardial infarction because its action can be applied at the onset of reperfusion in conjunction with other clinical services such as angioplasty. We have begun to elucidate the mechanisms of action through which the mechanical control of blood flow at reperfusion confers cardioprotection in the heart. The signaling pathway responsible for the transduction of postconditioning into cardioprotective signaling and the reduction in infarct size is likely to involve the posttranslational modification of eNOS through phosphorylation.

The results of this work suggest that phosphorylation of eNOS is sufficient to provide protection against reperfusion injury. Which downstream effectors are activated through eNOS phosphorylation will require further investigation. Moreover, there are currently no known pharmacological drugs capable of directing

the phosphorylation eNOS. The design of an assay to evaluate eNOS activity would be useful within the framework of large pharmacological drug screen. Identification of a compound capable of activating eNOS may provide an invaluable tool against acute myocardial infarction.

eNOS phosphorylation and postconditioning may also prove beneficial for the treatment of other pathological processes. The ability to augment NO bioavailabilty through the S1176D mutation raises the interesting possibility of therapeutic eNOS modulation. The beneficial effects of the S1176D mutation has already been reported in models of cerebral ischemia [64] and angiogenesis [63].

Finally, further investigation into the application of cumulative biomarker measurements and their correlation with disease severity is necessary. The application of MRSw sensors will need to be compared against the gold standard method for evaluating infarct size for these devices to become useful and reliable tools. The use of a biosensor capable of detecting cardiac biomarkers at a very early time frame with high sensitivity would be extremely valuable in future basic research.

Bibliography

1. Yellon, D.M. and D.J. Hausenloy, *Myocardial Reperfusion Injury.* N Engl J Med, 2007. **357**(11): p. 1121-1135.
2. Teerlink, J.R., S.Z. Goldhaber, and M.A. Pfeffer, *An overview of contemporary etiologies of congestive heart failure.* Am Heart J, 1991. **121**(6 Pt 1): p. 1852-3.
3. Jugdutt, B.I., *Nitric oxide and cardioprotection during ischemia-reperfusion.* Heart Fail Rev, 2002. **7**(4): p. 391-405.
4. Hansen, P.R., *Role of Neutrophils in Myocardial Ischemia and Reperfusion.* Circulation, 1995. **91**(6): p. 1872-1885.
5. Vinten-Johansen, J., et al., *Nitric Oxide and the Vascular Endothelium in Myocardial Ischemia-Reperfusion Injury.* Ann NY Acad Sci, 1999. **874**(1): p. 354-370.
6. Vinten-Johansen, J., *Postconditioning: a mechanical maneuver that triggers biological and molecular cardioprotective responses to reperfusion.* Heart Fail Rev, 2007.
7. Herrick, J., *Clinical features of sudden obstruction of the coronary arteries.* JAMA, 1912. **LIX**((23)): p. 2015-2022.
8. DeBoer, L.W., et al., *A flow- and time-dependent index of ischemic injury after experimental coronary occlusion and reperfusion.* Proceedings of the National Academy of Sciences, 1983. **80**(18): p. 5784-5788.
9. Reimer, K., et al., *The wavefront phenomenon of ischemic cell death. 1. Myocardial infarct size vs duration of coronary occlusion in dogs.* Circulation, 1977. **56**(5): p. 786-794.
10. Braunwald, et al., *Myocardial reperfusion: a double-edged sword?* Vol. 76. 1985, Ann Arbor, MI, ETATS-UNIS: American Society for Clinical Investigation.
11. Jennings, R.B., et al., *Myocardial necrosis induced by temporary occlusion of a coronary artery in the dog.* Archives of Pathology, 1960. **70**(1): p. 68-78.
12. Yellon, D.M. and D.J. Hausenloy, *Myocardial Reperfusion Injury.* New England Journal of Medicine, 2007. **357**(11): p. 1121-1135.
13. Bolli, R. and E. Marbán, *Molecular and Cellular Mechanisms of Myocardial Stunning.* Physiological Reviews, 1999. **79**(2): p. 609-634.
14. Manning, A.S. and D.J. Hearse, *Reperfusion-induced arrhythmias: Mechanisms and prevention.* Journal of Molecular and Cellular Cardiology, 1984. **16**(6): p. 497-518.
15. Ito, H., *No-reflow phenomenon and prognosis in patients with acute myocardial infarction.* Nat Clin Pract Cardiovasc Med, 2006. **3**(9): p. 499-506.
16. Piper, H.M., D. Garcña-Dorado, and M. Ovize, *A fresh look at reperfusion injury.* Cardiovascular Research, 1998. **38**(2): p. 291-300.

17. Bredt, D.S. and S.H. Snyder, *Nitric Oxide: A Physiologic Messenger Molecule.* Annual Review of Biochemistry, 1994. **63**(1): p. 175-195.
18. Dudzinski, D.M., et al., *The regulation and pharmacology of endothelial nitric oxide synthase.* Annual Review of Pharmacology and Toxicology, 2006. **46**(1): p. 235-276.
19. Dimmeler, S., et al., *Activation of nitric oxide synthase in endothelial cells by Akt-dependent phosphorylation.* Nature, 1999. **399**(6736): p. 601-605.
20. Fulton, D., et al., *Regulation of endothelium-derived nitric oxide production by the protein kinase Akt.* Nature, 1999. **399**(6736): p. 597-601.
21. Zhao, Z.Q., et al., *Inhibition of myocardial injury by ischemic postconditioning during reperfusion: comparison with ischemic preconditioning.* Am J Physiol Heart Circ Physiol, 2003. **285**(2): p. H579-88.
22. Kaljusto, M.L., et al., *Postconditioning in rats and mice.* Scand Cardiovasc J, 2006. **40**(6): p. 334-41.
23. Staat, P., et al., *Postconditioning the Human Heart.* Circulation, 2005. **112**(14): p. 2143-2148.
24. Hausenloy, D.J. and D.M. Yellon, *Survival kinases in ischemic preconditioning and postconditioning.* Cardiovasc Res, 2006. **70**(2): p. 240-53.
25. Kitakaze, M., et al., *Temporary acidosis during reperfusion limits myocardial infarct size in dogs.* Am J Physiol Heart Circ Physiol, 1997. **272**(5): p. H2071-2078.
26. Vinten-Johansen, J., et al., *Postconditioning--A new link in nature's armor against myocardial ischemia-reperfusion injury.* Basic Res Cardiol, 2005. **100**(4): p. 295-310.
27. Alderton, W.K., C.E. Cooper, and R.G. Knowles, *Nitric oxide synthases: structure, function and inhibition*.
28. McCabe, T.J., et al., *Enhanced Electron Flux and Reduced Calmodulin Dissociation May Explain "Calcium-independent" eNOS Activation by Phosphorylation.* Journal of Biological Chemistry, 2000. **275**(9): p. 6123-6128.
29. Garcin, E.D., et al., *Structural Basis for Isozyme-specific Regulation of Electron Transfer in Nitric-oxide Synthase.* Journal of Biological Chemistry, 2004. **279**(36): p. 37918-37927.
30. Sessa, W.C., *eNOS at a glance.* Journal of Cell Science, 2004. **117**(12): p. 2427-2429.
31. Goligorsky, M.S., *Endothelial nitric oxide synthase: from structure to function in one aspartic substitution.* Kidney Int, 0000. **75**(3): p. 255-257.
32. Kaminski, K.A., et al., *Oxidative stress and neutrophil activation--the two keystones of ischemia/reperfusion injury.* Int J Cardiol, 2002. **86**(1): p. 41-59.
33. Vinten-Johansen, J., *Involvement of neutrophils in the pathogenesis of lethal myocardial reperfusion injury.* Cardiovascular Research, 2004. **61**(3): p. 481-497.

34. Seubert, J.M., et al., *Role of epoxyeicosatrienoic acids in protecting the myocardium following ischemia/reperfusion injury.* Prostaglandins & Other Lipid Mediators, 2007. **82**(1–4): p. 50-59.
35. Lemasters, J.J., et al., *The mitochondrial permeability transition in toxic, hypoxic and reperfusion injury.* Molecular and Cellular Biochemistry, 1997. **174**(1): p. 159-165.
36. Sharov, V.G., et al., *Cyclosporine A attenuates mitochondrial permeability transition and improves mitochondrial respiratory function in cardiomyocytes isolated from dogs with heart failure.* Journal of Molecular and Cellular Cardiology, 2007. **42**(1): p. 150-158.
37. Argaud, L., et al., *Postconditioning Inhibits Mitochondrial Permeability Transition.* Circulation, 2005. **111**(2): p. 194-197.
38. Kilgore, K.S. and B.R. Lucchesi, *Reperfusion injury after myocardial infarction: The role of free radicals and the inflammatory response.* Clinical Biochemistry, 1993. **26**(5): p. 359-370.
39. Zweier, J.L., *Measurement of superoxide-derived free radicals in the reperfused heart. Evidence for a free radical mechanism of reperfusion injury.* Journal of Biological Chemistry, 1988. **263**(3): p. 1353-1357.
40. Becker, L.B., *New concepts in reactive oxygen species and cardiovascular reperfusion physiology.* Cardiovascular Research, 2004. **61**(3): p. 461-470.
41. Zweier, J.L. and M.A.H. Talukder, *The role of oxidants and free radicals in reperfusion injury.* Cardiovascular Research, 2006. **70**(2): p. 181-190.
42. Lemasters, J.J., et al., *The pH paradox in ischemia-reperfusion injury to cardiac myocytes.* EXS, 1996. **76**: p. 99-114.
43. Bond, J.M., B. Herman, and J.J. Lemasters, *Protection by acidotic pH against anoxia/reoxygenation injury to rat neonatal cardiac myocytes.* Biochemical and Biophysical Research Communications, 1991. **179**(2): p. 798-803.
44. Harrison, D.C., J.J. Lemasters, and B. Herman, *A pH-dependent phospholipase A2 contributes to loss of plasma membrane integrity during chemical hypoxia in rat hepatocytes.* Biochemical and Biophysical Research Communications, 1991. **174**(2): p. 654-659.
45. Bronk, S.F. and G.J. Gores, *pH-dependent nonlysosomal proteolysis contributes to lethal anoxic injury of rat hepatocytes.* American Journal of Physiology - Gastrointestinal and Liver Physiology, 1993. **264**(4): p. G744-G751.
46. Klein, H.H., et al., *Treatment of reperfusion injury with intracoronary calcium channel antagonists and reduced coronary free calcium concentration in regionally ischemic, reperfused porcine hearts.* Journal of the American College of Cardiology, 1989. **13**(6): p. 1395-1401.
47. Boden, W.E., et al., *Diltiazem in acute myocardial infarction treated with thrombolytic agents: a randomised placebo-controlled trial.* The Lancet, 2000. **355**(9217): p. 1751-1756.

48. Mehta, J.L., et al., *Impaired canine coronary vasodilator response to acetylcholine and bradykinin after occlusion-reperfusion.* Circ Res, 1989. **64**(1): p. 43-54.
49. Laufs, U., et al., *Upregulation of Endothelial Nitric Oxide Synthase by HMG CoA Reductase Inhibitors.* Circulation, 1998. **97**(12): p. 1129-1135.
50. Jones, S.P., et al., *Direct vascular and cardioprotective effects of rosuvastatin, a new HMG-CoA reductase inhibitor.* Journal of the American College of Cardiology, 2002. **40**(6): p. 1172-1178.
51. Di Napoli, P., et al., *Simvastatin reduces reperfusion injury by modulating nitric oxide synthase expression: an ex vivo study in isolated working rat hearts.* Cardiovascular Research, 2001. **51**(2): p. 283-293.
52. Minamishima, S., et al., *Hydrogen Sulfide Improves Survival After Cardiac Arrest and Cardiopulmonary Resuscitation via a Nitric Oxide Synthase 3–Dependent Mechanism in Mice.* Circulation, 2009. **120**(10): p. 888-896.
53. Chiari, P.C., et al., *Isoflurane Protects against Myocardial Infarction during Early Reperfusion by Activation of Phosphatidylinositol-3-Kinase Signal Transduction: Evidence for Anesthetic-induced Postconditioning in Rabbits.* Anesthesiology, 2005. **102**(1): p. 102-109.
54. Krolikowski, J., et al., *Role of Erk1/2, p70s6K, and eNOS in isoflurane induced cardioprotection during early reperfusion* Canadian Journal of Anesthesia / Journal canadien d'anesthésie, 2006. **53**(2): p. 174-182.
55. Hausenloy, D.J. and D.M. Yellon, *Survival kinases in ischemic preconditioning and postconditioning.* Cardiovascular Research, 2006. **70**(2): p. 240-253.
56. Montagnani, M., et al., *Insulin-stimulated Activation of eNOS Is Independent of Ca2+ but Requires Phosphorylation by Akt at Ser1179.* Journal of Biological Chemistry, 2001. **276**(32): p. 30392-30398.
57. Gao, F., et al., *Nitric Oxide Mediates the Antiapoptotic Effect of Insulin in Myocardial Ischemia-Reperfusion.* Circulation, 2002. **105**(12): p. 1497-1502.
58. Li, J., et al., *Insulin inhibits leukocyte–endothelium adherence via an Akt-NO-dependent mechanism in myocardial ischemia/reperfusion.* Journal of Molecular and Cellular Cardiology, 2009. **47**(4): p. 512-519.
59. Jones, S.P., et al., *Myocardial ischemia-reperfusion injury is exacerbated in absence of endothelial cell nitric oxide synthase.* Am J Physiol Heart Circ Physiol, 1999. **276**(5): p. H1567-1573.
60. Huang, P.L., et al., *Hypertension in mice lacking the gene for endothelial nitric oxide synthase.* Nature, 1995. **377**(6546): p. 239-242.
61. Gyurko, R., et al., *Modulation of mouse cardiac function in vivo by eNOS and ANP.* American Journal of Physiology - Heart and Circulatory Physiology, 2000. **278**(3): p. H971-H981.
62. Scotland, R.S., et al., *Functional Reconstitution of Endothelial Nitric Oxide Synthase Reveals the Importance of Serine 1179 in Endothelium-Dependent Vasomotion.* Circulation Research, 2002. **90**(8): p. 904-910.

63. Schleicher, M., et al., *The Akt1-eNOS Axis Illustrates the Specificity of Kinase-Substrate Relationships in Vivo.* Sci. Signal., 2009. **2**(82): p. ra41-.
64. Atochin, D.N., et al., *The phosphorylation state of eNOS modulates vascular reactivity and outcome of cerebral ischemia in vivo.* The Journal of Clinical Investigation, 2007. **117**(7): p. 1961-1967.
65. Michael, L.H., et al., *Myocardial ischemia and reperfusion: a murine model.* American Journal of Physiology - Heart and Circulatory Physiology, 1995. **269**(6): p. H2147-H2154.
66. Tarnavski, O., et al., *Mouse cardiac surgery: comprehensive techniques for the generation of mouse models of human diseases and their application for genomic studies.* Physiological Genomics, 2004. **16**(3): p. 349-360.
67. Lundberg, J.O., E. Weitzberg, and M.T. Gladwin, *The nitrate-nitrite-nitric oxide pathway in physiology and therapeutics.* Nat Rev Drug Discov, 2008. **7**(2): p. 156-167.
68. Jones, S.P., et al., *Myocardial ischemia-reperfusion injury is exacerbated in absence of endothelial cell nitric oxide synthase.* American Journal of Physiology - Heart and Circulatory Physiology, 1999. **276**(5): p. H1567-H1573.
69. Jones, S.P., et al., *Endothelial nitric oxide synthase overexpression attenuates myocardial reperfusion injury.* American Journal of Physiology - Heart and Circulatory Physiology, 2004. **286**(1): p. H276-H282.
70. Tsang, A., et al., *Postconditioning: A Form of "Modified Reperfusion" Protects the Myocardium by Activating the Phosphatidylinositol 3-Kinase-Akt Pathway.* Circulation Research, 2004. **95**(3): p. 230-232.
71. Hausenloy, D.J. and D.M. Yellon, *New directions for protecting the heart against ischaemia–reperfusion injury: targeting the Reperfusion Injury Salvage Kinase (RISK)-pathway.* Cardiovascular Research, 2004. **61**(3): p. 448-460.
72. Schulz, R., M. Kelm, and G. Heusch, *Nitric oxide in myocardial ischemia/reperfusion injury.* Cardiovascular Research, 2004. **61**(3): p. 402-413.
73. Zhao, Z.-Q., et al., *Inhibition of myocardial injury by ischemic postconditioning during reperfusion: comparison with ischemic preconditioning.* American Journal of Physiology - Heart and Circulatory Physiology, 2003. **285**(2): p. H579-H588.
74. Bolli, R., *The Late Phase of Preconditioning.* Circulation Research, 2000. **87**(11): p. 972-983.
75. Di Napoli, P., et al., *Chronic treatment with rosuvastatin modulates nitric oxide synthase expression and reduces ischemia–reperfusion injury in rat hearts.* Cardiovascular Research, 2005. **66**(3): p. 462-471.
76. Li, J., et al., *Nitric Oxide Suppresses Apoptosis via Interrupting Caspase Activation and Mitochondrial Dysfunction in Cultured Hepatocytes.* Journal of Biological Chemistry, 1999. **274**(24): p. 17325-17333.

77. Wang, G., et al., *Nitric oxide donors protect murine myocardium against infarction via modulation of mitochondrial permeability transition.* American Journal of Physiology - Heart and Circulatory Physiology, 2005. **288**(3): p. H1290-H1295.
78. Hausenloy, D. and D. Yellon, *Reperfusion injury salvage kinase signalling: taking a RISK for cardioprotection.* Heart Failure Reviews, 2007. **12**(3): p. 217-234.
79. Lacerda, L., et al., *Ischaemic postconditioning protects against reperfusion injury via the SAFE pathway.* Cardiovascular Research, 2009. **84**(2): p. 201-208.
80. Hausenloy, D.J., S. Lecour, and D.M. Yellon, *Reperfusion Injury Salvage Kinase and Survivor Activating Factor Enhancement Prosurvival Signaling Pathways in Ischemic Postconditioning: Two Sides of the Same Coin* Antioxidants & Redox Signaling., 2011. **14**(5): p. 893-907.
81. Ito, H., et al., *Clinical Implications of the `No Reflow' Phenomenon : A Predictor of Complications and Left Ventricular Remodeling inReperfused Anterior Wall Myocardial Infarction.* Circulation, 1996. **93**(2): p. 223-228.
82. Resnic, F.S., et al., *No-reflow is an independent predictor of death and myocardial infarction after percutaneous coronary intervention.* American Heart Journal, 2003. **145**(1): p. 42-46.
83. Reffelmann, T. and R. Kloner, *The no-reflow phenomenon: A basic mechanism of myocardial ischemia and reperfusion.* Basic Research in Cardiology, 2006. **101**(5): p. 359-372.
84. Moncada, S., *Adventures in vascular biology: a tale of two mediators.* Philosophical Transactions of the Royal Society B: Biological Sciences, 2006. **361**(1469): p. 735-759.
85. Cai, H. and D.G. Harrison, *Endothelial Dysfunction in Cardiovascular Diseases: The Role of Oxidant Stress.* Circulation Research, 2000. **87**(10): p. 840-844.
86. Jones, S.P. and R. Bolli, *The ubiquitous role of nitric oxide in cardioprotection.* Journal of Molecular and Cellular Cardiology, 2006. **40**(1): p. 16-23.
87. Gerczuk, P.Z. and R.A. Kloner, *An Update on Cardioprotection: A Review of the Latest Adjunctive Therapies to Limit Myocardial Infarction Size in Clinical Trials.* J Am Coll Cardiol, 2012. **59**(11): p. 969-978.
88. Kotani, J.-i., et al., *Plaque Gruel of Atheromatous Coronary Lesion May Contribute to the No-Reflow Phenomenon in Patients With Acute Coronary Syndrome.* Circulation, 2002. **106**(13): p. 1672-1677.
89. Kloner, R., et al., *Ultrastructural evidence of microvascular damage and myocardial cell injury after coronary artery occlusion: which comes first?* Circulation, 1980. **62**(5): p. 945-952.
90. Marzilli, M., et al., *Beneficial Effects of Intracoronary Adenosine as an Adjunct to Primary Angioplasty in Acute Myocardial Infarction.* Circulation, 2000. **101**(18): p. 2154-2159.

91. Ma, X., et al., *Diminished basal nitric oxide release after myocardial ischemia and reperfusion promotes neutrophil adherence to coronary endothelium.* Circulation Research, 1993. **72**(2): p. 403-412.
92. Lefer, D., et al., *Antineutrophil and myocardial protecting actions of a novel nitric oxide donor after acute myocardial ischemia and reperfusion of dogs.* Circulation, 1993. **88**(5): p. 2337-2350.
93. Pasceri, V., et al., *Effects of the Nitric Oxide Donor Nitroprusside on No-Reflow Phenomenon During Coronary Interventions for Acute Myocardial Infarction.* The American Journal of Cardiology, 2005. **95**(11): p. 1358-1361.
94. Wardell, K., A. Jakobsson, and G.E. Nilsson, *Laser Doppler perfusion imaging by dynamic light scattering.* Biomedical Engineering, IEEE Transactions on, 1993. **40**(4): p. 309-316.
95. Atochin, D.N., et al., *Mouse Model of Microembolic Stroke and Reperfusion.* Stroke, 2004. **35**(9): p. 2177-2182.
96. Smits, G.J., R.J. Roman, and J.H. Lombard, *Evaluation of laser-Doppler flowmetry as a measure of tissue blood flow.* J Appl Physiol, 1986. **61**(2): p. 666-672.
97. Humeau, A., et al., *Laser Doppler perfusion monitoring and imaging: novel approaches.* Medical & Biological Engineering & Computing, 2007. **45**(5): p. 421-435.
98. Li, X.-F. and Y.-P. Wang, *Laser Doppler flowmetry for assessment of myocardial microperfusion in the beating rat heart.* Vascular Pharmacology, 2007. **46**(3): p. 207-214.
99. A. Klassen, G., et al., *Red cell flux during the cardiac cycle in the rabbit myocardial microcirculation.* Cardiovasc Res, 1997. **34**(3): p. 504-514.
100. Postema, M., et al., *Ultrasound-induced encapsulated microbubble phenomena.* Ultrasound in Medicine & Biology, 2004. **30**(6): p. 827-840.
101. McCulloch, M., et al., *Ultrasound contrast physics: a series on contrast echocardiography, article 3.* Journal of the American Society of Echocardiography : official publication of the American Society of Echocardiography, 2000. **13**(10): p. 959-967.
102. Firschke, et al., *Myocardial perfusion imaging in the setting of coronary artery stenosis and acute myocardial infarction using venous injection of a second-generation echocardiographic contrast agent*. Vol. 96. 1997, Hagerstown, MD, ETATS-UNIS: Lippincott Williams & Wilkins.
103. Wei, K., et al., *Basis for detection of stenosis using venous administration of microbubbles during myocardial contrast echocardiography: bolus or continuous infusion?* Journal of the American College of Cardiology, 1998. **32**(1): p. 252-260.
104. Kaul, S., et al., *Detection of Coronary Artery Disease With Myocardial Contrast Echocardiography : Comparison With 99mTc-Sestamibi Single-Photon Emission Computed Tomography.* Circulation, 1997. **96**(3): p. 785-792.

105. Tei, C., et al., *Myocardial contrast echocardiography: a reproducible technique of myocardial opacification for identifying regional perfusion deficits.* Circulation, 1983. **67**(3): p. 585-593.
106. Lilly, L.S., *Pathophysiology of Heart Disease: A Collaborative Project of Medical Students And Faculty*2007: Wolters Kluwer/Lippincott Williams & Wilkins.
107. Albers, V., *Underwater Acoustic Handbook*1960, State College, Pa: The Pennsylvania State University Press.
108. Wei, K., et al., *Quantification of Myocardial Blood Flow With Ultrasound-Induced Destruction of Microbubbles Administered as a Constant Venous Infusion.* Circulation, 1998. **97**(5): p. 473-483.
109. Jayaweera, A., et al., *In vivo myocardial kinetics of air-filled albumin microbubbles during myocardial contrast echocardiography. Comparison with radiolabeled red blood cells.* Circulation Research, 1994. **74**(6): p. 1157-1165.
110. Keller, M., et al., *The behavior of sonicated albumin microbubbles within the microcirculation: a basis for their use during myocardial contrast echocardiography.* Circulation Research, 1989. **65**(2): p. 458-467.
111. Kaul, S., et al., *Assessment of regional myocardial blood flow with myocardial contrast two-dimensional echocardiography.* Journal of the American College of Cardiology, 1989. **13**(2): p. 468-482.
112. Scherrer-Crosbie, M., et al., *Echocardiographic determination of risk area size in a murine model of myocardial ischemia.* American Journal of Physiology - Heart and Circulatory Physiology, 1999. **277**(3): p. H986-H992.
113. Raher, M.J., et al., *In Vivo Characterization of Murine Myocardial Perfusion With Myocardial Contrast Echocardiography.* Circulation, 2007. **116**(11): p. 1250-1257.
114. Chalana, V., et al., *A multiple active contour model for cardiac boundary detection on echocardiographic sequences.* Medical Imaging, IEEE Transactions on, 1996. **15**(3): p. 290-298.
115. Hammoude, A., *Endocardial border identification in two-dimensional echocardiographic images: review of methods.* Computerized Medical Imaging and Graphics, 1998. **22**(3): p. 181-193.
116. Kass, M., A. Witkin, and D. Terzopoulos, *Snakes: Active contour models.* International Journal of Computer Vision, 1988. **1**(4): p. 321-331.
117. Chenyang, X. and J.L. Prince, *Snakes, shapes, and gradient vector flow.* Image Processing, IEEE Transactions on, 1998. **7**(3): p. 359-369.
118. Noble, J.A. and D. Boukerroui, *Ultrasound image segmentation: a survey.* Medical Imaging, IEEE Transactions on, 2006. **25**(8): p. 987-1010.
119. Cohen, L.D., *On active contour models and balloons.* CVGIP: Image Understanding, 1991. **53**(2): p. 211-218.
120. Mikic, I., S. Krucinski, and J.D. Thomas, *Segmentation and tracking in echocardiographic sequences: active contours guided by optical flow estimates.* Medical Imaging, IEEE Transactions on, 1998. **17**(2): p. 274-284.

121. Hamarneh, G. and T. Gustavsson. *Combining snakes and active shape models for segmenting the human left ventricle in echocardiographic images*. in *Computers in Cardiology 2000*. 2000.
122. Chenyang, X. and J.L. Prince. *Gradient vector flow: a new external force for snakes*. in *Computer Vision and Pattern Recognition, 1997. Proceedings., 1997 IEEE Computer Society Conference on*. 1997.
123. Scherrer-Crosbie, M., et al., *Myocardial Perfusion and Wall Motion in Infarction Border Zone: Assessment by Myocardial Contrast Echocardiography.* Journal of the American Society of Echocardiography, 2000. **13**(5): p. 353-357.
124. Loscalzo, J., *Nitric Oxide Insufficiency, Platelet Activation, and Arterial Thrombosis.* Circulation Research, 2001. **88**(8): p. 756-762.
125. Hale, S.L., et al., *Postconditioning fails to improve no reflow or alter infarct size in an open-chest rabbit model of myocardial ischemia-reperfusion.* American Journal of Physiology - Heart and Circulatory Physiology, 2008. **294**(1): p. H421-H425.
126. Yezzi, A., Jr., et al., *A geometric snake model for segmentation of medical imagery.* Medical Imaging, IEEE Transactions on, 1997. **16**(2): p. 199-209.
127. Ayata, C., et al., *Laser Speckle Flowmetry for the Study of Cerebrovascular Physiology in Normal and Ischemic Mouse Cortex.* J Cereb Blood Flow Metab, 2004. **24**(7): p. 744-755.
128. Anderson, J.L., et al., *ACC/AHA 2007 Guidelines for the Management of Patients With Unstable Angina/Non ST-Elevation Myocardial Infarction Executive Summary: A Report of the American College of Cardiology/American Heart Association Task Force on Practice Guidelines (Writing Committee to Revise the 2002 Guidelines for the Management of Patients With Unstable Angina/Non ST-Elevation Myocardial Infarction) Developed in Collaboration with the American College of Emergency Physicians, the Society for Cardiovascular Angiography and Interventions, and the Society of Thoracic Surgeons Endorsed by the American Association of Cardiovascular and Pulmonary Rehabilitation and the Society for Academic Emergency Medicine.* J Am Coll Cardiol, 2007. **50**(7): p. 652-726.
129. Apple, F.S., *Biomarkers in aggregate.* Nat Biotech, 2011. **29**(3): p. 236-237.
130. Gutterman, D.D., *Silent Myocardial Ischemia.* Circulation Journal, 2009. **73**(5): p. 785-797.
131. Sheifer, S.E., T.A. Manolio, and B.J. Gersh, *Unrecognized Myocardial Infarction.* Annals of Internal Medicine, 2001. **135**(9): p. 801-811.
132. Ammar, K.A., et al., *Defining unrecognized myocardial infarction: A call for standardized electrocardiographic diagnostic criteria.* American Heart Journal, 2004. **148**(2): p. 277-284.
133. Shapiro, M.G., et al., *Dynamic imaging with MRI contrast agents: quantitative considerations.* Magn Reson Imaging, 2006. **24**(4): p. 449-62.

134. Daniel, K.D., et al., *Multi-reservoir device for detecting a soluble cancer biomarker.* Lab Chip, 2007. **7**(10): p. 1288-93.
135. Kim, G.Y., et al., *Magnetic relaxation switch detection of human chorionic gonadotrophin.* Bioconjug Chem, 2007. **18**(6): p. 2024-8.
136. Taktak, S., et al., *Multiparameter magnetic relaxation switch assays.* Anal Chem, 2007. **79**(23): p. 8863-9.
137. Tsourkas, A., et al., *Magnetic relaxation switch immunosensors detect enantiomeric impurities.* Angew Chem Int Ed Engl, 2004. **43**(18): p. 2395-9.
138. Perez, J.M., et al., *Magnetic relaxation switches capable of sensing molecular interactions.* Nat Biotechnol, 2002. **20**(8): p. 816-20.
139. Perez, J.M., L. Josephson, and R. Weissleder, *Use of magnetic nanoparticles as nanosensors to probe for molecular interactions.* Chembiochem, 2004. **5**(3): p. 261-4.
140. Perez, J.M., et al., *DNA-based magnetic nanoparticle assembly acts as a magnetic relaxation nanoswitch allowing screening of DNA-cleaving agents.* J Am Chem Soc, 2002. **124**(12): p. 2856-7.
141. Sun, E.Y., R. Weissleder, and L. Josephson, *Continuous analyte sensing with magnetic nanoswitches.* Small, 2006. **2**(10): p. 1144-7.
142. Wunderbaldinger, P., L. Josephson, and R. Weissleder, *Crosslinked iron oxides (CLIO): a new platform for the development of targeted MR contrast agents.* Acad Radiol, 2002. **9 Suppl 2**: p. S304-6.
143. Zhao, M., et al., *Magnetic sensors for protease assays.* Angew Chem Int Ed Engl, 2003. **42**(12): p. 1375-8.
144. Daniel, K.D., et al., *Implantable diagnostic device for cancer monitoring.* Biosens Bioelectron, 2009. **24**(11): p. 3252-7.
145. Jaffe, A.S., L. Babuin, and F.S. Apple, *Biomarkers in Acute Cardiac Disease: The Present and the Future.* Journal of the American College of Cardiology, 2006. **48**(1): p. 1-11.
146. Tarnavski, O., et al., *Mouse cardiac surgery: comprehensive techniques for the generation of mouse models of human diseases and their application for genomic studies.* Physiol. Genomics, 2004. **16**(3): p. 349-360.
147. Thygesen, K., J.S. Alpert, and H.D. White, *Universal Definition of Myocardial Infarction.* Journal of the American College of Cardiology, 2007. **50**(22): p. 2173-2195.
148. Ling, Y., *Nuclear magnetic resonance readable sensors*, in *Harvard University--MIT Division of Health Sciences and Technology.*2010, Massachusetts Institute of Technology: Cambridge, MA. p. 104.
149. Scherrer-Crosbie, M., et al., *Infarct Size Assessment in Mice.* Echocardiography, 2007. **24**(1): p. 90-96.
150. Bello, D., et al., *Infarct morphology identifies patients with substrate for sustained ventricular tachycardia.* Journal of the American College of Cardiology, 2005. **45**(7): p. 1104-1108.

151. Stijntje, D.R., et al., *Comparison of Myocardial Infarct Size Assessed With Contrast-Enhanced Magnetic Resonance Imaging and Left Ventricular Function and Volumes to Predict Mortality in Patients With Healed Myocardial Infarction.* The American journal of cardiology, 2007. **100**(6): p. 930-936.
152. Takemura, G. and H. Fujiwara, *Doxorubicin-Induced Cardiomyopathy: From the Cardiotoxic Mechanisms to Management.* Progress in Cardiovascular Diseases, 2007. **49**(5): p. 330-352.
153. Robert, J., *Long-term and short-term models for studying anthracycline cardiotoxicity and protectors.* Cardiovascular Toxicology, 2007. **7**(2): p. 135-139.
154. Wallace, K.B., et al., *Serum troponins as biomarkers of drug-induced cardiac toxicity.* Toxicologic Pathology, 2004. **32**(1): p. 106-121.